

Argonne National Laboratory

REACTOR DEVELOPMENT PROGRAM PROGRESS REPORT

APRIL 1968

The facilities of Argonne National Laboratory are owned by the United States Government. Under the terms of a contract (W-31-109-Eng-38) between the U. S. Atomic Energy Commission, Argonne Universities Association and The University of Chicago, the University employs the staff and operates the Laboratory in accordance with policies and programs formulated, approved and reviewed by the Association.

MEMBERS OF ARGONNE UNIVERSITIES ASSOCIATION

The University of Arizona
Carnegie Institute of Technology
Case Institute of Technology
The University of Chicago
University of Cincinnati
Illinois Institute of Technology
University of Illinois
Indiana University
Iowa State University

The University of Iowa
Kansas State University
The University of Kansas
Loyola University
Marquette University
Michigan State University
The University of Michigan
University of Minnesota
University of Missouri

Northwestern University
University of Notre Dame
The Ohio State University
Purdue University
Saint Louis University
Washington University
Wayne State University
The University of Wisconsin

LEGAL NOTICE

This report was prepared as an account of Government sponsored work. Neither the United States, nor the Commission, nor any person acting on behalf of the Commission:

A. Makes any warranty or representation, expressed or implied, with respect to the accuracy, completeness, or usefulness of the information contained in this report, or that the use of any information, apparatus, method, or process disclosed in this report may not infringe privately owned rights; or

B. Assumes any liabilities with respect to the use of, or for damages resulting from the use of any information, apparatus, method, or process disclosed in this report.

As used in the above, "person acting on behalf of the Commission" includes any employee or contractor of the Commission, or employee of such contractor, to the extent that such employee or contractor of the Commission, or employee of such contractor prepares, disseminates, or provides access to, any information pursuant to his employment or contract with the Commission, or his employment with such contractor.

Printed in the United States of America

Available from

Clearinghouse for Federal Scientific and Technical Information

National Bureau of Standards, U. S. Department of Commerce

Springfield, Virginia 22151

Price: Printed Copy \$3.00; Microfiche \$0.65

ARGONNE NATIONAL LABORATORY
9700 South Cass Avenue
Argonne, Illinois 60439

REACTOR DEVELOPMENT PROGRAM
PROGRESS REPORT

April 1968

Robert B. Duffield, Laboratory Director
Stephen Lawroski, Associate Laboratory Director

<u>Division</u>	<u>Director</u>
Chemical Engineering	R. C. Vogel
Idaho	M. Novick
Metallurgy	M. V. Nevitt
Reactor Engineering	L. J. Koch
Reactor Physics	R. Avery
Remote Control	D. P. Mingesz (Acting)

Report Coordinated by
L. B. Fosdick and A. Glassner

Issued June 12, 1968

FOREWORD

The Reactor Development Program Progress Report, issued monthly, is intended to be a means of reporting those items of significant technical progress which have occurred in both the specific reactor projects and the general engineering research and development programs. The report is organized in accordance with budget activities in a way which, it is hoped, gives the clearest, most logical overall view of progress. Since the intent is to report only items of significant progress, not all activities are reported each month. In order to issue this report as soon as possible after the end of the month editorial work must necessarily be limited. Also, since this is an informal progress report, the results and data presented should be understood to be preliminary and subject to change unless otherwise stated.

The issuance of these reports is not intended to constitute publication in any sense of the word. Final results either will be submitted for publication in regular professional journals or will be published in the form of ANL topical reports.

The last six reports issued
in this series are:

October 1967	ANL-7391
November 1967	ANL-7399
December 1967	ANL-7403
January 1968	ANL-7419
February 1968	ANL-7427
March 1968	ANL-7438

REACTOR DEVELOPMENT PROGRAM

Highlights of Project Activities for April 1968

EBR-II

The reactor was operated for 587 MWdt in Runs 27D through 27H during April. Throughout the month the primary aim was to identify the source of fission-gas leakage from the core. Suspected experimental sub-assemblies were removed from the core in four lots as leakage recurred. The last lot removed included the last of the fueled experimental subassemblies in the core, and further operation for 148 MWdt in Run 27H produced no further leakage by the end of the month. The cumulated total of EBR-II operation is 16,704 MWdt.

Normal productive operations were continued in the FCF hot and cold lines. Additional runs were made to produce 70% enriched fission elements for use in experimental programs.

ZPR-3

Doppler-reactivity measurements with Assembly 51, the first core of the FTR Phase-B critical program, were completed. Axial and radial traverses are in progress for measurements of reaction rate and material-reactivity worths.

The worths of selected core drawers at the core-reflector interface have been tabulated, and a calculation has been made of the sensitivity of the neutron multiplication factor to incremental fuel changes at the core boundary.

ZPPR

The Request for Proposal for the ZPPR computer and related equipment has been issued as part of a joint Request for Proposal for three Argonne on-line experimental computer systems.

Installation of the reactor assembly was about one week ahead of schedule at the end of the month. Installation was about 65% complete on the mechanical items and 70% complete on the instrumentation and controls.

ANL requested occupancy of the escape tunnel on April 10 in order to complete work on the seal doors which may become the critical item for completion of the facility.

TABLE OF CONTENTS

	<u>Page</u>
I. LIQUID-METAL FAST BREEDER REACTORS--CIVILIAN	1
A. Fuel Development--LMFBR	1
1. Metallic	1
2. Oxide	2
3. Carbide--Fabrication and Evaluation	3
4. Fuel Cladding and Structure--Jacket Alloys	4
B. Physics Development--LMFBR	7
1. Theoretical Reactor Physics--Fast Critical Experiments--Theoretical Support	7
2. Experimental Reactor Physics--Fast Critical Experiments--Experimental Support (Idaho)	9
3. Experimental Reactor Physics--Fast Critical Experiments--Experimental Support (Argonne)	10
4. ZPR-3 Operations and Analysis	11
5. ZPR-6 and -9 Operations and Analysis	15
6. ZPPR Operations and Analysis	20
7. ZPR Fuel and Nonfissile Materials--Technical Assistance	22
8. ZPR Fuel and Nonfissile Materials--Procurement	23
9. ZPPR Construction	30
10. FFTF Critical Experiment Program	31
C. Component Development--LMFBR	33
1. Sodium Technology Development--Engineering Development	33
2. Reactor Mechanisms Development--Materials Evaluation	34
3. Fuel Handling, Vessels and Internals	35
D. Systems and Plant--LMFBR	36
1. 1000-MWe Plant	36
E. EBR-II	38
1. Research and Development	38
a. Reactor Experimental Support--Reactor Analysis and Testing	38
b. Nuclear Analysis Methods Development	60
c. Reactor System Testing, Surveillance, and Evaluation	66

TABLE OF CONTENTS

	<u>Page</u>
d. Fuel Swelling and Driver Surveillance	67
e. Mark-II Driver Fuel Element Development	69
f. Equipment--Fuel Related	72
g. Equipment--Reactor and Primary Coolant System	73
h. Secondary Sodium and Power Systems	74
i. New Subassemblies Design and Experimental Support	75
j. Process Chemistry	76
k. Experimental Irradiation and Testing	78
l. FCF Process Analysis and Testing	83
m. FCF Equipment Improvement	83
n. FCF Experimental Support--Hot Fuel Examination Facility (HFEF)--Feasibility and Cost Study	84
o. Reactor Improvements, Nuclear Instrument Test Facility Study	84
p. Feasibility Study of Fuel Failure Detection--Chemical and Mechanical Methods	85
q. EBR-II Materials-Coolant Compatibility	87
2. Operations--Reactor Plant	90
3. Operations--Fuel Cycle Facility	91
Publications	98
II. GENERAL REACTOR TECHNOLOGY	99
A. Applied and Reactor Physics Development--Research and Development	99
1. Reactor Code Center	99
2. Theoretical Reactor Physics	99
B. Reactor Fuels and Materials Development	102
1. Fuels and Claddings--Behavior of Reactor Materials	102
2. Fuels and Claddings--Chemistry of Irradiated Materials	106
3. Fuels and Claddings--Thermodynamics of Fuel Materials	108
4. Techniques of Fabrication and Testing--Basic Fabricability--Research and Development	108
5. Engineering Properties of Reactor Materials--Research and Development	110

TABLE OF CONTENTS

	<u>Page</u>
C. Engineering Development--Research and Development	110
1. Development of Master-Slave Manipulator Systems	110
2. Heat Transfer, Fluid Flow, and Mechanics of Materials	112
D. Chemistry and Chemical Separations	116
1. Aqueous and Volatility Processes--Research and Development--Fluoride Volatility Process	116
2. Closed Cycle Processes--Research and Development--Compact Pyrochemical Processes	119
3. General Chemistry and Chemical Engineering--Research and Development	122
Publications	128
III. NUCLEAR SAFETY	129
A. Other Reactor Kinetics--Research and Development	129
1. Accident Analysis and Safety Evaluation	129
2. Fuel Meltdown Studies with TREAT	130
3. Materials Behavior, Equation of State, and Energy Transfer	132
4. Coolant Dynamics	142
B. Operations	146
1. TREAT Operations	146
C. Engineered Safety Features Technology--Research and Development	146
1. Energy Absorption Containment	146
2. One-dimensional Code Containment Structure	148

1	Introduction
2	1.1 Background and Motivation
3	1.2 Scope and Objectives
4	1.3 Organization of the Report
5	2. Literature Review
6	2.1 General Chemistry and Physics
7	2.2 Specific Topics
8	2.3 Summary
9	3. Experimental Methods
10	3.1 Materials and Apparatus
11	3.2 Procedures
12	3.3 Data Collection
13	3.4 Error Analysis
14	4. Results and Discussion
15	4.1 Data Analysis
16	4.2 Discussion of Results
17	4.3 Comparison with Literature
18	4.4 Conclusions
19	5. Conclusions and Future Work
20	5.1 Summary of Findings
21	5.2 Future Work
22	References
23	Appendix A: Supplementary Data
24	Appendix B: Glossary
25	Appendix C: Bibliography
26	Appendix D: Index

I. LIQUID-METAL FAST BREEDER REACTORS--CIVILIAN

A. Fuel Development--LMFBR

1. Metallic

a. Fuel Element Performance (W. F. Murphy)

Last Reported: ANL-7438, pp. 3-4 (March 1968).

Each of four fuel elements irradiated in Subassembly XA07 (see Progress Report for September 1967, ANL-7382, Table II.D.1, p. 73) has been sectioned transversely near the midlength of the fuel column (at the point of maximum burnup, 4.4 to 4.6 a/o). The fuel had a nominal composition of U-15 w/o Pu-10 w/o Zr. The three annular zones observed in these sections (see Progress Report for November 1967, ANL-7399, pp. 1-4) have been analyzed to determine the distribution of uranium, plutonium, zirconium, and technetium. The results of the analyses are given in Fig. I.A.1 for the center, middle, and outer zones.

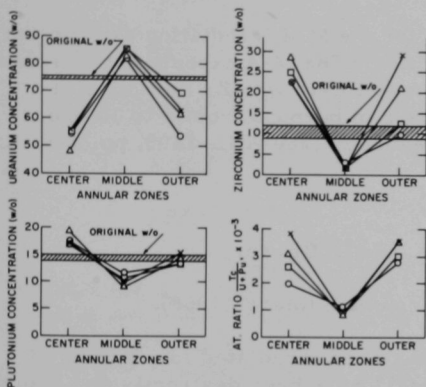


Fig. I.A.1. Compositional Variation of Transverse Sections of U-Pu-Zr Fuel Pins. The symbols represent four different sets of data.

graphy reported previously (see ANL-7399, Table I.A.1, p. 3). The initial ratio of plutonium to uranium was about 1:5, and changes in this ratio indicate that some movement of these elements also has occurred.

The analyses showed that considerable amounts of zirconium and technetium migrated from the middle zone, which is in agreement with results of beta-gamma autoradiography

These analytical results indicate depletion of some fission products in the middle zone, and significant changes in the original alloy composition have occurred in all zones. The mechanism for this behavior is not known at this time, but the following factors are probable contributors:

- (1) phase transformations in the alloy (two transformations are known to exist at 595 and 655°C in the unirradiated alloy);
- (2) temperature distributions over the lifetime of the element (variations produced by changes in geometry, thermal conductivity, and reactor power);
- (3) temperature gradients (variations produced by changing

Irradiation of Subassembly XG05 in EBR-II was terminated after 12,640 MWd, which is 92% of the planned exposure. This subassembly contains two metallic fuel pins (U-15 w/o Pu-10 w/o Zr and U-15 w/o Pu-10 w/o Ti) that are clad in V-20 w/o Ti alloy. The estimated burnup of heavy atoms for these two elements is 6.9 a/o. The capsules that contain these elements will be examined by neutron radiography at the EBR-II site.

Fifteen U-15 w/o Pu-10 w/o Zr fuel elements (Group M-3) have accumulated about 0.8 a/o burnup in EBR-II. The primary objectives of this experiment and the design and operating parameters of these elements have been given previously (see Progress Report for December 1967, ANL-7403, Table II.A.3, p. 4).

Twenty-nine fuel elements for the M-4 irradiation experiment have been fabricated and passed inspection. The M-4 experiment will investigate the irradiation behavior of U-15 w/o Pu-12 w/o Zr fuel alloy at a linear heat rating of 14 kW/ft in the range of burnups from 1 to 10 a/o. Design parameters have been given previously (see ANL-7403, pp. 4-5).

2. Oxide

a. Fuel Element Performance (F. L. Brown)

Last Reported: ANL-7438, pp. 4-6 (March 1968).

Two of the fuel elements that were irradiated to a burnup of 3.5 a/o in experimental Subassembly XO11 have been destructively examined. Transverse sections were taken from Element TVOV-1 (irradiated at a maximum linear heat rating of ~19.5 kW/ft) and from the severely overheated Element HOV-4.

Melting of the Hastelloy-X cladding of Element HOV-4 during irradiation was a result of the loss of sodium bond from the capsule that contained this element. Photomicrographs and autoradiographs of the transverse sections (taken from the midplane of the fuel column and from $2\frac{1}{2}$ in. below the midplane) showed that the fuel in each of these sections has at least two once-molten annular zones plus areas that appeared to be incomplete dendrites at the fuel periphery. The alpha-autoradiographs showed little or no indication of plutonium inhomogeneity in the main body of the fuel, but there was some evidence that plutonium was concentrated in particles in the periphery. The beta-gamma autoradiographs indicated the presence of high concentrations of fission products adjacent to the central void and high concentrations at random locations near the periphery.

Fission-gas release from Element TVOV-1 (based on the estimated burnup) was 53% of the theoretical volume generated. Photomicrographs and autoradiographs were made of TVOV-1 at the location of

maximum cladding temperature, 575°C. The presence of a large central void and the extensive development of columnar grains were attributed to the low smeared density of this element, 77% of theoretical. The alpha-autoradiograph showed possible depletion of plutonium in the periphery of the fuel; however, loss of fuel from the periphery during specimen preparation may be the reason for the light band that was observed adjacent to the cladding. The beta-gamma autoradiograph showed variations in fission-product concentration across the section examined. The maximum diameter of the area of high fission-product density corresponded to a ring of porosity.

A reaction layer that averaged about 0.0025 in. thick was found at the interface of the fuel and the V-20 w/o Ti cladding of TVOV-1; the maximum depth observed was 0.005 in. A layer that was similar in appearance and in etching characteristics, but only 0.002 in. thick, was found in the plenum $2\frac{1}{2}$ in. above the fuel column.

3. Carbide--Fabrication and Evaluation

a. Fuel Element Performance (J. H. Kittel)

Last Reported: ANL-7438, p. 6 (March 1968).

The status of carbide fuels under irradiation in EBR-II is shown in Table I.A.1. Irradiation of Subassembly XG05 was terminated at the request of other experimenters sharing the subassembly. The subassembly was dismantled in the Fuel Cycle Facility, and the elements are being returned to Illinois for destructive examination.

TABLE I.A.1. Status of Mixed-carbide Fuel Irradiations in Progress in EBR-II

S/A No.	Specimen Number	Design Parameters					Operating Conditions				
		Fuel Composition (w/o)	Fuel Form ^a	Effective Density (%)	Cladding Composition (w/o)	Cladding OD (in.)	Cladding Thickness (in.)	Max (kW/ft)	Max Cladding Temp (°C)	Burnup to Date	
										a/o	fiss/cc x 10 ⁻²⁰
XG05 ^c	SMV-2	UC-20 PuC	VIPAC	83.8	304 SS	0.296	0.021	24.0	675	6.9	19.2
XG05 ^c	HMV-5	UC-20 PuC	VIPAC	80.0	Hastelloy-X	0.295	0.015	26.6	685	7.2	18.9
XG05 ^c	NMV-11	(U _{0.8} Pu _{0.2})C	VIPAC	82.9	Nb-1 Zr	0.281	0.012	25.5	635	7.2	19.7
X008	NMP-2	(U _{0.8} Pu _{0.2})C	PELLET	81.6	Nb-1 Zr	0.284	0.013	17.4	545	4.4	11.9
X008	NMV-4	UC-20 PuC	VIPAC	80.0	Nb-1 Zr	0.283	0.013	27.0	645	6.6	17.5
X008	NMV-7	UC-20 PuC	VIPAC	80.0	Nb-1 Zr	0.283	0.013	26.0	630	6.5	17.3
X008	NMV-12	(U _{0.8} Pu _{0.2})C	VIPAC	85.5	Nb-1 Zr	0.284	0.014	26.7	645	6.6	18.6
X008	HMV-1	UC-20 PuC	VIPAC	80.0	Hastelloy-X	0.295	0.015	25.2	660	6.0	15.9
X008	HMV-4	UC-20 PuC	VIPAC	80.0	Hastelloy-X	0.295	0.016	27.2	690	6.5	17.1
X008	HWMP-1	(U _{0.8} Pu _{0.2})C	PELLET	81.4	Hastelloy-X + W	0.296	0.020	16.9	565	4.4	11.8
X008	HWMP-1	(U _{0.8} Pu _{0.2})C	VIPAC	82.9	Hastelloy-X + W	0.295	0.018	26.4	685	6.5	17.8
X015	NMP-1	(U _{0.8} Pu _{0.2})C	PELLET	81.6	Nb-1 Zr	0.284	0.013	16.5	535	2.1	5.6
X015	NMV-3	UC-20 PuC	VIPAC	80.0	Nb-1 Zr	0.284	0.013	26.0	635	3.1	8.2
X015	HMV-2	UC-20 PuC	VIPAC	80.0	Hastelloy-X	0.295	0.015	27.0	685	3.0	8.0
X015	TVMV-1	(U _{0.8} Pu _{0.2})C	VIPAC	83.7	V-20 Ti	0.298	0.021	23.4	640	2.8	7.7

^aVIPAC = Vibratorily compacted into cladding; PELLET = Pressed and sintered pellets.

^bBased on effective density.

^cIrradiation completed.

4. Fuel Cladding and Structure--Jacket Alloys

a. Irradiation Studies of Fuel Jacket Alloys (R. Carlander)

Last Reported: ANL-7438, pp. 7-8 (March 1968)

Tests are being conducted to evaluate the effects of irradiation on the mechanical properties of vanadium alloys in comparison with other potential cladding materials for LMFBR, such as Type 304 stainless steel, Hastelloy-X and Inconel 625. When possible, the comparisons are made between specimens that were irradiated in the same EBR-II subassemblies to obtain identical irradiation conditions.

Postirradiation tube-burst tests were conducted at 550°C with specimens of V-15 w/o Ti-7.5 w/o Cr, Type 304 stainless steel, Hastelloy-X, and Inconel 625. The specimens had been irradiated in Subassembly XO13 in EBR-II to a nominal fluence of 5×10^{21} at $600 \pm 100^\circ\text{C}$. The results of the tests are given in Table I.A.2. The ratios of the irradiated to unirradiated test values were calculated to compare the effects of irradiation on the strengths and ductilities of the alloys. The values are plotted in Figs. I.A.2 and I.A.3.

The increase in the rupture strength at 550°C due to irradiation was greater for V-15 w/o Ti-7.5 w/o Cr than for both Type 304 stainless steel and for Hastelloy-X, but less than for Inconel 625 (see Fig. I.A.2). The maximum increase in rupture strength of V-15 w/o Ti-7.5 w/o Cr alloy was 32%, as compared with maximum increases of 41, 21, and 14% for Inconel 625, Hastelloy-X, and Type 304 stainless steel, respectively.

TABLE I.A.2. Tube-burst Properties at 550°C of Specimens of Cladding Materials from EBR-II Subassembly XO13

Material	Fluence ($\text{n}/\text{cm}^2 \times 10^{21}$)	Tangential Rupture Strength (kg/mm^2)	$\Delta D/D$ (%)	Material	Fluence ($\text{n}/\text{cm}^2 \times 10^{21}$)	Tangential Rupture Strength (kg/mm^2)	$\Delta D/D$ (%)
V-15 w/o Ti-7.5 w/o Cr	-	71.1	6.1	304 SS	3.7	44.8	10.0
V-15 w/o Ti-7.5 w/o Cr	-	70.5	6.2	304 SS	3.9	45.6	3.6
V-15 w/o Ti-7.5 w/o Cr	-	73.0	6.1	304 SS	4.0	44.3	3.2
V-15 w/o Ti-7.5 w/o Cr	-	72.4	8.1	304 SS	5.3	46.2	3.0
V-15 w/o Ti-7.5 w/o Cr	0.2	77.2	7.2	Hastelloy-X	-	56.2	13.2
V-15 w/o Ti-7.5 w/o Cr	0.5	77.6	8.9	Hastelloy-X	-	56.2	14.0
V-15 w/o Ti-7.5 w/o Cr	1.1	83.4	5.8	Hastelloy-X	-	56.6	14.2
V-15 w/o Ti-7.5 w/o Cr	2.0	83.4	2.0	Hastelloy-X	-	58.1	13.5
V-15 w/o Ti-7.5 w/o Cr	3.6	90.5	3.8	Hastelloy-X	3.5	68.8	8.1
V-15 w/o Ti-7.5 w/o Cr	4.7	94.7	4.9	Hastelloy-X	3.7	67.6	3.7
304 SS	-	41.2	10.9	Inconel 625	-	63.7	9.5
304 SS	-	41.9	10.7	Inconel 625	-	65.3	12.7
304 SS	-	40.6	12.1	Inconel 625	-	64.1	14.5
304 SS	-	39.4	12.1	Inconel 625	-	64.1	13.0
304 SS	-	38.7	11.0	Inconel 625	0.2	88.6	9.2
304 SS	-	38.7	11.3	Inconel 625	1.1	90.5	15.7
304 SS	-	39.4	12.5	Inconel 625	3.3	88.6	7.0
304 SS	-	39.4	12.4	Inconel 625	3.3	87.9	3.3
304 SS	0.2	38.8	14.7	Inconel 625	3.5	88.2	4.4
304 SS	1.2	40.1	11.2	Inconel 625	3.6	89.2	10.5
304 SS	3.6	41.7	6.3				

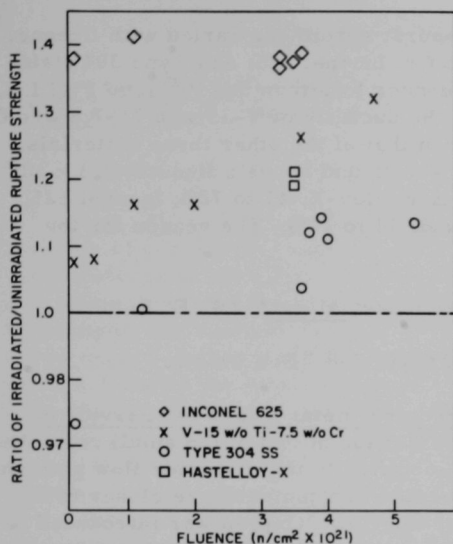
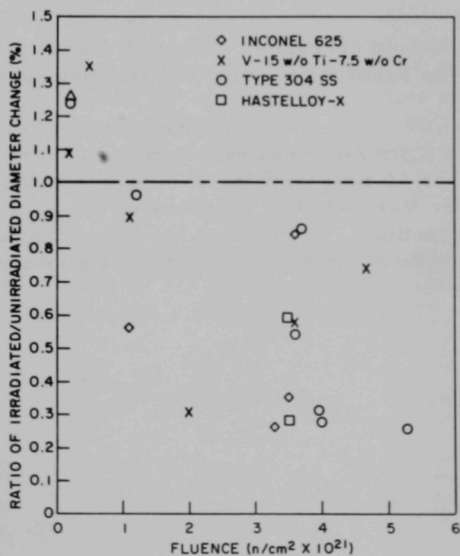


Fig. I.A.2. Effect of Irradiation on the Rupture Strengths (at 550°C) of Specimens of Cladding Materials from EBR-II Subassembly XO13

Fig. I.A.3. Effect of Irradiation on the Percent Diameter Increase (at 550°C) of Specimens of Cladding Materials from EBR-II Subassembly XO13



The ductility of the tube-burst specimens varied with fluence. The ductility of V-15 w/o Ti-7.5 w/o Cr, Inconel 625, and Type 304 stainless steel appeared to increase at fluences less than 5×10^{20} (see Fig. I.A.3). However, at fluences above 3×10^{22} , the ductility of V-15 w/o Ti-7.5 w/o Cr alloy decreased by a lesser extent than that of the other three materials. The following decreases in ductility were found above a fluence of 3×10^{22} : V-15 w/o Ti-7.5 w/o Cr, 26 to 42%; Hastelloy-X, 41 to 72%; Inconel 625, 16 to 74%; and Type 304 stainless steel, 14 to 74%. The reason for the scatter in the results is not known.

b. Sodium Corrosion of Fuel Jacket Alloys* (W. E. Ruther)

Last Reported: ANL-7427, pp. 7-8 (Feb 1968).

(i) Development of Refractory-metal Alloys for Service in Oxygen-contaminated Sodium. The cold traps of two of the small refreshed autoclave systems were cleaned and modified to insure better flow patterns of sodium. The traps can now be operated at a temperature closer to the melting point of sodium and still maintain flow. Oxygen was introduced to the autoclave system via the gas phase, and the system was allowed to equilibrate for 4 days with the cold trap at $\sim 100^\circ\text{C}$.

Initial exposure of vanadium wire to this system resulted in rapid corrosion. Possibly insufficient time was allowed for equilibration. The exposure of vanadium is being repeated.

The dynamic test of vanadium alloys at 600°C (at a speed of 6.1 m/sec) has been terminated after 107 days. Maximum weight change was $+0.4 \text{ mg/cm}^2$ for V-20 w/o Ti; minimum weight change was $\pm 0.03 \text{ mg/cm}^2$ for V-10 w/o Cr. Sections of the samples are being microscopically examined. A final test has been started at 500°C that will complete this phase of the scheduled dynamic exposures.

*Errata in Progress Report for January 1968, ANL-7419, p. 4, under the heading (ii) Corrosion of Nickel Alloys in Flowing Sodium. Second sentence should read, "Fluence was $7.2 \times 10^{20} \text{ n/cm}^2$ ($4.7 \times 10^{19} > 1.35 \text{ MeV}$)."

B. Physics Development--LMFBR

1. Theoretical Reactor Physics--Fast Critical Experiments--Theoretical Support (F. W. Thalgot, R. B. Nicholson and R. G. Palmer)

Last Reported: ANL-7438, p. 9 (March 1968).

a. Shape Factors for Large Cores in ZPPR. A computer study of a series of cores with composition similar to ZPPR Core I has been carried out to determine the effect of core volume on shape factor (the ratio of spherical critical volume to cylindrical critical volume). Critical size was varied by changing the enrichment of the fuel plates. The peak of the shape-factor curve occurs in the vicinity of a length-to-diameter (L/D) ratio of 0.93. Figure I.B.1 shows the predicted variation of peak shape factor with core size. Also shown are the results of five measurements of shape factor for small cores correlated linearly.* Differences in core and reflector compositions appear to be responsible for the fairly large discrepancy between the two curves. It would seem that the experimental curve has little applicability to the analysis of large oxide cores in ZPPR. Work is continuing on the variation of shape factor with L/D for large cores.

b. Reactivity Worths in ZPPR Core I. One-dimensional calculations were performed by MACH-1 of the reactivity worths versus radius of a core drawer with and without a B₄C blade, 28 by 1.945 by 0.280 in., containing 350 g ¹⁰B. At the core center the special region was treated as an equivalent cylindrical rod. At other radii, it was treated as an annulus and corrected for flux depression with the results obtained for a central rod. It was found that eight control blades at a radius of 40 cm have the required reactivity worth of 1.5% Δk/k, and that a drawer with control blade is worth 2.28 core drawers.

c. Modifications to WINDOW. The WINDOW code (see Progress Report for February 1968, ANL-7427, pp. 9-10) has been modified to automate the calculation of broad-group neutron cross sections as follows:

$$\langle \sigma \rangle = \frac{\int_{\text{Br.Gr.}} \sigma(E) \phi(E) dE}{\int_{\text{Br.Gr.}} \phi(E) dE}.$$

The smoothed neutron spectrum $\phi(E)$ comes from a fundamental-mode calculation by the MC² code, and $\sigma(E)$ is obtained by Lagrangian interpolation from a table of values at discrete energies produced by cell calculations of the RAPPLE/RABID type.

d. ²³⁸U Cross Sections for RABBLE. A code has been written for the CDC-1604 to compute typical resonance parameters for ²³⁸U in the

* Davey, W. G., Nucl. Sci. and Eng. 19, 259-273 (1964).

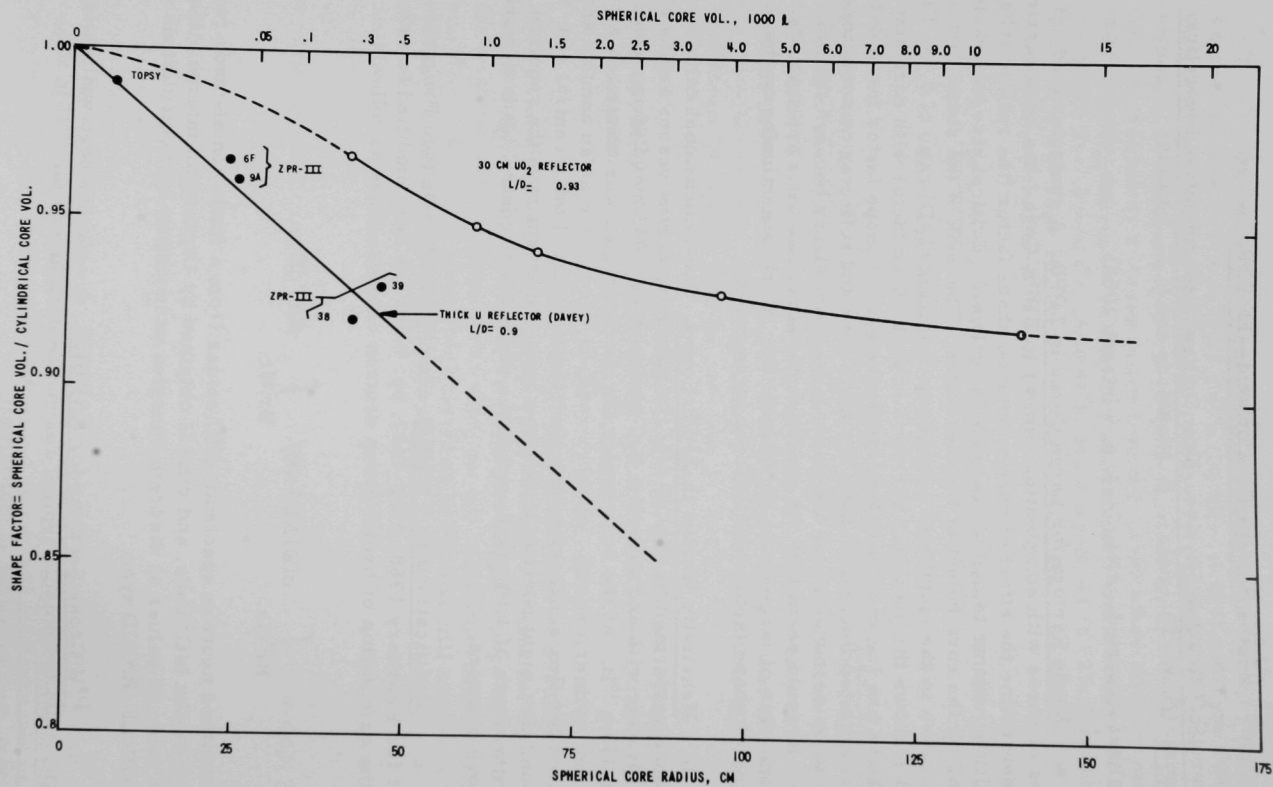


Fig. I.B.1. Shape Factor vs. Radius for Large Cores in ZPPR

unresolved region for use in the RABBLE code. The code will allow the punching in RABBLE input format of N samples, each containing R resonances, for each broad-energy group. The neutron widths are based on a chi-squared distribution ($\nu = 1$) and on the average value of the width measured in the resolved region. S- and P-wave resonances are treated. Ordering of the widths in each sample is obtained from a routine that generates random numbers. Presently a constant resonance spacing is assumed.

2. Experimental Reactor Physics--Fast Critical Experiments--
Experimental Support (Idaho) (W. G. Davey)

Last Reported: ANL-7438, pp. 10-11 (March 1968).

a. Neutron Spectrometry

(i) High-count-rate Electronics. Efforts to improve the pre-amplifier and linear amplifier for the proton-recoil spectrometer continued. Data taken in AFSR showed that a dc-coupled charge-sensitive preamplifier matched to a pole-zero-corrected linear amplifier gave satisfactory response to overload pulses under high-count-rate conditions.

Preliminary comparisons with the previously used amplifiers were encouraging. The pole-zero-corrected amplifiers substantially reduced distortion of the proton spectrum, but showed a need for base-line restoration. A base-line restorer that is presently being constructed should greatly improve the amplifier response to overloads.

A pile-up detector is being designed for rejecting pulses that ride on the "hill sides" of large overload pulses, thus further reducing spectrum distortion. The additional dead time will be accounted for by interfacing the detector to the live-time clock.

b. Heterogeneity Studies. Analyses of ^{235}U and ^{238}U exposures in AFSR have been completed and the analysis of exposure of a thick (30-mil) ^{239}Pu foil in AFSR is almost complete. In addition, a 42-Whr exposure of ^{235}U and a 150-Whr exposure of ^{238}U in ZPR-3 have been performed. The latter two exposures indicate that counting statistics for foil exposures in ZPPR should be obtainable at acceptable reactor power levels.

The 38 gamma-ray peaks selected for use cover the energy range from 50 to 2500 keV, include half-lives from 23.5 min to 40 days, and provide information on 14 mass chains plus ^{239}U and ^{239}Np activities. Out of these, 9 mass chains and ^{239}Np have two or more lines from individual isotopes or pairs of isotopes in equilibrium. This allows checking the identification of a gamma-ray peak against other parameters than half-life.

An exposure of ^{232}Th foils in AFSR has been made, and counting is in progress. Preliminary inspection of the spectra shows a predominance of gamma rays from ^{233}Pa . Exposures of ^{235}U , ^{238}U , and ^{239}Pu in various AFSR spectra will be initiated soon.

c. Computer Applications. The Request for Proposal for the ZPPR computer and related equipment has been issued as part of a joint Request for Proposals for three Argonne on-line experimental computer systems. The other two systems, for the Reactor Physics Division, will serve the ZPR-6 and -9 reactors and the Fast Neutron Generator. The document has been submitted to computer manufacturers; response within five weeks is expected.

Development and programming of the ZPPR fuel inventory program on the CDC-1604 is continuing. The proposed input format and program operation has been formulated and is being circulated for comment.

3. Experimental Reactor Physics--Fast Critical Experiments-- Experimental Support (Argonne)

a. On-line Computer Applications (R. Gold)

Last Reported: ANL-7399, pp. 20-22 (Nov 1967).

(i) Computer Processing of Sampling--Oscilloscope Data. The DDP-24 computer has been used with a sampling oscilloscope to average out noise and fluctuations, and estimate true pulse shape.

A sampling oscilloscope is useful for fast pulses, but when the signal contains noise and fluctuations, as with nuclear detectors, the "true" pulse shape cannot be seen readily. The computer extracts that information.

The oscilloscope is a Tektronix 564, with 3S3 sampling-probe unit and 3T77 sampling-sweep unit. Analog X and Y signals are available from the oscilloscope at 1 V per scale division. These are passed through amplifiers which invert their polarity and shift their zero, and are digitized by two ADC's with 5-MHz clocks.

The sampling-sweep unit generates a clock pulse when a sampling has occurred. This pulse commands the ADC's to digitize the signals. The time (X) information is digitized to 512 channels, the amplitude (Y) information to 1024 channels.

The ADC address-advance pulses go to the computer input scalars. On completion of conversion, the computer reads the data. Subsequent samplings are ignored until data transfer is complete and the scalars are reset.

During staircase-sweep retrace, the sampling-sweep unit blanks the CRT beam so that samplings taken then will not be displayed. A portion of the blanking voltage is applied to the ADC's to inhibit conversion of those samplings.

The averaging program is in FORTRAN-IV with machine-language instructions intermixed. To start a run, the operator types in the oscilloscope vertical gain and sweep-speed settings. He then signals the computer to begin taking data. For each value of X-ADC reading, the computer keeps a record of the number of samplings with that reading, the sum of the readings from the Y-ADC for those samplings, and the sum of the squares of those readings.

The progress of the run is monitored on the computer CRT display, which shows the mean and standard deviation of the pulse shape. The operator may use the information to decide when enough data have been accumulated.

After the operator terminates the run, he looks at the CRT display and types in the time at which the pulse began to rise from the baseline or zero level, in terms of horizontal divisions on the CRT graticule. The computer averages the amplitudes for all samplings preceding the specified time, and uses that average as the baseline level. The baseline is subtracted from the average amplitude at each time point, and the difference is numerically integrated.

The output is a graph with the pulse shape shown as three curves (see Fig. I.B.2). The middle curve gives the mean amplitude at each sampling time; the two outer curves are displaced from the mean by the standard deviation of a single sampling.

The time scale is referenced to the earliest sampling recorded, whereas the voltage scale is referenced to the baseline. A vertical line crosses the pulse-shape traces at the time that was selected as the end of the baseline. Scaling is adjusted so that the pulse-shape traces fill the graph as much as possible and still have round-number scale markings. The time integral of the pulse shape is also written on the graph.

4. ZPR-3 Operations and Analysis (W. G. Davey and R. L. McVean)

Last Reported: ANL-7348, pp. 12-16 (March 1968).

a. Mockup Studies. Experiments with Assembly 51 continued. The Doppler reactivity measurements were completed, and the data are being analyzed. Axial and radial traverses through the core and reflector are underway. These traverses include reaction-rate measurements using plutonium and depleted uranium fission counters and a BF_3 proportional counter. Material-reactivity-worth traverses will also be made using boron-10, plutonium, and depleted uranium samples.

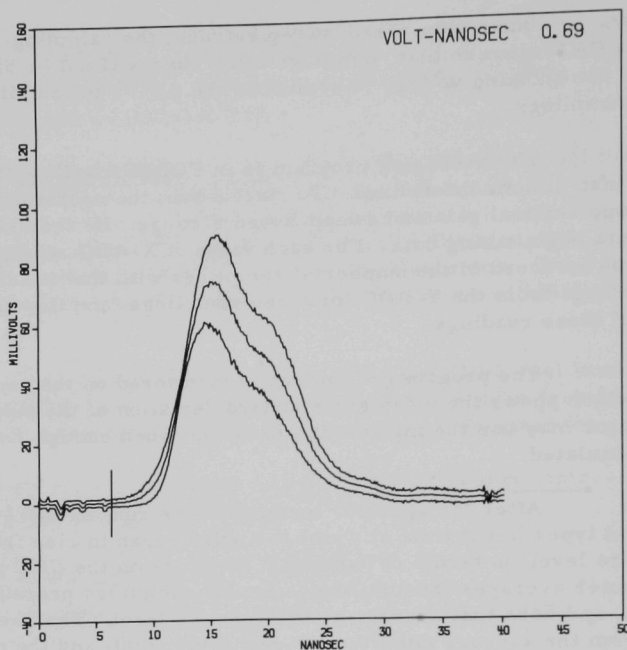


Fig. I.B.2 Computer-processed Output Graph

(i) Approach to Critical. The details of the approach to critical for Assembly 51 which have not been reported previously are given here.

The initial step was to load the radial and axial reflector, leaving 218 central drawers, 109 drawers in each half of the assembly, for core materials. Of these 218 drawers, the outer 160 drawers were inserted in the matrix as "preloaded" core drawers. Preloaded core drawers were loaded exactly as in the intended final critical system except that the columns of fissile material were replaced with depleted uranium. The remaining 58 central drawers, including the ten control and safety rods, were loaded with the normal fuel content for the initial loading in the approach to critical. Subsequent loadings in the approach to critical were achieved by replacing the depleted uranium in the "preloaded" core drawers with fuel. After each incremental fuel loading, the halves of the reactor were brought together and subcritical multiplication count rates taken with the two control rods completely withdrawn and again with the control rods completely inserted. Two methods were used to establish progressive estimates of critical mass and safe intermediate fuel increments. Plots were constructed for the inverse count rate versus mass in various forms to monitor the approach to critical.

A typical curve from one of the five counting channels, in which the product of the inverse count rate and the square of the mass versus the mass is plotted, is shown in Fig. I.B.3. The criticality region indicated in the figure is defined as being between the fuel loading where the assembly would go critical with two control rods fully inserted, and the fuel loading where the assembly would go critical with two control rods fully withdrawn. Criticality was achieved with one control rod partially inserted and the other fully inserted. The total loading was 215 kg of fissile material, including the full inventory of the partially inserted control rod. At this point, the safety rods were loaded with additional fuel from adjacent drawers to increase their total reactivity worth above the minimum of $1\frac{1}{2}\%$ $\Delta k/k$ as required in the ZPR-3 Operating Limits. The edge of the core was also adjusted to a more nearly cylindrical shape. With these changes, this particular loading is known as the reference core for Assembly 51. A full description of the reference core and safety-rod reloading is given in the Progress Report for January 1968, ANL-7419, p. 11.

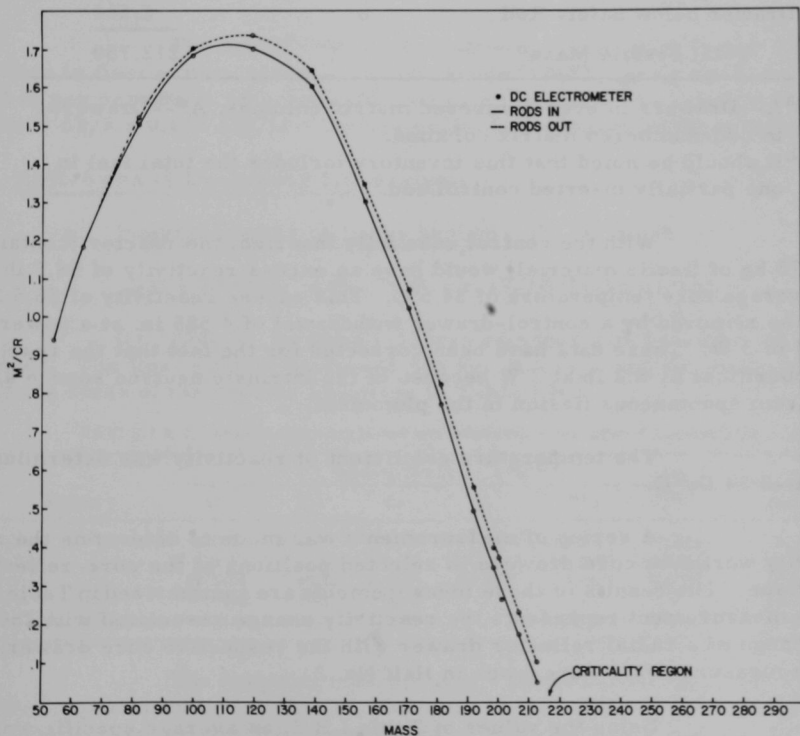


Fig. I.B.3. Approach to Critical with Assembly 51

(ii) Worth of Core Drawers at Core-reflector Interface. The reference core is used as the reference loading for most of the experiments on Assembly 51. Table I.B.1 summarizes the fissile inventory in the reference loading.

TABLE I.B.1. Fissile Inventory in Assembly-51 Reference Core

Core Drawer Type	Number of Drawers	Fissile Mass
		$^{239}\text{Pu} + ^{241}\text{Pu} + ^{235}\text{U}$ (kg)
Type A ^a	110	114.905
Type A* ^a	96	76.606
Control Rod	2	2.109
Safety Rod	8	12.718
Drawer above Safety Rod	8	3.848
Drawer below Safety Rod	8	2.564
Total Fissile Mass ^b		212.750

^aA--Drawers in even-numbered matrix columns; A*--Drawers in odd-numbered matrix columns.

^bIt should be noted that this inventory includes the total fuel in one partially inserted control rod.

With the control rods fully inserted, the reactor (containing 212.75 kg of fissile material) would have an excess reactivity of 58.5 Ih at an average core temperature of 34.5°C. This excess reactivity of 58.5 Ih may be removed by a control-drawer withdrawal of 4.585 in. at a power level of 3 W. These data have been corrected for the fact that the reactor is subcritical by 8.2 Ih at 3 W because of the intrinsic neutron source arising from spontaneous fission in the plutonium.

The temperature coefficient of reactivity was determined to be -2.34 Ih/°C.

A series of measurements was made to determine the reactivity worths of core drawers in selected positions at the core-reflector interface. The results of these measurements are summarized in Table I.B.2. Each measurement represents the reactivity change associated with the interchange of a radial reflector drawer with the respective core drawer. All these measurements were made in Half No. 2.

Using the values of Table I.B.2, an average specific worth of 86.75 Ih/kg of fissile material is obtained at a radius of 30.98 cm. The excess reactivity of 58.48 Ih represents 0.67 kg of fissile mass at the core edge.

TABLE I.B.2. Summary of Worths of Core Drawers at Core-reflector Interface

Drawer	Fissile Mass ^a (kg)	Worth (lh)	Specific Worth (lh/kg)	Radius (cm)
2-J-17	0.79798	67.67	84.80	30.90
2-L-21	0.79798	56.54	70.85	32.53
2-M-11	0.79798	77.21	96.76	29.62
2-O-10	1.04459	95.68	91.60	30.90
2-J-18	1.04459	85.61	81.96	32.13
2-K-20	1.04459	80.84	77.39	32.53
2-P-22	1.04459	94.67	90.63	30.48
2-L-20	1.04459	104.45	99.99	28.74

^a $^{239}\text{Pu} + ^{241}\text{Pu} + ^{235}\text{U}$.

Subtraction of 0.67 kg from the total inventory of 212.75 kg gives a critical mass of 212.08 kg of fissile material with fully inserted control rods. No corrections are included for heterogeneity or for the perturbation to the average regional composition due to the reloading of the safety rods.

The sensitivity of the neutron multiplication factor k to a change in fissile mass at the boundary can be found by using the value 1.036×10^3 lh per percent k as calculated for this assembly. The relationship becomes $\Delta k/k = 0.178 \Delta M/M$ for incremental fuel changes at the core boundary.

5. ZPR-6 and -9 Operations and Analysis

a. Integral Studies of Large Systems (W. Y. Kato)

Last Reported: ANL-7438, pp. 17-18 (March 1968).

(i) ZPR-9. Assembly 23 was removed and Assembly 24 was loaded. The final critical mass was 505 kg. Average atomic concentrations and the sizes of the regions are given in Table I.B.3.

TABLE I.B.3. Atomic Concentrations and Dimensions for ZPR-9 Assembly 24

Region	Atomic Densities $\times 10^{-21}$					Outer Radius (cm)	
	Fe	Ni	Cr	C	^{238}U		
Core	6.8313	0.8635	1.9496	43.4188	13.2997	1.1626	25.88
Buffer	6.8313	0.8635	1.9496	43.3299	14.5596	0.0311	30.66
Driver	22.3486	2.8252	6.3785	43.3399	0.1624	2.2765	50.85
Steel Reflector	77.7700	0.8910	2.0360	-	-	-	64.38
Depleted Reflector	4.3320	0.5400	1.1400	-	39.9300	0.0810	80.95

The material concentrations in the central zone were adjusted experimentally so that k_{∞} was unity at the center of the central zone, and the carbon and depleted concentrations were selected so as to maximize the neutron flux in the energy region of the ^{239}Pu alpha uncertainty (i.e., 1-10 keV).

The integral alpha values (i.e., the capture-to-fission ratios) for $^{239}\text{Pu} + ^{235}\text{U}$ are being measured by two different methods. The null-reactivity types of measurements were made first. In this method the neutron source is equal to the absorption at the center of the central zone, and no adjoint weighting of the terms in the alpha expression is necessary. These measurements are complete, and data reduction is in progress.

The second set of alpha measurements is in progress. The technique utilizes that described by Redman and Bretscher.* A ^{252}Cf source is used to establish the worth of fission neutrons.

b. Heterogeneity Effects (C. E. Till)

Last Reported: ANL-7419, p. 17 (Jan 1967).

(i) Fine-structure Measurements in Assembly 6 of ZPR-6. The normal loading pattern in the single-drawer unit cell of Assembly 6 is shown at the bottom of Fig. I.B.4. A simple change in this loading pattern was made

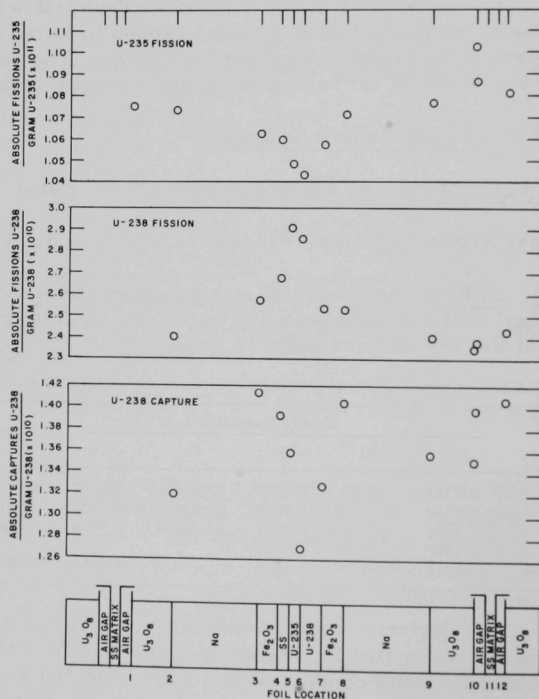


Fig. I.B.4. Fine Structure in ^{235}U Fission, ^{238}U Fission, and ^{238}U Capture in the Normal Configuration of ^{238}U in Assembly 6 of ZPR-6

*Redman and Bretscher, Nucl. Sci. Eng. 27, 34 (1967).

by bunching all the ^{238}U to alter the effects of heterogeneity. The change was made in an 80-drawer region at the center of Assembly 6. The altered loading pattern of a drawer is shown at the bottom of Fig. I.B.5. The gain in reactivity associated with the change in the loading pattern was 93 lh (0.206% $\Delta k/k$). The fine structure in the fission rates of ^{235}U and ^{238}U , and the capture rate in ^{238}U , were measured using ^{235}U and ^{238}U foils in both the normal and bunched loading patterns. The ^{238}U foils were placed between each plate in the central drawer of one half of the reactor, 2 in. from the midplane, and the ^{238}U foils were similarly placed in the other half. The foils were counted relatively, and in some cases, checked by radiochemical techniques.

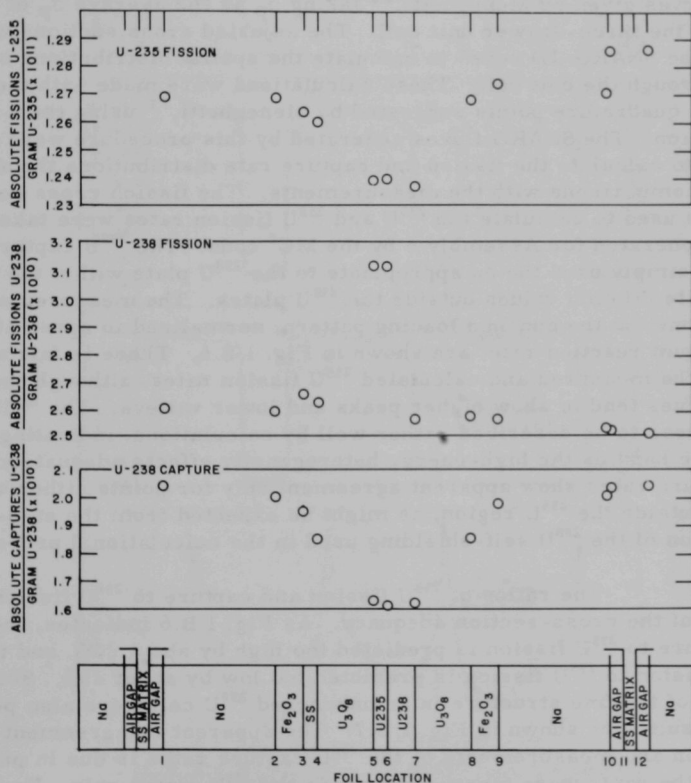


Fig. I.B.5. Fine Structure in ^{235}U Fission, ^{238}U Fission, and ^{238}U Capture in Bunched Configuration of ^{238}U in Assembly 6 of ZPR-6

Figure I.B.4 illustrates that the ^{235}U fission rate in the normal loading pattern decreases significantly in the vicinity of the ^{235}U fuel plate. The ^{238}U capture rate distribution behaves analogously; the ^{238}U fission rate increases sharply near the ^{235}U fuel plate.

The comparable results for the bunched pattern are shown in Fig. I.B.5.

(ii) Comparisons of Measurements with Calculations of the Fine Structure in Assembly 5 of ZPR-6. The fine-structure measurements in Assembly 5 (See Progress Report for April 1967, ANL-7329, pp. 25-33) have been analyzed using ENDF/B cross section data in the following manner. The MC² code* was used to generate broad-group cross sections for a homogeneous mixture with the same overall number densities as the plate-type heterogeneous core. The ²³⁸U capture cross sections then were corrected for the differences in σ_p between the homogeneous and heterogeneous geometries, using curves given by Meneghetti,** taking σ_p as the average σ_p of the ²³⁸U plates in the three-drawer unit cell. The adjusted cross sections were then used in the SNARG-1D code† to calculate the spatial distributions of the fluxes through the unit cell. These calculations were made with the modified Gaussian quadrature points suggested by Meneghetti,†† using the $n = 16$ approximation. The SNARG fluxes generated by this procedure were then used directly to calculate the fission and capture rate distributions through the cell for comparisons with the measurements. The fission cross sections that were used to calculate the ²³⁵U and ²³⁸U fission rates were taken from the set generated for Assembly 5 by the MC² code. The ²³⁸U capture cross sections simply used the σ_p appropriate to the ²³⁸U plate within the plate, and infinite dilution values outside the ²³⁸U plates. The measurements and calculations for the bunched loading pattern, normalized to agree at the point of maximum reaction rate, are shown in Fig. I.B.6. There is fair agreement between the measured and calculated ²³⁵U fission rates, although the measured values tend to show higher peaks and lower valleys. The ²³⁸U fission rates appear to be described rather well by calculations, indicating that the procedure handles the high-energy heterogeneity effects adequately. The ²³⁸U capture rates show apparent agreement only for points either well within or well outside the ²³⁸U region, as might be expected from the step-function description of the ²³⁸U self-shielding used in the calculational procedure.

The ratios of ²³⁸U fission and capture to ²³⁵U fission provide an index of the cross-section adequacy. As Fig. I.B.6 indicates, the ratio of ²³⁸U capture to ²³⁵U fission is predicted too high by about 20%, and the ratio of ²³⁸U fission to ²³⁵U fission is predicted too low by about 25%. Similar analyses of the fine structure in an unbunched ²³⁸U cell were also performed. These results are shown in Fig. I.B.7. The apparent disagreement between calculation and measurements of the ²³⁸U capture rates is due in part to the fact that the rates were measured outside the ²³⁸U plates only. For this case the ratio of ²³⁸U capture to ²³⁵U fission was predicted too high by about 24%, and the ratio of ²³⁸U fission to ²³⁵U fission was predicted lower by 19% than the measured value.

*Toppel, B. J., *et al.*, ANL-7318 (June 1967).

**Meneghetti, D., ANL-7320 (Oct 1966).

†Duffy, G., *et al.*, ANL-7271 (June 1966).

††Meneghetti, D., Nucl. Sci. Eng. 11, 295 (1962).

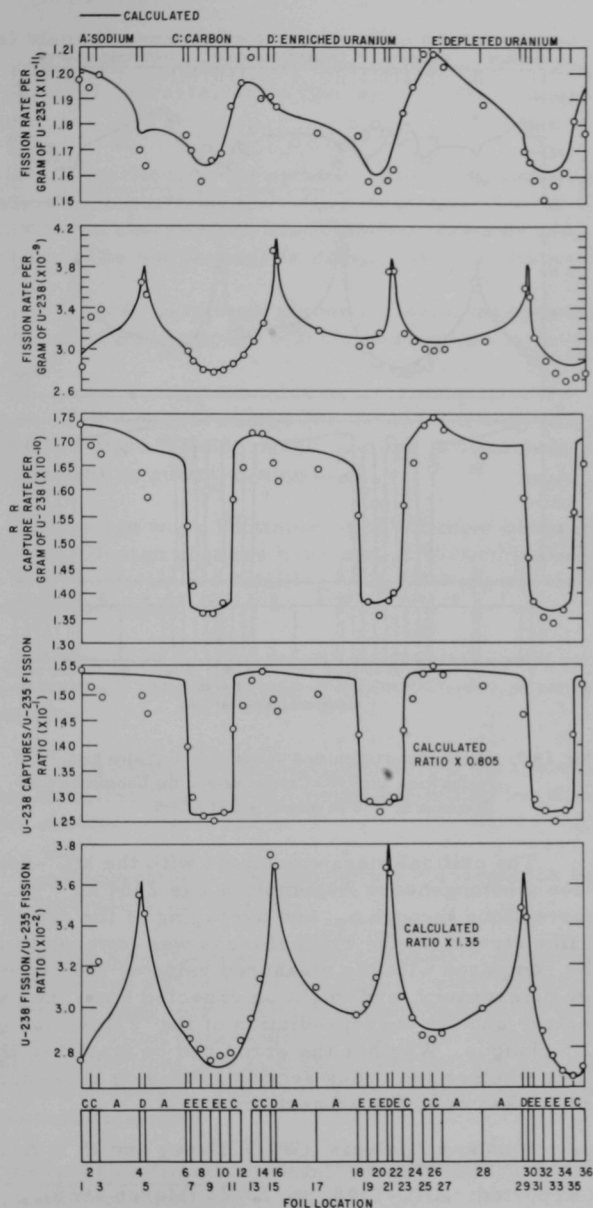


Fig. I.B.6. Measured and Calculated Values of ^{235}U Fission Rate, ^{238}U Fission Rate, ^{238}U Capture Rate, and Their Ratios in a Bunched Configuration of ^{238}U in Assembly 5 of ZPR-6

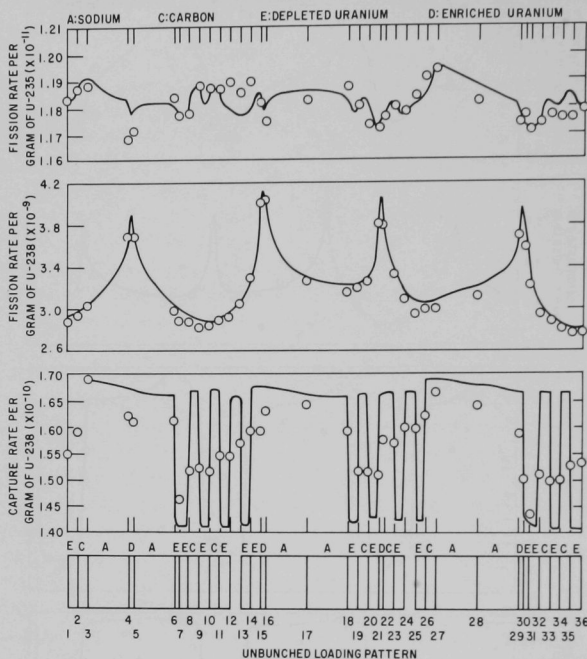


Fig. I.B.7. Measured and Calculated Values of ^{235}U Fission Rate, ^{238}U Fission Rate, and ^{238}U Capture Rate in the Unbunched Configuration of ^{238}U in Assembly 5 of ZPR-6

The critical mass calculated with the MC^2 -generated cross-section sets for a homogeneous Assembly 5 was 2554 kg ^{235}U . After the heterogeneity corrections through α_p , and averaging of the cross sections over the unit-cell fine structure, the critical mass was lowered to 2112 kg. These values may be compared with the measured value of 1583 kg of ^{235}U . This is a rather large discrepancy, and might be expected from the overprediction of the ^{238}U capture and the underprediction of the ^{238}U fission given by the calculational technique. Whether the error can be traced to the ENDF/B data for ^{238}U , or whether the cross section averaging procedure is simply inadequate, is not known at the present time.

6. ZPPR Operations and Analysis (W. G. Davey and P. I. Amundson)

Last Reported: ANL-7348, pp. 20-22 (March 1968).

a. Basic Studies of Large Plutonium Systems

(i) Program. Definitive design work for the ZPPR Core I continues. Evaluations of average cell compositions in each zone are in progress

as the initial step of a preanalysis program to be carried out for all ZPPR cores. The exact cell compositions await additional data about certain fuel and diluent physical characteristics that will be available upon completion of fabrication.

(ii) Experimental Equipment. The development of major reactor-associated experimental devices continues. The design of the perturbation sample changer has been finished, checked, and approved for construction. The bid package is being reviewed by potential vendors.

Orders have been placed for selected perturbation sample materials. Assembly of samples will commence upon receipt of the initial order.

The detail drawings for the axial traverse drive system have been finished and checked. A bid package is presently being assembled and will be sent to potential suppliers.

Design work continues on the sample changer for the axial traverse system. Design changes have been incorporated to amplify the capabilities of this system for handling both box-type reactivity-coefficient samples and foil packages.

Fabrication of parts for an initial autorod is complete and it is being assembled. Bench testing of the rod-drive portion of the system will begin shortly.

The criticality monitoring system for the vault and work-room is being installed. Cables are being assembled for data transmission to the reactor control console.

Preparations are underway for acceptance tests and storage of the initial shipment of ZPPR fuel.

b. Doppler Coefficients. Three alternative proposals for the drive system were evaluated and one was selected. Detail design work on the chosen system is in progress. The design has been discussed in detail with Reactor Physics Division personnel to ensure compatibility with the Doppler samples, and modifications are in progress to incorporate recent changes in the Doppler-sample design. The final dimensional checkout is complete except for these modifications.

c. Sodium Coefficients. Development work on the axial-sample drive mechanism continues.

d. Reactor Technique Development

(i) Precision Reactivity Measurements. A computer code has been written to predict the errors in reactivity measurements due to reactor

noise. The computation is based on the integral of the autorod noise spectrum. Calculated data are in good agreement with ZPR-3 measurements in indicating substantially larger errors at lower detector efficiencies and/or lower power levels. The results indicate a substantial improvement by this method as compared to the assumption of a constant rod-noise spectrum $W(\omega) = W(0)$.

(ii) Foil Techniques. The analysis of ^{235}U and ^{238}U exposures and identification of peaks for the ^{239}Pu exposure permit selection of the gamma-ray peaks of interest and the specification of the foil-counting system for ZPPR. Requests for quotations have been submitted for the major system components.

Computer programs which will locate gamma-ray peaks, integrate them and subtract background, give standard deviations, etc., are almost complete. Parts of these programs are now operational (see Sect. I.B.2).

(iii) Automation of Data Acquisition. This program covers work on control and readout equipment for the experiments on ZPPR that require automation.

(a) Digital Position Indicators. The display portion of the prototype of the digital position indicator is complete. Development continues on the remainder of the system.

(b) Digital Multiplexer. Development and testing of the digital multiplexer continues.

(c) Autorod Control. Construction of the autorod control system continues.

(d) Data Acquisition and Recording System. A vendor has been selected to supply the system. Operating procedures for this system are being formulated.

(iv) Training. The Idaho Division Reactor Technology Training Course is complete. Technicians and staff of ZPPR are now engaged in a systems training program which will cover in detail all major aspects of ZPPR operations and maintenance.

7. ZPR Fuel and Nonfissile Materials--Technical Assistance

a. Fuel Element Fabrication Development (J. E. Ayer)

Last Reported: ANL-7403, pp. 20-22 (Dec 1967).

Work continued on the development of procedures for making modular oxide-core plates for ZPPR. Previously, UO_2 discs (4.22 cm in diameter and 0.51-cm thick) were hot pressed, five specimens at a time. In one instance

11 specimens were hot pressed at the same time. The die, punches, and spacers for the pressings were made from CS-grade graphite, a coarse, soft, and relatively weak material. During this reporting period dies, punches, and spacers were made from ATJ-grade graphite, which is fine-grained, hard surfaced, and stronger than the CS grade. The specimen shape also was changed to a square (5.08-cm side with a thickness of 0.51 cm) that is approximately the size of the modular fuel plates for the ZPPR.

Three pressings, each with five specimens in a stack, were made at a pressure of 125 kg/cm^2 and at a maximum temperature of 1625 to 1630°C . Each pressing was above 1600°C for 15 min; for each, hard-surface paper liners were used. The first five specimens released cleanly from the mold and were in relatively good condition. Unlike the completely black appearance of specimens pressed in CS-grade graphite, these were dark brownish-red except at the edges. Some of the corners were chipped. A flowing argon blanket was used during the second pressing to reduce weight loss in the top specimen in the stack* and to extend the life of the die, punches, and susceptor. The argon flow was maintained at a rapid rate after power shutoff until the die assembly was below red heat; then the flow was reduced to $1 \text{ ft}^3/\text{hr}$. The specimens from this pressing released cleanly and had the brownish-red color of the previous run, but corner chipping had increased; the second specimen from the top had fractured into several pieces. Thermal shock was considered the best explanation for the fracture of the specimen. Therefore, again under a flowing argon blanket, the third pressing was slowly cooled by gradually reducing the power. This procedure resulted in more severe fracture. The second and third specimens from the top of the stack broke into several pieces; the second also stuck to the spacer, indicating some surface reaction. This result suggests that the temperature was too high for pressing UO_2 in ATJ graphite.

8. ZPR Fuel and Nonfissile Materials--Procurement

Last Reported: ANL-7419, pp. 21-25 (Jan 1968).

a. Process Materials

(i) Plutonium; 11.5% ^{240}Pu Ingots. Approximately 3933 kg of plutonium metal ingots of approximately uniform composition are required to manufacture the basic U-28.3% Pu-2.5% Mo ZPR fuel elements. This quantity of plutonium must be drawn from several sources that produce quite different isotopic compositions. Most of these products have ^{239}Pu : ^{240}Pu : ^{241}Pu : ^{242}Pu ratios that, although not constant, vary in an ordered manner. Therefore, it is possible to achieve a considerable normalization of the isotopic composition by blending to a constant ^{240}Pu content. Further

*The weight loss was probably due to oxidation of the top specimens, resulting in the formation of volatile oxides.

normalization is achieved by adjusting the composition of the fuel elements to a constant $^{239}\text{Pu} + ^{241}\text{Pu}$ content. Review of the compositions available from the various sources indicated that by blending to 11.5% ^{240}Pu it would be possible to achieve compositions within the following specification limits:

Isotope	Weight Percent
^{238}Pu	<0.2
^{239}Pu	85.70 to 87.60
^{240}Pu	11.2 to 11.8
^{241}Pu	1.0 to 2.5
^{242}Pu	0.25 to 0.50

Permission was granted to have the ZPR plutonium blended to 11.5% ^{240}Pu and cast as ingots in the AEC Hanford Plant. An order was placed with Isochem Inc. to begin this work in Jan 1967. By March 1968, Isochem Inc. and its successor contractor, the Atlantic Richfield Hanford Corp., had completed orders for the ingoting and analysis of 2600 kg plutonium. Modification No. 3 to the order was placed on March 8, 1968 for ingoting an additional 600 kg plutonium to complete a cumulative total of 3200 kg of plutonium ingots by June 30, 1968. Blending Lot No. 21 covering plutonium to complete this amount was approved on April 24, 1968. On April 30, 1968, 2841 kg plutonium had been ingoted and about 67 kg were in process. Shipments of a total of 2176 kg plutonium have been made to fuel fabricators.

Experience has shown that a three-month lead time is required from start of plutonium processing to shipment to the fabricator. A month is required for composition verification by the fabricator. In order to save time, melt samples were prepared at Hanford for simultaneous analysis by ARHCO and NUMEC. The sample preparation, sample and ingot identification, and packaging for shipment were witnessed and certified by an observer appointed from Battelle Pacific Northwest Laboratory.

The quantity of plutonium produced during each month that the order has been in effect and cumulatively are shown by the second and third columns of Table I.B.4. The average of isotopic analyses and 2σ variation of the analyses is reported in columns 5 through 9; the americium content and range are shown in the last two columns.

(ii) Plutonium; 27.5% ^{240}Pu . It has been necessary to reschedule the fabrication of the 27.5% ^{240}Pu elements from FY 1969 to early FY 1970 in order not to interrupt the fabrication schedule of the 11.5% ^{240}Pu fuel elements. The AEC Richland Operations Office has been requested to delay processing the 27.5% ^{240}Pu to the last quarter of FY 1969 so that the ^{241}Am , a decay product of the 6% of ^{241}Pu in this material, will be as low as possible at the time of fabrication.

TABLE I.B.4. Summary of ARHCO Ingot Production and Analyses

Month Ingoted	kg Pu per month	kg Pu Cumulative	No. of Analyses (n)	^{238}Pu (w/o)		^{239}Pu (w/o)		^{240}Pu (w/o)		^{241}Pu (w/o)		^{242}Pu (w/o)		^{241}Am (ppm)	
				\bar{x}	$\pm 2\sigma$	\bar{x}	$\pm 2\sigma$	\bar{x}	$\pm 2\sigma$	\bar{x}	$\pm 2\sigma$	\bar{x}	$\pm 2\sigma$	\bar{x}	Range
Feb 1967	176.6	176.7	53	0.038	0.024	86.746	0.445	11.504	0.194	1.565	0.368	0.137	0.038	598	1007
Mar	281.8	458.4	91	0.032	0.017	86.796	0.349	11.609	0.292	1.492	0.370	0.130	0.021	474	1076
Apr	344.7	803.1	112	0.039	0.032	86.710	0.374	11.536	0.302	1.566	0.202	0.149	0.040	338	604
May	275.0	1078.0	91	0.040	0.027	86.542	0.520	11.519	0.362	1.704	0.285	0.183	0.040	314	785
June	259.3	1337.3	85	0.049	0.027	86.660	0.507	11.490	0.347	1.687	0.264	0.177	0.32	466	849
July															
Aug															
Sept	24.4	1361.7	10	0.056	0.030	86.711	0.070	11.487	0.176	1.683	0.111	0.177	0.022	911	1126
Oct	71.0	1432.7	24	0.054	0.025	86.813	0.304	11.456	0.236	1.513	0.103	0.160	0.004	1106	1775
Nov	54.6	1487.3	18	0.074	0.014	85.883	0.406	11.569	0.388	2.303	0.228	0.211	0.012	740	323
Dec	574.2	2061.5	188	0.061	0.029	86.317	0.784	11.490	0.233	1.916	0.404	0.211	0.064	580	416
Jan 1968	161.1	2222.6	49	0.049	0.025	86.752	0.374	11.473	0.288	1.566	0.078	0.149	0.016	423	290
Feb	253.1	2475.7	81	0.056	0.027	86.562	0.548	11.498	0.351	1.706	0.290	0.175	0.031	488	202
Mar	169.0	2644.7	Analysis data not yet complete												
Apr	270.0	2841.0 ^a													

^aThis amount corrected to current data supplied by ARHCO.

(iii) Stainless Steel. Additional stainless steel wire was acquired to be formed into jacket end plugs. Although the mill analyses showed this wire to have been made from TP-304L ingot, the carbon analyses of the wire were slightly above the TP-304L carbon range. In order to expedite production of the end plugs, the wire was accepted as a deviation to ANL Specification PF-1600.

Identical tubing specifications, except for dimensions, were prepared for the oxide-element jacket sleeves and the calandria tubes. In order that the jackets will be uniform for each oxide-fuel-element contract and for the calandria, ANL is ordering this tubing and will supply it to the fuel-fabrication contractors. Bids are due for the tubing on April 30.

(iv) Fuel-element Production. The Dow Chemical Co. completed the manufacture of 4171 fuel elements containing 758.1 kg plutonium in March 1968. Dow consolidated and remelted the solid scrap from their machining operations and this material was cast as plate stock measuring 2.00 x 0.200 x ~10 in. long. Ninety-four castings weighing 108.5 kg and containing 29.9 kg of plutonium were supplied to the Laboratory with their analyses. These castings will be fabricated at ANL into 4-in. instrument traverse fuel elements.

Dow developed a "fast-recycle" chemical process for recovery of their machining chips and crucible skulls, involving calcining, nitric acid dissolving, oxalate precipitation, hydrofluorination, and reduction. The plutonium recovered in this process contained $1\frac{1}{2}$ to 10% uranium and about 1900 ppm americium, but otherwise, the recovered plutonium met ANL Specification PF-1607 for zero-power reactor-fuel plutonium. Dow quite successfully used this material to fabricate fuel elements meeting all of the requirements of Specification PF-1600. NUMEC was extremely cautious about accepting recycle fuel from the Dow operation and submitted

a proposal for the use of this material which was prohibitive in cost. Since the "fast-recycle" plutonium could not be economically used at NUMEC, the scrap-recovery operation was stopped at Dow.

Dow is dismantling the ZPPR fuel-element-production line. Contaminated equipment is being cleaned and will be reused at Dow where possible. The fuel-element welding machines and vacuum-glovebox balances, as well as leak-detection and inspection equipment, are being shipped to ANL. This equipment will be used in the manufacture of special fuel elements and will be maintained in operating condition should fuel-element production be required to back up the commercial source.

(v) Fuel Fabrication at NUMEC. NUMEC signed a contract with ANL on July 28, 1967, for the fabrication of 5379 U-28.3% Pu-2.5% Mo fuel elements containing 1000 kg plutonium. The contract has two follow-on options. Option No. 1 is for 3091 fuel elements containing 575 kg of plutonium and Option 2 is for 3366 fuel elements containing 625 kg of plutonium. The monthly and cumulative deliveries of fuel elements from NUMEC are shown in Table I.B.5.

TABLE I.B.5. Fuel Elements Produced by NUMEC and Dow

Month 1968	Element Size (in.)						Monthly Total	Cumulative Total	Pu (kg)	
	1	4	5	6	7	8			Monthly	Cumulative
NUMEC Jan		140	213	151	121	218	843	843	161.8	161.8
NUMEC Feb		110	220	106	110	98	644	1483	117.4	279.2
NUMEC March		139	194	218	253	121	925	2412	175.8	455.0
NUMEC April ^a		54	148	239	389	210	1040	3422	213.0	668.0
NUMEC Totals		443	775	714	873	647	3422	-	668.0	-
Dow Totals	118	739	1085	779	720	727	4168		760	
Total Fabricated	118	1182	1860	1493	1593	1374		7590		1428

^aApril production does not include Shipment 51, which is included in Table I.B.6. NUMEC elements are as-received at ANL during each month. Plutonium is as shown by the IBM fuel-element data cards supplied with each shipment and is subject to ANL verification.

The shipments of fuel elements from March 27 through April 29 contained 202 kg of plutonium--double the rate of 100 kg plutonium per month scheduled in the contract. The numbers of fuel elements produced at NUMEC in April and cumulative production to April 30 are summarized in Table I.B.6.

NUMEC's work on chip and skull recovery was reviewed at a meeting on April 23. Twelve 1- to 4-kg chip remelts had been induction melted in a vacuum glovebox. Carbon crucibles were plasma-coated with ZrO₂. Vacuum and inert atmospheres were tried with and without flux additions to the melts. The best results were achieved with clean chips of recent origin which were "Oxylene" washed and magnetically and hand sorted

to remove iron and tramp impurities. The chips were tableted to reduce bulk volume and to achieve better thermal transfer. Temperatures of approximately 1600°C were required to melt the tablets. Ingot yields on the clean chips were 50 to 75% of the weight charged. Very poor results were obtained with oxidized chips (4 to 5 weeks old) and crucible skulls. Fluoride flux was tried on these but was not effective in removing the oxide and the fluorides caused difficulty in the furnace operation. The development process was scaled up to 8 kg in the production furnace, and ingot yields were near 80% of the metal charged. The analyses of the ingots showed high carbon, iron, and aluminum contents; however, there appeared to be no reason why the recovered ingot material should not be used in ternary alloy melts if small enough proportions were used so that the specified impurity limits were not exceeded.

TABLE I.B.6. NUMEC April and Cumulative Fuel Production

	April 1968	Cumulative
Ternary Alloy Melts	71	359
Inspected Core Plates	900	3890
Fuel Elements Shipped	985 ^a	3522 ^a
Plutonium Shipments (kg)	202.0 ^a	683.3 ^a
Fuel Elements on Order		5379

^aFigures from NUMEC records are subject to ANL verification. These figures include 13 fuel elements that have been rejected by ANL inspection and 64 fuel elements (2%) of production that have been selected for de jacketing, inspection and sampling, and includes Shipment 51 not included in Table I.B.5.

NUMEC had made four ternary alloy melts which incorporated 10 to 15% of recovered metal. The analysis of these melts met the specification and the core-plate castings were similar in appearance to core plates made from virgin metal. Permission was granted to fabricate the castings into fuel elements which have now been received at ANL and are being evaluated. NUMEC has submitted revised process specifications and manufacturing instructions for ANL review prior to incorporating chip-melt operations in the fuel-fabrication process.

(vi) Quality Evaluation of ZPR Fuel. The ANL inspection, sampling, and analytical program has continued. Several fuel elements were de jacketed at the request of the ANL Special Materials Division, sampled, and re jacketed as smaller fuel elements for use as control standards in the gamma-spectrometric assay program. An attempt is being made to salvage useable cores from all evaluation elements, and these cores are being used for the fabrication at ANL of instrument traverse, thermocouple, and other special fuel elements.

The charge-in compositions, NUMEC analyses, and ANL analyses are being statistically compared. The bias between charge-in compositions and analytical data was brought to NUMEC's attention in a meeting April 3. This trend has continued although the correspondence between ANL analysis of samples from de jacketed elements and NUMEC laboratory results now appears to be quite good. Results from eleven melts were examined for which both ANL and NUMEC plutonium assays and isotopic analyses were available. The following $^{239}\text{Pu} + ^{241}\text{Pu}$ percentages were derived from these data:

	By ANL Analysis	By NUMEC Analysis
11 melt avg, $^{239}\text{Pu} + ^{241}\text{Pu}$	24.88 w/o	24.87 w/o
Standard deviation σ	± 0.17 w/o	± 0.17 w/o

The oxygen and nitrogen analyses of samples taken at ANL from fuel elements are considerably above those shown by NUMEC on melt samples. Similar results have been noted for the Dow elements, and it may be that these levels increase with exposure of the core plates to air before jacketing.

The ANL receiving inspection is current to within one week of receipt of the fuel elements. Rejections are presently less than 0.5%, and have been from nicks, scratches, weld craters, and nonperpendicularity of the fuel-element ends to the jacket sleeves.

Analyses and mass spectrometry are four to six weeks behind as a result of the analytical load backlog from the ZPR and LMFBR, which compete for analytical time. In order to reduce this load, and hopefully reduce the analysis lag, the rate of sampling is being reduced by 50 percent in May 1968.

b. Oxide-fuel Elements. Specification ZPR-1614 was prepared to cover the manufacture of ZPR depleted and enriched UO_2 and $(\text{U,Pu})\text{O}_2$ -loaded fuel rods. The specification was written so that combined or separate subcontracts can be let for jacket tubing, jacket-component fabrication, depleted UO_2 rods ($^{235}\text{U}_{0.16}$ $^{235}\text{U}_{0.84}\text{O}_2$), and ($^{235}\text{U}_{0.46}$ $^{238}\text{U}_{0.56}\text{O}_2$) rods, as well as three compositions of $(\text{U,Pu})\text{O}_2$ rods. Copies of the specification were submitted for AEC comment. A plan and schedule for procurement of oxide fuel rods was submitted, which will require a high-priority effort to the ZPR oxide-fuel procurement.

Dow Chemical Co. completed process studies on the fabrication of UO_2 pellets and produced two pilot-scale runs of 500 and 200 pellets each. The pilot-production pellets were sinterable ADU-derived UO_2 blended with

1.0 w/o stearic acid and 1.0 w/o Carbowax 4000. The mix was prepressed at 10,000 psi and granulated through a 28 mesh screen. The resulting granules were weight charged into the pelleting die and pressed at 30,000 psi. The length-to-diameter ratio of the green pellets was 1.5:1. The first production run was sintered at 1650°C for 4 hr; 90% of the pellets fell within the density range of 93 to 95% of theoretical density. The second lot of pellets was sintered at 1635°C; the density was 92 to 93% of theoretical density.

Work on (U,Pu)O₂ started in March. Some difficulty was experienced in establishing the correct heating cycle in the gloveboxed sintering furnace. The heating rate, time at temperature, and hydrogen atmosphere were found to require very close control for the (U_{0.85},Pu_{0.15})O₂ and (U_{0.71},Pu_{0.29})O₂ compositions. When sintering parameters were established, density, shrinkage, dimensional control, and pellet-surface characteristics were found to be within acceptable limits for small lots, and a run of approximately 800 pellets has been started to establish statistics for (U,Pu)O₂.

c. Nonfissile Elements

(i) Iron Oxide (D. E. Mitchell)

Delivery of acceptable iron oxide plates from Lake Products is underway. The delivery schedule is 1500 plates per week, which will assure delivery of the 9900 plates required early in July.

(ii) Sodium and Sodium Carbonate (D. E. Mitchell)

DK Aerospace Co. is cutting, forming, and welding cans for the sodium and sodium carbonate elements. They were forced to move the sodium-filling operation outside of Chicago because of fire restrictions imposed by the city. The relocated installation has been set up. In full production, DK will have seven welding stations operating on a two-shift basis. They have installed a manual sodium-filling station as a backup to automated equipment in case of downtime on the automated unit. To assure meeting the requirement for 21,000 sodium elements by July in addition to the sodium carbonate elements, a limited fabrication of sodium elements is scheduled in Central Shops at ANL.

Preproduction sodium carbonate wafers have been received from NUMEC. Their schedule provides for ample sodium carbonate elements to meet current requirements.

(iii) Boron Carbide Elements (F. B. Huke)

Boron carbide elements are being procured for ZPR-3 programs supporting FFTF. Development of specifications has been a

cooperative effort among ANL-ID, ANL-ILL, and PNL. Core material is being designed to fit the jacket sleeves of sodium carbonate elements, and jacketing will be done for the ANL shops. Specifications are in the final approval stage, and it is expected that procurement will be initiated during the first week of May.

9. ZPPR Construction (H. Lawroski)

Last Reported: ANL-7438, pp. 22-24 (March 1968).

Installation of the reactor assembly was approximately one week ahead of schedule at the end of April. It is estimated that the installation is 65% complete for the mechanical items and 70% complete for the instrumentation and controls.

Installation of the matrix tubes on the stationary half of the reactor was completed. Measurements indicated that the matrix face has a slight general tilt (0.010 in. maximum at the top) toward the movable half of the reactor. The maximum variation from a vertical plane through the center of the face is approximately ± 0.005 in., which is acceptable.

The alignment plates with the strongback beams were installed on the movable half of the reactor. The plates were adjusted to compensate for the configuration of the stationary half-matrix so that the two halves would match closely. Installation of the matrix tubes was completed, and disassembly of the alignment equipment was started.

Reactor frames for both halves of the reactor were assembled, and the rod-drive mounting plates were installed. Final alignment of the rod-drive mounting plates will be done after both reactor matrices are completed. One frame with rod-drive mounting plate was placed on the stationary table. Control and experimental wireways were installed, and work was started on installing wiring for the control and safety rod systems on the reactor.

The loading platform was cleaned and brought into the reactor cell.

Inspection and leak testing of the initial 288 ZPPR fuel-storage containers received by ANL yielded 18 rejects due to leakage and unacceptable deposits inside the containers. These rejected containers were returned to the vendor for rework. An additional shipment of containers was made by the vendor.

The construction contractor was unable to obtain a satisfactory leak test of the escape-tunnel connection to the reactor cell. ANL requested occupancy of the tunnel on April 10 in order to begin work on the seal doors which may become the critical item for completion of the facility. The installation contractor began work on the doors.

10. FFTF Critical Experiment Program (D. Meneghetti)

Last Reported: ANL-7438, pp. 24-26 (March 1968).

a. Analysis of Safety-rod Worths of ZPR-3 Assembly 51. Calculations of both the presently used spiked and initial-loading unspiked safety-rod worths have been made for a 10-in. removal position. Analyses used the six-group ANL cross-section Set #29601 in the Argonne two-dimensional discrete-ordinate transport code, 2D-SNARG in the S_2 approximation. Results are given in Table I.B.7. The sensitivity of the calculated values to the composition surrounding the rod was estimated for the spiked-rod case. Results of calculations using neighboring-drawer composition values are also given in Table I.B.7 for comparison with the values obtained by use of overall-core-average composition surrounding the rod.

TABLE I.B.7. Calculated % $\Delta k/k$ for 10-in. Removal of a Safety Rod for ZPR-3 Assembly 51

Safety Rod Type	% $\Delta k/k$, Calc Composition Surrounding the Rod		% $\Delta k/k$, ^a Exp
	Overall Core Average	Neighboring Drawers	
Unspiked	-0.13	-	-0.115
Spiked	-0.26	-0.23	-0.238

^aEstimated.

b. Additional Studies of a Simple Method for Approximating Solutions of Axially Split Cylindrical Cores. A method was described (see ANL-7427 and -7438) by which a finite cylindrical reactor in coordinates r and z may be viewed as a finite slab reactor in coordinates x , y , and z , making use of a chord-buckling $B_y^2(x)$, which forces $\phi(x)$ to be of the same form as the known cylindrical solution $\phi(r)$. In this description x is identified with r . It is possible to define another chord-buckling $B_y^2(x)$ such that $\phi(x)$ is of the same form as $\phi(u)$, where $\phi(u)$ gives the distribution of neutron flux along a chord rather than along a radius. If the distance from the origin of the cylindrical coordinates to the chord is y_0 ,

$$u = \sqrt{r^2 - y_0^2}$$

in analogy with the previous derivation it may be shown that

$$B_y^2 = \frac{-1}{\phi} \left[\frac{y_0^2}{r^2} \frac{d^2 \phi}{dr^2} + \frac{r^2 - y_0^2}{r^3} \frac{d\phi}{dr} \right],$$

This reduces to the previously obtained expression when the chord coincides with the diameter, i.e., when $y_0 = 0$.

For a bare cylinder of critical radius r_c , the radial distribution is $\phi = \phi_0 J_0\left(\frac{2.405 r}{r_c}\right)$, and the radial buckling is $B_r^2 = \left(\frac{2.405}{r_c}\right)^2$. The value of B_y^2 is then given analytically as a function of u by

$$B_y^2 = B_r^2 \left[\frac{y_0^2}{u^2 + y_0^2} + \left(\frac{u^2 - y_0^2}{u^2 + y_0^2} \right) \frac{J_1\left(\frac{2.405\sqrt{u^2 + y_0^2}}{r_c}\right)}{\left(\frac{2.405\sqrt{u^2 + y_0^2}}{r_c}\right) J_0\left(\frac{2.405\sqrt{u^2 + y_0^2}}{r_c}\right)} \right],$$

where the range of u is $0 \leq u \leq \sqrt{r_c^2 - y_0^2}$.

In Tables I.B.8 and I.B.9 the values of B_y^2/B_r^2 are listed for $y_0/r_c = 1/3$ and $y_0/r_c = 2/3$, respectively, as a function of $u/\sqrt{r_c^2 - y_0^2}$.

TABLE I.B.8. Ratio of Effective Chord Buckling to Radial Buckling of a Cylinder for $y_0/r_c = 1/3$

$u/\sqrt{r_c^2 - y_0^2}$	B_y^2/B_r^2	$u/\sqrt{r_c^2 - y_0^2}$	B_y^2/B_r^2
0.025	0.4552	0.525	0.5741
0.075	0.4568	0.575	0.6093
0.125	0.4600	0.625	0.6547
0.175	0.4650	0.675	0.7150
0.225	0.4718	0.725	0.7982
0.275	0.4808	0.775	0.9192
0.325	0.4922	0.825	1.1104
0.375	0.5065	0.875	1.4554
0.425	0.5243	0.925	2.2617
0.475	0.5464	0.975	6.2936

TABLE I.B.9. Ratio of Effective Chord Buckling to Radial Buckling of a Cylinder for $y_0/r_c = 2/3$

$u/\sqrt{r_c^2 - y_0^2}$	B_y^2/B_r^2	$u/\sqrt{r_c^2 - y_0^2}$	B_y^2/B_r^2
0.025	0.2159	0.525	0.2446
0.075	0.2163	0.575	0.2530
0.125	0.2171	0.625	0.2637
0.175	0.2183	0.675	0.2779
0.225	0.2200	0.725	0.2973
0.275	0.2222	0.775	0.3254
0.325	0.2249	0.825	0.3696
0.375	0.2284	0.875	0.4490
0.425	0.2327	0.925	0.6338
0.475	0.2380	0.975	1.5557

C. Component Development--LMFBR

1. Sodium Technology Development--Engineering Development

a. Sodium Quality Measurement (S. B. Skladzien)

Last Reported: ANL-7438, pp. 26-27 (March 1968).

(i) Laboratory Techniques. A new sampling valve for the GC-5 gas chromatograph was received, installed, and tested under pressure and vacuum; it appears to operate satisfactorily. Blanket-gas samples taken from the sodium analytical loop before and after hydroxide was added are being analyzed for changes in hydrogen concentration.

(ii) In-line Techniques. The response of the in-line oxygen-monitoring devices to changes in oxygen concentration in the sodium of the analytical loop is being determined. The concentration is changed by raising or lowering the cold-trap temperature; after each temperature change, the in-line devices are observed frequently to determine when the system has returned to equilibrium. Then readings from the in-line instruments are correlated with plugging-meter data and with the oxygen-concentration values obtained from distillation samples. From these data, calibration curves and cell constants are being determined for the two United Nuclear Corp. oxygen cells.

b. Sodium Quality Control (S. B. Skladzien)

Last Reported: ANL-7427, pp. 27-28 (Feb 1968).

The direct-water-reaction technique for cold-trap-residue analysis has been tested with sodium metal, sodium oxide, and mixtures of both. The reaction of water with both of these species has proceeded as postulated, so the water-reaction method has been judged suitable for analytical work.

The most recent effort has been to react water quantitatively with sodium hydride. Because the commercially available sodium hydride used was found to contain ~30 w/o nonhydride material, it was purified by distillation in a sealed evacuated capsule, which resulted in the separation of a liquid hydrocarbon. Although analyses of a series of the purified samples indicated only ~95 w/o sodium hydride, the alkalinity of the resulting solution agreed with the amount of hydrogen given off, indicating that the reaction between sodium hydride and water was quantitative.

Because of the algebraic limitations that exist in direct-water-reaction analysis (see Progress Report for January 1968, ANL-7419, p. 29), the presence or absence of sodium hydroxide in a residue is important.

Therefore, the oxide-hydroxide equilibrium with sodium present was investigated to find whether hydroxide can be expected in a cold-trap residue. Thermodynamic examination showed that sodium hydroxide in the presence of molten sodium at cold-trap temperatures is not stable and therefore should not be found in a cold-trap residue.

2. Reactor Mechanisms Development--Materials Evaluation

a. Fission Gas Pressure Transducer (J. R. Folkrod)

Last Reported: ANL-7438, pp. 29-30 (March 1968).

(i) Null-balance System. The transducer that has been tested since February 9 still is operating at 900°F, and the pressure has been increased from 80 to 350 psig. Thus, the pressure transducer now is being tested to its design temperature and pressure.

Operation at 350 psig is good. The variation in readout caused by the change of the electrical contact resistance is 5 psig; the process pressure (fission gas) is within this range. Thus accuracy is ± 2.5 psig over the pressure range, or $\pm 0.715\%$ at full scale (350 psig).

The electronic system, upgraded for improved stabilization so that the system will not hunt or cycle frequently when the process-gas pressure is stable, has been put in its final form.

b. Signal Lead Connectors for Sodium Service (A. P. Grunwald)

Last Reported: ANL-7438, p. 30 (March 1968).

Fabrication and assembly of the FFTF fuel-channel coupling and connector device are essentially finished. Heat treatment of springs, installation of the connector, and seal-welding of pipes required about three weeks longer than had been scheduled. The adapter flange and mounting assembly for tests in the sodium furnace have been delivered. The tests are about to begin.

c. Failed Fuel Locating Method Development (F. Verber)

Last Reported: ANL-7438, pp. 30-31 (March 1968).

In a preliminary safety review of the design for the failed fuel monitoring loop, structural features and anchor points of the loop were established tentatively.

Water will simulate sodium in a flow mockup of the gas-disengagement chamber, 1-in. vertical pipe section and 2-in. horizontal pipe section, of the loop that is being fabricated with transparent acrylic

tubing. The effect of liquid flow rate on the liquid level in the 1-in. vertical pipe will be determined. The test data will be used to check the calculated additional height of liquid in the 1-in. pipe caused by the pressure drops through the 12 radial holes, the annulus between the 1-in. pipe and the 4-in. pipe, and the 2-in. horizontal pipe. That will establish the elevation of the sodium vapor trap and the gas loop.

Electric heaters for the loop are on hand. The surge tank is being fabricated, and temperature instrumentation and power-control equipment are being procured.

Preliminary tests of the gas loop (with 0.001-in.-thick Mylar window) were made to determine its ability to detect krypton-85 in the helium cover gas above the sodium. The results indicate that a krypton-85 concentration of $0.0001 \mu\text{Ci/ml}$ of helium will be readily detectable at 50 cpm above a background of 50 cpm. At that concentration, the total activity in 15 liters of cover gas (assuming complete mixing) would be $1.5 \mu\text{Ci}$. If the krypton that enters the cover gas does not disperse immediately throughout the system but is entrained as a slug in the helium, the concentration of krypton-85 in the counting chamber will, at times, be somewhat higher than $0.0001 \mu\text{Ci/ml}$, which would give greater sensitivity for detecting activity in the system.

3. Fuel Handling, Vessels and Internals

a. Core Component Test Loop (CCTL) (R. A. Jaross)

Last Reported: ANL-7399, pp. 45-47 (Nov 1967).

The initial FFTF prototype fuel assembly for testing in the CCTL has been received from Pacific Northwest Laboratory. This subassembly will be flowtested in the CCTL for about 5 months at or near full design flow of 400 gpm at an isothermal average sodium temperature of 1060°F so as to determine the hydraulic, mechanical, and metallurgical integrity of the FFTF subassembly design. Examination of the assembly's mechanical integrity, fuel-spacer wear, and corrosion or erosion effects will be reported by PNL.

The CCTL modifications to accommodate the FFTF prototype subassembly are being completed (the design of the loop was described previously*). The test arrangement now provides a 4° tilt on the fuel assembly and removable sodium-pressure instrumentation. Sodium inlet and outlet transition pieces have been designed and fabricated. Before the

*Armstrong, R. H., Smith, F. A., Bohne, L., Folkrod, J. R., Janicek, J., Kimont, E., Kush, R., Skladzien, S., and Venkateswarlu, A., FARET Fuel Assembly Flow Test Loop, American Nuclear Society, 11th Annual Meeting, Gatlinburg, Tennessee (June 21-24, 1965).

high-flow high-temperature tests begin, the loop will be filled with sodium and operated at low temperatures. During initial operation of the loop, the performance of the mechanical pump will be checked and the calculated displacements of the piping will be confirmed by measurements with strain gauges.

Because of the timely arrival of the first FFTF prototype fuel subassembly from PNL and the desire for early testing of it, two other planned modifications to the loop have been deferred. One of these would have incorporated a 4-in. gate valve in the loop so that flow could be controlled more closely than by means of the variable-speed feature of the pump. The other modification would have provided mechanical access to the test vessel for dynamic material-corrosion tests and surveillance.

D. Systems and Plant--LMFBR

1. 1000-MWe Plant

a. Contract Management and Technical Review (L. W. Fromm)

Last Reported: ANL-7438, pp. 31-32 (March 1968).

(i) The Babcock & Wilcox Co. Subcontract. Preparation of conceptual system design descriptions continues. ANL comments on the first draft of the reactor shielding system design description were forwarded to Babcock & Wilcox, who now are preparing a second draft.

In the performance analysis of the reference fuel pin, fuel temperatures in the hot channel, nominal hot channel, and average channel at the beginning and end of life were calculated.

Task-III parametric studies and safety studies of molten-fuel release, sodium fires, core meltdown, and pump coastdown accidents continue.

Descriptions of the turbine-generator, the steam-piping system, and the condensate feedwater systems have been prepared. Work has begun on the cost estimate of the overall plant.

(ii) Westinghouse Corp. Subcontract. The Task-I report is about 90% complete. One topical report has been received.

Under Task II, the reactor auxiliary-systems components have been sized. Conceptual system design descriptions are being written for the fuel-handling, reactor auxiliary, reactor- and intermediate-cooling, and steam-generation systems. Cost estimates have been completed for the primary and intermediate cover-gas purification and supply systems.

Reactor correlation equations have been applied successfully in the core-optimization computer code for preparation of the Task-III parametric studies.

Task-IV effort has been initiated.

(iii) General Electric Co. Subcontract. The draft of the Task-I report is nearly finished.

Task-III core parametric studies are being made for both oxide and carbide fuels. For oxide fuels, the effects of power flattening have been studied by analysis of 2-, 3-, 4-, and 6-zone core configurations. The interrelation between allowable cladding strain, fuel swelling, and fuel density as a function of cladding temperature and burnup is being studied.

Conceptual designs of the reference core and control-rod mechanisms are nearly finished.

Features of the inert-gas-handling system have been established and conceptual system design descriptions have been prepared. The number-of-loops study has been completed. The scope of Task-III work for the architect-engineer has been defined and a schedule was agreed on regarding information flow to the architect-engineer and completion of the work.

(iv) Combustion Engineering, Inc. Subcontract. The fourth quarterly technical report has been received. ANL has reviewed and commented on three of the five conceptual system design descriptions.

Numerous calculations have been made of projected accidents such as loss of flow, control-rod ejection, control-rod withdrawal, gas bubbles, and subassembly drop during refueling.

The method of cooling spent fuel during transfer from the reactor core to storage was modified to provide greater reliability and safety.

In the Task-III parametric studies, the effect of derating fuel burnup on economics and doubling time was determined.

(v) Atomics International Subcontract. The study is approximately 40% complete. The Task-I report is being printed.

Funding limitations for the remainder of FY 1968 have caused some work to be rescheduled. Conceptual system design descriptions in Tasks II and III that have not been prepared will be deferred until next fiscal year, as will drawings and plant-arrangement layouts. Task-III work that is continuing includes the fuel-handling review, parametric study, nuclear uncertainty analysis, steam-generator study, and review of plant arrangement. Several plant arrangements will be studied to determine the effects of alternate arrangements and design features on plant capital cost.

E. EBR-II1. Research and Developmenta. Reactor Experimental Support--Reactor Analysis and Testing
(R. R. Smith)

Last Reported: ANL-7438, pp. 33-42 (March 1968).

(i) Nuclear Analysis

(a) The Application of Correlation Techniques for Establishing the Reactor Transfer Function. At present, methods used for evaluating the reactor transfer function are limited at low frequencies. For the method based on the periodic insertion of reactivity with a rotating oscillator rod, the limitation is imposed by a tendency for the rod to rub and seize at the lower frequencies. For the method based on the steep ramp withdrawal of reactivity (rod-drop technique), the low-frequency limitation is a consequence of the limited capability of the existing equipment for processing and storing digital information. Furthermore, both methods are seriously affected by changes of the bulk sodium temperature during measurements at the lower frequencies. As a consequence of these limitations, low-frequency feedback information is essentially unavailable.

To extend the range of feedback measurements into the low-frequency region, an effort is being made to perfect a technique based on the trapezoidal insertion of reactivity. In this method, reactivity is periodically perturbed through the programmed motion of a conventional control rod over a carefully fixed and specified distance in the linear portion of the control-rod calibration curve. The output power wave, as sensed by an ion chamber, is then cross-correlated with the excitation function to give the reactor transfer function. One major advantage inherent in this method is the ability to reduce the reactivity perturbation to values as low as ± 1.0 lh with acceptable reproducibility. By keeping the reactivity perturbations small, temperature variations in the bulk sodium are greatly reduced at the lower frequencies, for which feedback effects, between the primary heat exchanger discharge and pump inlets, become important.

On the other hand, the use of small reactivity perturbations, i.e., of the order of ± 1.5 lh, tends to decrease the ratio of flux signal to background noise, thereby reducing the accuracy with which the transfer function may be established. An illustration of noise magnitude relative to the neutron flux signal is given in Fig. I.E.1, which depicts a CalComp plot of the power output and the control-rod position. In this particular instance, the control rod was programmed for a total travel of approximately 0.1 in., which corresponds to a reactivity change of approximately 3.0 lh.

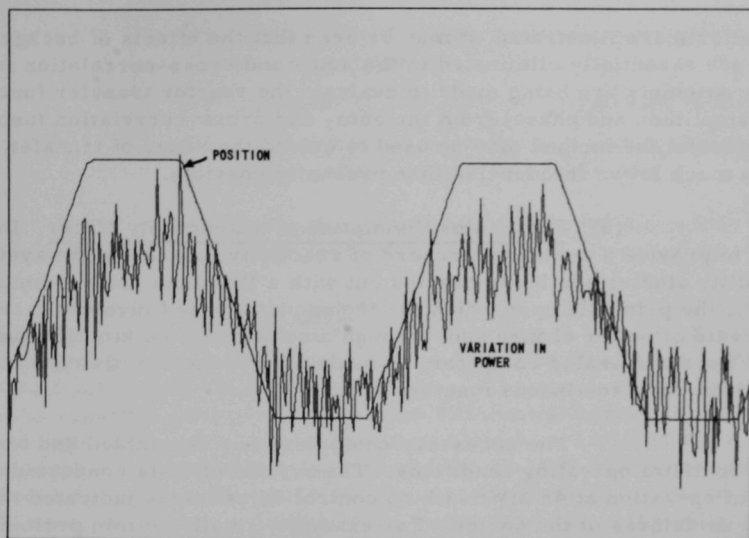


Fig. I.E.1. Alternating Power Component and Control-rod Position

In an attempt to reduce the effects of background noise, data, typified by that given in Fig. I.E.1, were processed by establishing the autocorrelation function of control-rod position (actually, reactivity) and the cross-correlation function of control-rod position with the alternating component of the neutron flux. From Fig. I.E.2, in which the results of

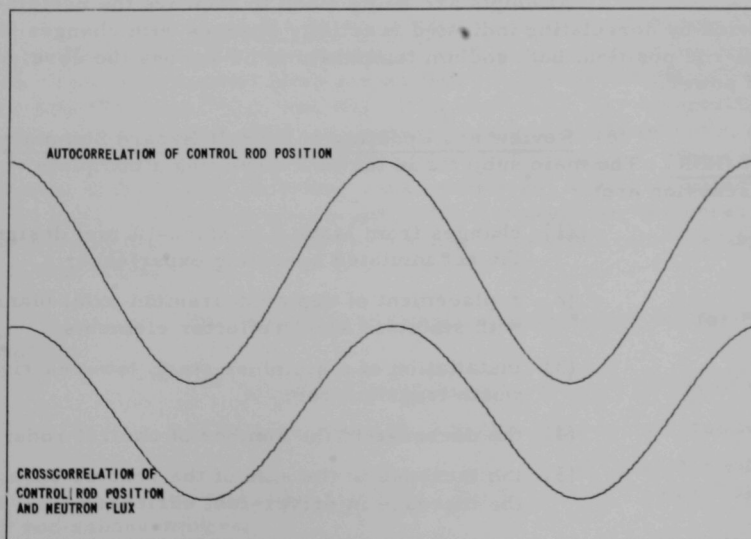


Fig. I.E.2. Correlation Functions of Power and Control-rod Position

such efforts are illustrated, it may be seen that the effects of background noise are essentially eliminated in the auto- and cross-correlation functions. Attempts are being made to evaluate the reactor transfer function (both amplitude and phase) from the auto- and cross-correlation functions. If successful the method may be used to extend the range of transfer function to much lower frequencies than presently possible.

(b) The Analog Simulation of a Reactivity Meter. In an effort to provide a continuous record of reactivity balance in the system, feasibility studies are being carried out with a Beckman analog computer. Briefly, the principle upon which the technique is based involves a sensing of the rate of power change and, through a solution of the kinetic equations with a Beckman analog computer, an evaluation of the reactivity vested in the system as a continuous function of time.

The necessary equipment was assembled and tested under realistic operating conditions. The results of tests conducted under 10 hr of operation at 45 MWt with no control adjustments indicated the potential usefulness of the device. For example, small, 17-min periodic variations in the power output were sensed and recorded by the instrument as periodic reactivity variations with a ± 1.5 -Ih amplitude.

The results of calibration tests conducted with rod drops and control-rod movements indicated a potential sensitivity of the instrument under actual operating conditions of approximately 0.1 Ih.

Attempts are being made to improve the usefulness of the device by correlating indicated reactivity changes with changes in control-rod position, bulk sodium temperature ΔT across the core, and integrated power.

(c) Review and Updating of EBR-II Hazard Summary Report (HSR). The main subjects in the HSR requiring a complete review and discussion are:

- (1) changes from Mark-I to Mark-IA fuel design and the accumulated operating experience;
- (2) replacement of depleted-uranium axial blankets with stainless steel reflector elements;
- (3) installation of a stainless steel, low-reactivity-worth transient rod;
- (4) the decrease in the number of control rods;
- (5) the increase in the size of the reactor core and the increase in driver-fuel enrichment;

- (6) installation of encapsulated experimental irradiation experiments;
- (7) operation of EBR-II as an irradiation facility;
- (8) replacement of a portion of the radial-blanket region with stainless steel elements.

All these areas have safety considerations that are covered in varying degrees in the EBR-II Hazard Summary Report.

(d) Feedback Analysis of Run 27. The feedback was calculated for two rod-drop experiments at reduced flow in Run 27. Figures I.E.3 and I.E.4 give the results for operating conditions of 30 MWt with 75% flow and of 22.5 MWt with 54% flow, respectively. The similarity of the two sets of data is expected since the temperature differential across the core is the same in both cases. The prompt feedback (first 2 or 3 sec) is about 15% higher in these experiments than it was in the 45-MWt full-flow experiments performed during Run 26. At 10 sec, it is about 5% higher. The increase may be real, but also may be partly the result of error in the calibration of the stainless steel rod. Since the Run-27 calibration drops were relatively "noisy," the calibration from Run 26 was used.

The extension of rod-drop experiments to times beyond 10 sec produced additional information on delayed feedback processes. Attempts are continuing to include the effects of delayed feedback into a unified mathematical feedback model.

(e) Mark-IIA Safety Analysis. Nineteen different hypothetical EBR-II Mark-IIA core loadings (see Table I.E.1) are currently being studied. The experimental fuels are assumed to consist of 20% $^{239}\text{PuO}_2$ or ^{239}PuC , 30% $^{235}\text{UO}_2$ or ^{235}UC , and 50% $^{238}\text{UO}_2$ or ^{238}UC . The composition of a Mark-IIA driver subassembly, an oxide experimental subassembly, and a carbide experimental subassembly are given in Table I.E.2. The critical enrichment of the Mark-IIA driver subassembly has been calculated for each of the 19 cores. The enrichments and critical masses for the cores are tabulated in Table I.E.3 to characterize a range of possible core loadings of EBR-II with Mark-II fuel.

The following assumptions were employed for these calculations:

- (1) spherical geometry with a shape factor of 0.94;
- (2) three types of core are under consideration:

(a) homogeneous mixtures of Mark-IIA subassemblies, experimental subassemblies, and 14 Mark-IA control and safety rod subassemblies;

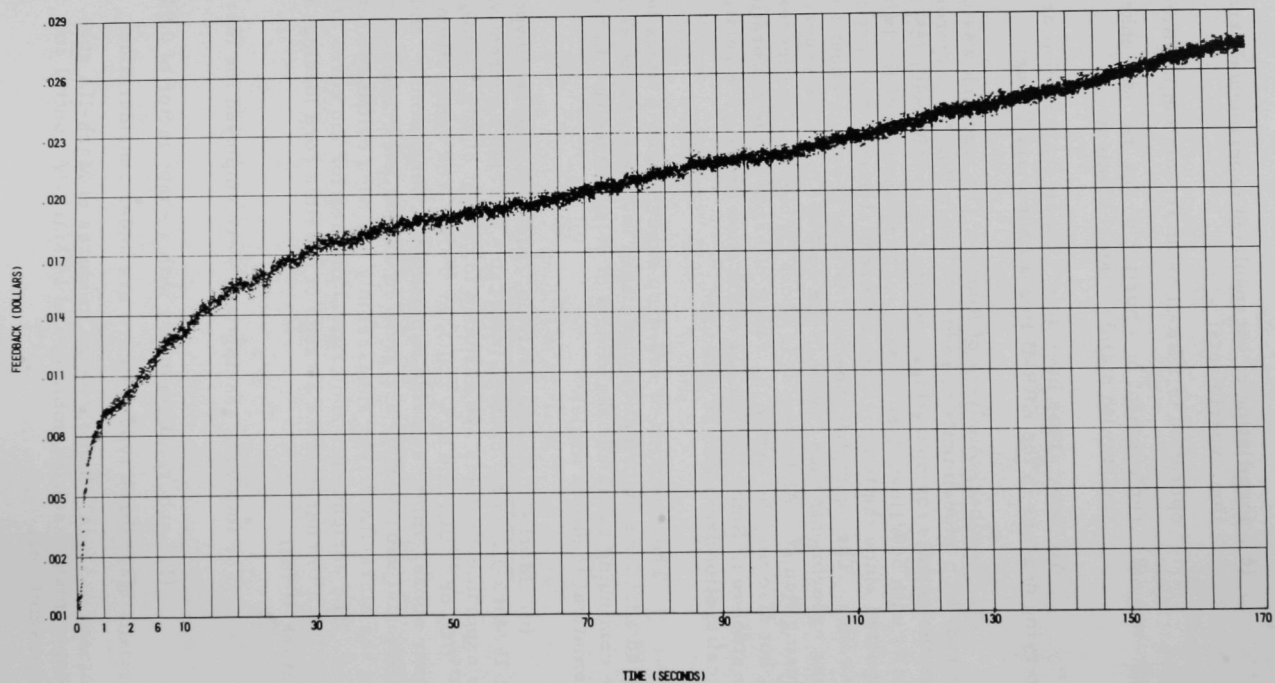


Fig. I.E.3. Feedback at 30 MW and 75% Flow for Run 27

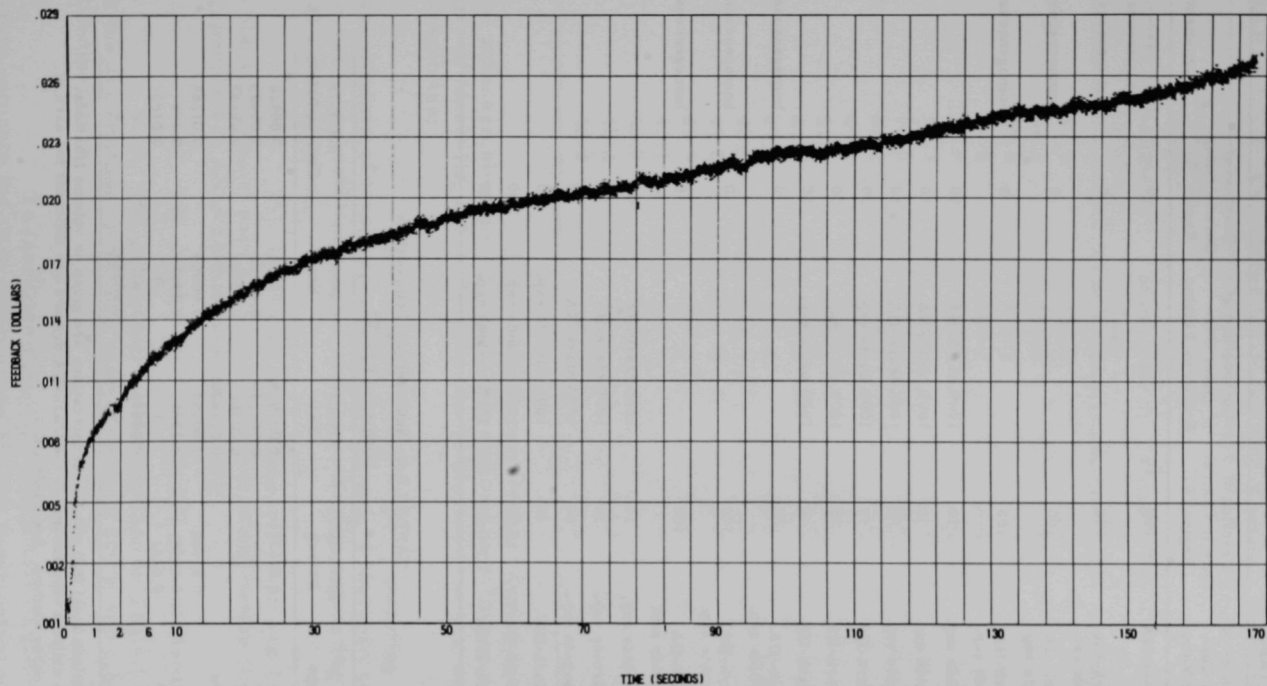


Fig. I.E.4. Feedback at 22.5 MW and 54% Flow for Run 27

TABLE I.E.1. Core Loadings for EBR-II Mark-IIA Safety Analysis

Core No.	Composition of Central Core Region by Volume	Fraction of Core in Central Region (%)	Composition of Outer Core Region by Volume	Fraction of Core in Outer Region (%)	Comments
1	100% Mark-IIA	100	-	0	Base Case-- homogeneous core
2	90% Mark-IIA 10% oxide exp.	100	-	0	homogeneous core
3	70% Mark-IIA 30% oxide exp.	100	-	0	homogeneous core
4	50% Mark-IIA 50% oxide exp.	100	-	0	homogeneous core
5	100% oxide exp.	10	100% Mark-IIA	90	
6	100% oxide exp.	30	100% Mark-IIA	70	
7	100% oxide exp.	50	100% Mark-IIA	50	
8	100% Mark-IIA	90	100% oxide exp.	10	
9	100% Mark-IIA	70	100% oxide exp.	30	
10	100% Mark-IIA	50	100% oxide exp.	50	
11	90% Mark-IIA 10% carbide exp.	100	-	0	homogeneous core
12	70% Mark-IIA 30% carbide exp.	100	-	0	homogeneous core
13	50% Mark-IIA 50% carbide exp.	100	-	0	homogeneous core
14	100% carbide exp.	10	100% Mark-IIA	90	
15	100% carbide exp.	30	100% Mark-IIA	70	
16	100% carbide exp.	50	100% Mark-IIA	50	
17	100% Mark-IIA	90	100% carbide exp.	10	
18	100% Mark-IIA	70	100% carbide exp.	30	
19	100% Mark-IIA	50	100% carbide exp.	50	

TABLE I.E.2. Subassembly Composition
(atoms/cc x 10⁻²⁴)

Isotope	Mark-IIA Driver	Oxide Exp	Carbide Exp	Mark-IA Control/Safety
U	0.01132	0.005925	0.00688	0.00928
²³⁵ U	b	0.002240	0.00260	0.00485
²³⁸ U	b	0.003685	0.00428	0.00443
²³⁹ Pu	0	0.001470	0.001705	0
Na	0.01148	0.00958	0.00958	0.01268
SS ^a	0.2255	0.2255	0.2255	0.208
Fs ^a	0.0222	0	0	0.0185
O	0	0.01479	0	0
C	0	0	0.008585	0

^aStainless steel (SS) and Fs concentrations are given as volume fractions.^bThe critical enrichments of the Mark-IIA drivers are different for each of the cores studied. See Table I.E.3.

TABLE I.E.3. Calculated Mark-IIA Enrichments: Critical Masses

Core No.	Mark-IIA Driver Enrichment (a/o)	Mass ^{235}U (kg)	Mass ^{239}Pu (kg)	Mass $^{235}\text{U} + ^{239}\text{Pu}$ (to nearest kg)
1	47.9	205.7	0	206
2	48.3	196.6	5.8	202
3	49.6	176.9	17.3	194
4	52.5	159.3	28.8	188
5	48.8	198.6	5.8	204
6	51.3	181.2	17.3	198
7	56.6	165.5	28.8	194
8	48.2	196.6	5.8	202
9	49.1	175.8	17.3	193
10	51.1	157.2	28.8	186
11	47.8	193.7	6.7	200
12	47.4	168.3	20.1	188
13	46.5	142.9	33.5	176
14	47.2	193.0	6.7	200
15	45.5	163.8	20.1	184
16	43.1	138.0	33.5	172
17	48.0	194.2	6.7	201
18	48.2	170.1	20.1	190
19	48.4	145.9	33.5	179

(b) a central core region consisting of experimental subassemblies and an outer core region consisting of a homogeneous mixture of Mark-IIA subassemblies and 14 Mark-IA control and safety rod subassemblies;

(c) a central core region consisting of a homogeneous mixture of Mark-IIA subassemblies and 14 Mark-IA control and safety rod subassemblies, and an outer core region consisting of experimental subassemblies;

(3) inner and outer blankets, 10.15 and 43.9 cm thick (both blankets consist primarily of depleted uranium having the compositions specified in ANL-5719 Addendum, p. 18);

(4) cross-section Set No. 238 generated with the MC² code;

(5) subassembly compositions in Table I.E.2 calculated under the assumptions of sodium temperature of 800°F and other elements at room temperature.

To facilitate these and future calculations, a code was written to compute the core composition for any combination of experimental subassemblies with Mark-IIA driver and Mark-IA control-rod subassemblies.

(f) Generalized Power and Flow Coefficients. A formula for the power-reactivity decrement (PRD) has been modified in the following manner:

Let $P(Q, R)$ be the generalized PRD. Then $P(Q/R, 1)$ is the full-flow PRD which corresponds to the same ΔT as for the generalized conditions (Q, R) .

Calling $\theta = Q/R$, then $[\partial P(\theta, 1)]/\partial \theta$ is the slope of the full-flow PRD curve, P versus Q as usually plotted. The generalized power coefficient can be expressed in terms of reactor properties and the slope of the full-flow PRD curve as

$$\frac{\partial P(Q, R)}{\partial Q} = \left(\frac{1}{R} - \frac{1}{R^{0.4}} \right) C_1 \alpha + \left(\frac{1}{R} - 1 \right) [C_2 + (C_3/k)] \alpha + \frac{1}{R} \frac{\partial P(\theta, 1)}{\partial \theta},$$

and the generalized flow coefficient is

$$\frac{\partial P(Q, R)}{\partial R} = \left(\frac{0.4}{R^{1.4}} - \frac{1}{R^2} \right) Q C_1 \alpha - \frac{[C_2 + (C_3/k)] Q \alpha}{R^2} - \frac{Q}{R^2} \frac{\partial P(\theta, 1)}{\partial \theta},$$

where

Q = power;

R = fraction of full flow;

α = effective linear thermal-expansion coefficient of fuel;

k = effective thermal conductivity of fuel;

C_1, C_2, C_3 = positive constants derived from thermal expansion effects.

The conditions under which the power coefficient changes from negative to positive and under which the flow coefficient changes from positive to negative are obtained by setting the above expressions equal to zero. Specifically, a positive power coefficient requires that the slope of the full-flow PRD curve be

$$\frac{\partial P(\theta, 1)}{\partial \theta} > -C_1 \alpha (1 - R^{0.6}) - \alpha [C_2 + (C_3/k)] (1 - R) \quad (1)$$

$$\approx -0.053(1 - R^{0.6}) - 0.311(1 - R). \quad (1a)$$

Similarly, a negative flow coefficient requires that the slope of the full-flow PRD curve be:

$$\frac{\partial P(\theta, 1)}{\partial \theta} > -C_1 \alpha (1 - 0.4R^{0.6}) - \alpha [C_2 + (C_3/k)] \quad (2)$$

$$\approx -0.053(1 - 0.4R^{0.6}) - 0.311. \quad (2a)$$

Equations (1a) and (2a) were obtained from Eqs. (1) and (2) by using calculated values of the constants C_1 , C_2 , and C_3 from multi-group diffusion analyses, with k assumed to be $0.06 \text{ cal/sec-cm-}^\circ\text{C}$. The remaining parameter, α , was then determined by the best fit to the reduced-flow PRD data at the beginnings of Runs 25, 26, and 27. Since the reduced-flow data yielded approximately the same value for α , namely, $23 \times 10^{-6} \text{ }^\circ\text{C}^{-1}$, at the start of each run, it is strongly implied that Eqs. (1a) and (2a) would be approximately correct at the start of any run for which the initial burnup averages about 0.5%. This being the case, the presence of positive power coefficients or negative flow coefficients under any condition of power and flow may be anticipated from Eqs. (1a) and (2a) at the start of a run as soon as the full-flow PRD curve has been determined.

Observations of the PRD at reduced flow throughout the course of Run 26 have indicated that either α or the C 's increased markedly throughout this run. This tendency will be watched in future runs.

(g) Temperature of a Fuel Pin Whose Thermal Conductivity Is a Linear Function of Temperature. The differential equation for temperature t as a function of radius r is

$$k(t)dt = q''dr = 0.5q'''r dr,$$

where

k = thermal conductivity;

q'' = heat flux, radially outward;

q''' = heat source per unit volume.

Recent measurements have shown that k may be expressed as

$$k = a + bt,$$

where a and b are parameters for a given fuel sample, which vary with irradiation-induced swelling, and t is the temperature in degrees centigrade (zero temperature at pin surface, r_p).

Substitution of this form into the differential equation and integration yields the following expression for temperature within the pin:

$$t(r) = \left(-a + \sqrt{a^2 + \frac{1}{2} q''' (r_p^2 - r^2) b} \right) / b.$$

The axial temperature expansion of the pin is proportional to the area average of $t(r)$ over the cross section. A computer program was prepared which evaluates the average temperature for various values of a and b . Table I.E.4 gives the average pin temperature at a reactor power of 45 MWt for various values of the constants a and b obtained from data at various degrees of swelling.

TABLE I.E.4. Average Pin Temperature

Swelling (% $\Delta V/V$)	a	b ($\times 10^5$)	t_{avg} ($^{\circ}\text{C}$)
Unirradiated	0.0688	5.65	488
2.66	0.0631	4.22	491
5.49	0.0547	3.88	495
6.78	0.0574	3.93	494
12.3	0.0471	3.13	500

Under these assumptions, the average pin temperature rises only slightly during the course of burnup as shown in the table. Even this slight rise in fuel temperature, however, may bring substantial quantities of fuel into the gamma-phase region, for which expansion effects are large. This may, in part, account for the large contribution of the fuel-reactivity effect to the power coefficient that was observed in reduced-flow measurements toward the end of Run 26.

(h) Physics Measurements for Runs 27D through 27G.

Table I.E.5 gives the results of pertinent physics measurements for Runs 27D through 27G.

TABLE I.E.5. Results of Physics Measurements for Runs 27D-27G

	27D	27E	27F	27G
PRD ^a at 45 MWt, 1h	44.1	47.2	40.4	41.9
Estimated Δk , 1h	-	+7	-34	+73
Measured Δk , 1h	-	+24	-60	+90
Control-rod bank, in.	11.0	11.25	12.25	11.0
Total control-rod worth, 1h	1390	1414	1383	-
Safety-rod worth, % $\Delta k/k$	-	-	1.05	-

^aCorrected to 11-in. control-rod banked condition.

Control-rod calibrations were established during Runs 25E, 25F, and 27D. The safety rods were measured by subcritical counting methods during Run 27F.

Analyses of the PRD's measured during the various startups of Run 27 do not indicate any significant trend in the value of the differential power coefficient at specific power levels as a function of power accumulation. Because of the significant loading changes that have been made throughout Run 27, however, small trends in the measured PRD could easily be masked by larger effects associated with the loading changes.

(i) Release of Fission Product Species to the EBR-II Cover Gas. In addition to the two small fission-product gas releases experienced during March (see ANL-7438, pp. 36-42), several additional releases occurred during April. Two of the April releases occurred while the reactor was operating at 45 MWt and five occurred at zero power following changes in primary coolant flow or subassembly movement. The April fission-product releases are summarized in Table I.E.6 along with all other previous releases observed in the operation of EBR-II. Previous releases were reported in the Progress Report for December 1967, ANL-7403, pp. 35-42, and in the Progress Report for March 1968, ANL-7438, pp. 36-42.

(a) Description of Events

(1) April 6 Releases. The reactor was taken to power on March 30 and until 0356 on April 6 operated at 45 MWt with no evidence indicative of a fission product release. At 0355, April 6, the beginning of a relatively sharp increase in the signal from the Fission Gas Monitor (FGM) was noted. Prior to the increase, the FGM signal was steady at 16.5 cps. At 0356 hours, the FGM alarmed at a counting rate of 22.5 cps and a rapid shutdown of the reactor was begun.

The results of a radiometric analysis conducted on a primary-tank cover-gas sample taken at 0400 hours, and counted at 0405, confirmed the release. At 1015 hours, the primary pumps were turned off. Shortly thereafter, an increase was noted in the FGM signal. A cover gas sample taken at 1025 hours confirmed the additional release.

Highlights of the FGM response preceding, during, and following the two releases are shown in Fig. I.E.5. An inspection of the xenon activities in the cover gas and the FGM record indicate that the release occurred at approximately 0345 hours. At no time preceding, during, or following the indicated release was there any indication of an increase in the signal from the Fuel Element Rupture Detection (FERD) system. Similarly, no changes in the reactivity balance of the system or abnormal temperature indications were observed.

TABLE I.E.6. Summary of Fission Product Release Incidents in EBR-II

Date	Time of Release	Reactor Power Level (MW)	MWdt of Operation since Previous Release	FGM ^a Response	FERD ^b Response	Approximate Increase in Xenon Activity ($\Delta\mu\text{Ci/cc} \times 10^3$)		Indication of Sodium Bond Loss	Comments
						¹³³ Xe	¹³⁵ Xe		
1. 5/24/67	1200	45	12,771 ^c	Very Large	Negative	1800 ^d	1800		Primary coolant sodium sample taken on 5/8 and analyzed on 5/18 showed possible bond loss. Results of second sample taken on 5/19 confirmed loss, but were not obtained until 30 min before 5/24 gas release.
2. 6/11/67	0215	30	115	Large	Negative	Negligible	8	None	Intentional confirmatory release.
3. 6/19/67	2115	10	0.7	Large	Negative	250	13	None	Intentional release to obtain further information.
4. 6/28/67	1430	7.5	150 ^e	Large	Negative	270	3.5	None	Intentional release to confirm suspect subassembly--X011 removed with no subsequent indication of fission product release.
5. 11/23/67	1000	20	1,888 ^f	Large	Negative	Negligible	3.0	None	
6. 11/24/67	1415	25	2	Large	Negative	Negligible	1.5	None	
7. 11/24/67	2100	25	7	Small	Negative	Negligible	Negligible	None	
8. 11/24/67	2330	0	<0.5	Small	Negative	Negligible	Negligible	None	Confirmatory release--reactor operated at 30 MW for 8 hr following first release--third release followed primary pump shutdown--lack of ¹³³ Xe inventory indicated fresh driver-type fuel.
9. 12/6/67	1800	45	430	Negative	Negative	270	160		Analyses of xenon buildup indicates probable loss of sodium bond.
10. 3/5/68	1500	45	636	Small	Negative	75	25	None	
11. 3/11/68	0900	30	52	Indefinite	Negative	25	1.5	None	Occurred during reduced flow testing following series of several scrams.
12. 3/12/68	0800	0	10	Negative	Negative	25	<0.5	None	
13. 3/12/68	1500	0	0	Negative	Negative	7	<0.5	None	Apparently associated with changes in primary coolant flow.
14. 4/6/68	0400	45	286	Large	Negative	75	95	None	Approximately 300 MWdt logged between 3/30 and 4/6.
15. 4/6/68	1015	0	0	Small	Negative	130	135	None	Followed immediately after stopping of primary coolant pumps.
16. 4/11/68	2015	0	90	Barely Perceptible	Negative	130	22	None	Followed reduction in flow after scram from 45 MW.
17. 4/16/68	0230	0	68	Negative	Negative	125	17	None	Followed reduction in flow after scram from 45 MW.
18. 4/19/68	1215	45	49	Small	Negative	90	25		
19. 4/19/68	1330	0	0	Large	Negative	150	140		Radiochemical analysis of primary coolant sodium and analysis of xenon decay, inconclusive--cannot be verified that bond loss did not occur.
20. 4/20/68	2000	0	0	Negative	Negative	35	50		Occurred after rapid shutdown following 1215 release and subsequent stopping of pumps.
									Followed lifting of X028 during fuel-handling operations.

^aFission Gas Monitor.^bFuel Element Rupture Detection (monitor of delayed neutrons).^cThis number represents total MWdt of EBR-II operation prior to first fission product release.^dEstimated value of increase.^eOf this total, the reactor was operated only 0.5 MWdt prior to release with suspect Subassembly X011 reinserted in core.^fAt the time of release, only 1.5 MWdt had been logged since insertion of new subassemblies.

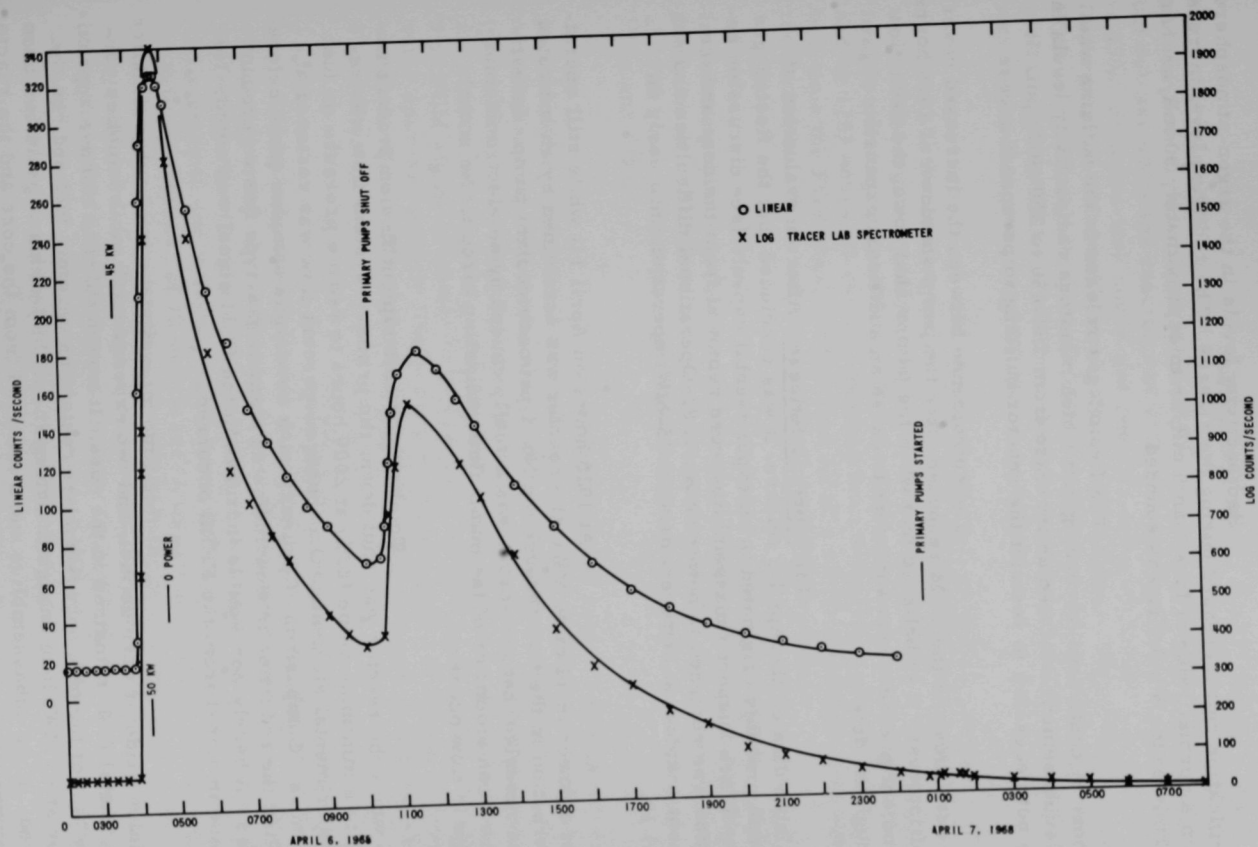


Fig. LE.5. FGM Data, April 6-7, 1968

Radioactivity levels in the argon-atmosphere purification cell increased during the release. The radiation level increased from a normal value of less than 5 mR/hr to approximately 90 mR/hr. An alarm, set for 5 mR/hr, was sounded.

The fission-gas release to the building was minor. A continuous-recording unit which monitors radioactivity levels in the subbasement indicated an increase from 150-250 to 350-400 cpm. It was not necessary to restrict the reactor building to personnel access.

The coincidence between the increased cover-gas activities and the FGM response after the pump shutdown at 1015 hours is of interest. It is believed that when the pumps shut down, the reduction in coolant pressure was sufficient to cause an additional expansion of gas through the defect.

(2) April 11 Release. After an evaluation of available data on the April 6 release, it was concluded that the fission-gas release probably originated in an experimental capsule (see discussion below). Three suspect subassemblies were removed from the core and the reactor was returned to power on April 8. Operational difficulties and subsequent shutdowns, however, delayed 45-MWt operation until early on April 10.

At 1916 hours on April 11, while still operating at a power level of 45 MWt, the reactor was scrammed by an indicated perturbation in the flow through the No. 1 primary coolant pump. Investigation revealed that the scram was actually caused by an electronic-tube failure in an amplifier of the pump-flow-indicating circuit. No actual change in flow occurred.

To check for an incipient fission product release while the reactor was shut down, the primary-system flow was reduced to a minimum value (23%) at 2009 hours to reduce pressure on fuel and experimental elements. One-hundred-percent flow was restored at 2022 hours. Comparison of primary-tank cover-gas samples taken before and after the reduction in flow indicated a small gas-type fission product release. A barely perceptible increase in the FGM signal was noted. No increase in signal from the FERD occurred.

At this time nine experimental subassemblies containing oxide or carbide fuel, and two experimental subassemblies containing metal fuel, remained in the core. It was decided to remove approximately half of the nine subassemblies containing ceramic fuel and run the reactor at 45 MWt long enough to determine if the leaking capsule had been removed. Four subassemblies were removed from the core and the reactor was returned to power on April 14.

(3) April 16 Release. At 0142 hours on April 16, after approximately 36 hr of 45 MWt operation, a spurious low-primary-sodium-flow signal caused a reactor scram. To check for a fission product release while the reactor was shut down, the primary flow was reduced to 23%. Primary-tank cover-gas samples collected before and after the flow reduction indicated a small fission-gas release. No increase in the FGM or FERD signals occurred. The remaining ceramic-fueled experimental subassemblies were then removed from the core and the reactor was returned to power at 0300 hours on April 18.

(4) Releases of April 19 and 20. At 1215 hours on April 19, the reactor operator noticed a slight but persistent increase in the FGM signal. Analyses of cover-gas samples taken immediately confirmed a fission-gas release. At 1224 hours, a rapid shutdown was initiated, and by 1253 hours all control rods had been withdrawn from the core. At this time the FGM signal had leveled off at a value 28% higher than before the increase. There was no increase in the FERD signal.

In an attempt to induce an additional gas release, the primary pumps were stopped at 1322 hours to reduce pressure on the core. Results of radiometric analyses of a cover-gas sample taken at 1335 hours indicated no perceptible increase in the concentrations of ^{133}Xe and ^{135}Xe .

At 1343 hours, the primary pumps were restarted and brought to full flow. Shortly thereafter, the FGM signal began to increase. At 1403 hours, the FGM alarmed and at 1405 hours the reactor building was evacuated. An air monitor located in the subbasement of the reactor building indicated a tenfold increase in activity during this time. The FGM signal continued to increase and at 1507 hours reached a peak value approximately 30 times the normal background level due to tramp uranium. The FGM response during these two releases is illustrated in Fig. I.E.6.

Fuel-handling operations were conducted on April 20 to remove the final two experimental metallic-fuel subassemblies remaining in the core. Three driver-fuel subassemblies were also removed for reactivity adjustment. The results of analyses conducted for xenon activity prior to and following the removal of each subassembly revealed that an activity increase of 10 to 20% occurred in conjunction with the transfer of XO28, an experimental subassembly containing elements of U-Pu-Zr alloy and also four elements of Mark-IA U-Fs alloy. These results suggest that lifting XO28 through approximately 10 ft of sodium decreased the pressure differential sufficiently to cause an additional release. No increase in activity was detected while handling the other subassemblies.

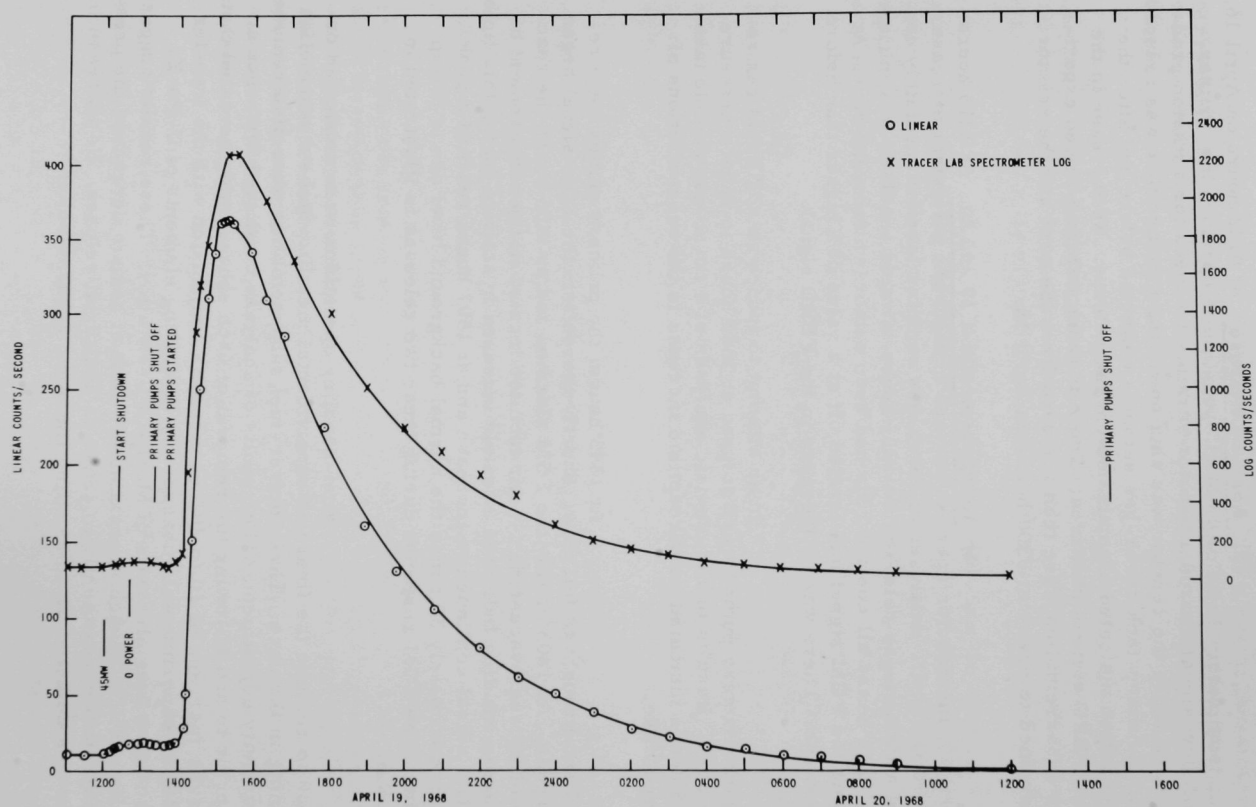


Fig. I.E.6. FGM Data, April 19-20, 1968

Pertinent ^{133}Xe and ^{135}Xe activities for the period April 6 through April 20 are plotted in Fig. I.E.7. Power operation for this period with the significant events discussed in this section are shown in Fig. I.E.8.

(b) Discussion. A detailed evaluation of all the data resulting from the March and April fission product releases leads to the following observations:

The evidence supports the postulate that the source of fission products is an experimental capsule rather than a driver element, and the fission product releases have been predominantly gaseous. These conclusions are supported by three main areas of investigation:

- (1) the magnitude of the radioactivity increases relative to the tramp uranium background;
- (2) fractionation of the fission product species (see ANL-7438, pp. 39-41);
- (3) primary-sodium analysis.

On the basis of signal-to-background ratios for the primary-tank cover-gas activities and the FGM response, it was concluded after the April 6 incidents that the release was very likely the result of a failure in an experimental capsule. For the total gas release, the signal-to-background ratio measured for ^{133}Xe was found to be approximately 25; for ^{135}Xe , approximately 44; and for the FGM, approximately 53. (For the cases of ^{135}Xe and the FGM response, corrections were made for radioactive decay between the initial peak and the secondary release.) The results of bare-pin tests conducted previously in EBR-II have indicated that the upper limit for the signal-to-background ratio for a single driver-fuel element is approximately ten. (Although the bare-pin tests were conducted on fresh fuel at an EBR-II power level of 10 MWt and 70% flow, it has been assumed that the signal-to-background ratio would not be significantly greater for a release from a high-burnup driver element under 45 MWt operation.) The conclusion based on these ratios is that the failure involved either a single experimental capsule or four to eight driver-fuel elements. Since a single experimental capsule failure was more probable than multiple failures in driver elements, subsequent action was directed toward removal of experimental fuel-bearing subassemblies. The magnitude of the April 19 release (FGM signal-to-background ratio > 30) also supports this contention.

Evidence of substantial fractionation, first observed during the March fission product releases, was also observed in April. On the basis of half-life considerations, the results of radiometric analyses conducted on cover-gas samples following the April 11 release indicate that a

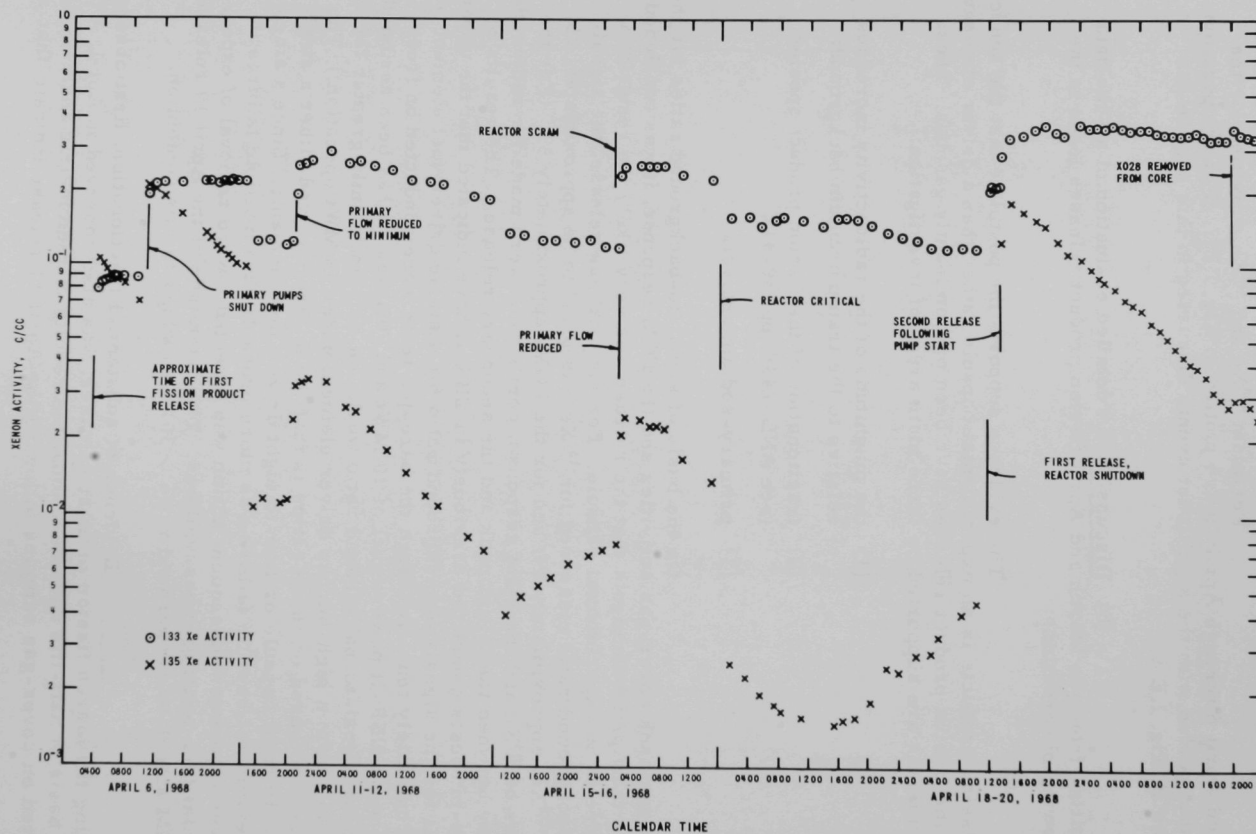


Fig. I.E.7. Xenon Activity in EBR-II Cover Gas during April 1968

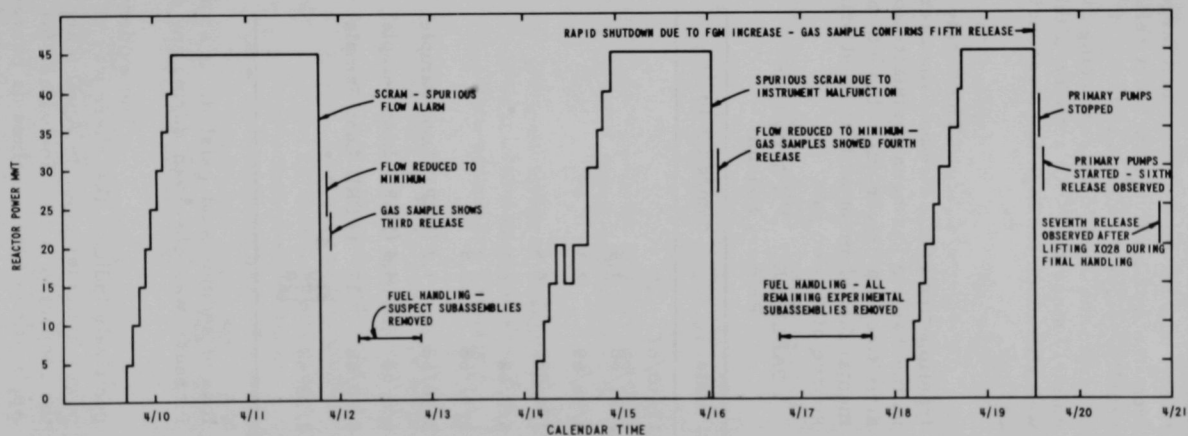
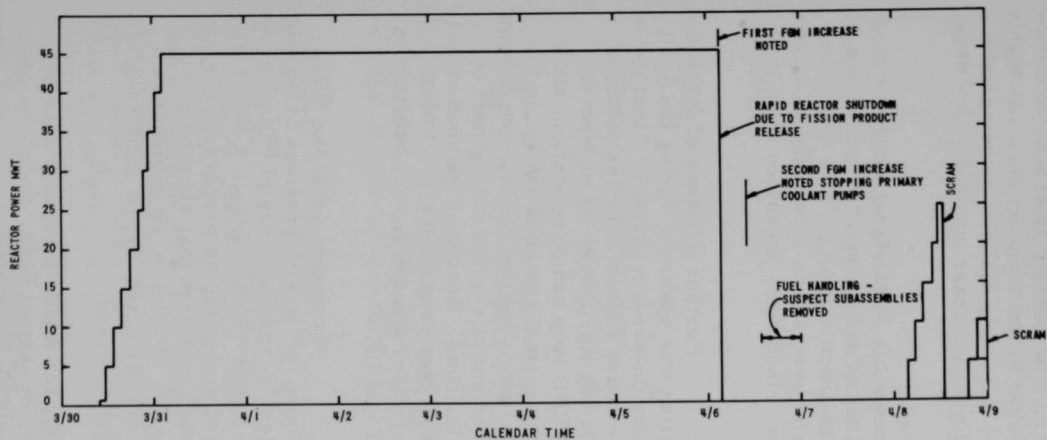


Fig. I.E.8. EBR-II Operation for April 1968

very large fractionation of ^{133}Xe and ^{135}Xe occurred. For example, the ^{133}Xe and ^{135}Xe activities increased by factors of approximately 2 and 3, respectively, but, because of the much larger holdover in the cover gas of ^{133}Xe from the April 6 fission product release, the relative increases indicate a heavily weighted release in favor of ^{133}Xe . The possibility of a hideout bubble from the April 6 release being dislodged by the pump shutdown is highly unlikely since the ^{135}Xe activity, although seriously discriminated against, was still much too high to be reconciled with a release occurring five days earlier.

The barely perceptible FGM signal and the strong fractionation of ^{135}Xe reduce the credibility of driver-fuel failure. Since no mechanism has been postulated for the fractionation of ^{133}Xe and ^{135}Xe activities in a driver-fuel element, a defective capsule containing an experimental fuel element with a failed primary cladding is presumed to be the source of fission gas.

TABLE I.E.7. ^{131}I Activity in Primary Sodium

Date	dpm/g ($\times 10^{-3}$)
12/10/67	20
2/27/68	1.4
2/28/68	2.3
3/4/68	4.4
3/5/68	6.1
3/11/68	7.5
3/30/68	1.2 (FERD Loop Sample)
4/6/68	4.4 (FERD Loop Sample)
4/20/68	17 (FERD Loop Sample)
4/23/68	$\begin{cases} 20 \\ 20 \end{cases}$

Further evidence of fractionation was observed during the April 16 fission-product release. Most of the primary sodium samples collected during April were taken from the FERD loop sampling station, since the normal sampling station in the primary-sodium-purification system was out of service during part of this time. Results of radiochemical analyses conducted for ^{131}I in the primary sodium are summarized in Table I.E.7.

A comparison of the ^{131}I activity levels with previous background levels, and the decay of ^{135}Xe (between releases) with a simple 9.2-hr half-life indicating no precursor, lead to the conclusion that except for the April 19 release, no evidence of a

loss of sodium bond existed. It should also be noted that no FERD signal increase was observed during any of the releases.

The evidence for the April 19 release does not positively indicate that there was no loss of sodium bond. From the time-power histories prior to April 6 and April 20, when the samples were taken, the respective saturation values for ^{131}I were established as 42 and 39%. Application of these values as corrections to the radiochemically measured results leads to the conclusion that a small iodine release is indicated.

On the other hand, the signal-to-background ratio for this case, approximately 3, is still substantially less than the signal-to-background ratios established from the FGM (≈ 30) and from the ^{135}Xe analyses (≈ 40). This evidence supports the theory that the release of April 19, assuming the most pessimistic conditions, consisted primarily of fission-product gases.

(c) Conclusions

(1) Significant increases in the ^{133}Xe and ^{135}Xe activities in samples from the primary-tank cover gas were observed on April 6, 11, 16, 19, and 20. Subsequent behavior of the fission product species is characteristic of gas-type releases.

(2) The releases of April 6, 11, and 19 were verified by the FGM.

(3) No evidence of a bond-type failure was indicated by the FERD.

(4) Analysis of ^{131}I activity in the primary sodium and analyses of ^{135}Xe decay between releases indicate no significant loss of sodium bond during the April releases.

(5) Fractionation of the fission product species in favor of the long-lived isotopes has been consistently indicative of a release from an experimental capsule.

(6) Four of the releases followed changes in primary-coolant flow, and there appears to be a correlation between the static pressure in the core and the driving force necessary to cause a bubble release from a defective capsule.

(7) The slight increases in ^{133}Xe and ^{135}Xe activities during the transfer of experimental Subassembly XO28 following the April 20 fission-gas release must be considered significant and, if real, implies that XO28 contains the suspect capsule. Contrary to this evidence, however, is the fact that the magnitude of the gas releases, as much as 30 times normal background, indicates a ceramic-fueled experiment. Recoil-release rates of rare-gas precursor species from U-Pu-Zr ternary alloys and U-Fs driver fuel should be approximately the same, but since no ceramic fuels were in the reactor at the time of the last release, the U-Pu-Zr alloys (such as those in XO28) must be considered.

Although XO28 is the prime suspect, the possibility of a failed driver-fuel element should not be rejected. To reconcile the failure of a driver element with the intensities and fractionation phenomena observed, however, it is necessary to postulate extensive cracking of the metallic fuel or fuel melting--effects which are logically associated with the loss of sodium bond.

b. Nuclear Analysis Methods Development (P. J. Persiani)

Last Reported: ANL-7438, pp. 43-46 (March 1968).

(i) Study of Improved Control Rods. The control-rod calculations (see Progress Report for February 1968, ANL-7427, pp. 46-48, and ANL-7438, pp. 44-45) have been continued with emphasis on determining the influence of the B_4C enrichment. Table I.E.8 gives some results.

TABLE I.E.8. Calculated Reactivities for Movement of
Ten Full Poison Control Rods in Ring 5

(The volume fraction of B_4C is 0.406 in all cases)

Case No. ^a	Location of "Poison Section"	Description of "Poison Section"	k
10	Bottom at core top	Boron in B_4C enriched to 69 a/o ^{10}B	0.9594
12	Bottom at core bottom	Boron in B_4C enriched to 69 a/o ^{10}B	0.8637
15	Bottom at core top	B_4C replaced by stainless steel	0.9913
16	Bottom at core top	Boron in B_4C enriched to 92% ^{10}B	0.9551
17	Bottom at core top	Natural boron in B_4C	0.9748
18	Bottom at core bottom	Natural boron in B_4C	0.9469

^aThe numbering of the cases as used in ANL-7427 and ANL-7438 has been retained; therefore some case numbers are missing.

The total calculated control worth of a natural boron system (cases 17 and 18 of Table I.E.8) is a Δk of 2.8%. This can be compared with a Δk of 9.6% for boron enriched to 69 a/o (cases 10 and 12). Replacing stainless steel with B_4C in the blanket causes a Δk of 1.6, 3.2 and 3.6% for boron enrichment of 20 (natural), 69, and 92%, respectively (cases 10, 15, 16, and 17). This replacement is approximated in the core by cases 12, 15, and 17, from which Δk of 4.4 and 12.8% can be derived for the cases of natural and 69% enriched boron, respectively. The increasing reactivity effect with enrichment apparently "saturates out" faster in the blanket than in the core, probably because of the harder core spectrum.

(ii) Power Distribution with Driver Subassemblies in Row 7. The influence of fuel in Row 7 on the power distribution in the outer blanket region of the EBR-II is being studied for a blanket system and a reflector system. Fuel subassemblies were positioned at a corner of Row 7, the center position of a side, the entire side, and the entire row. Each problem was run under SNARG-2D for $S_N = 4$, X-Y geometry with a twofold symmetry. The power distribution over the reactor was obtained with PYRO. Current

efforts are directed at comparing the power distributions to determine power changes in Rows 10 and 11. A code, PLOTPOWD, is being written to plot power distribution (in kW) as total events, as differences, or percent change on a rectangular display diagram.

(iii) Irradiation of Oxide-fuel Subassembly in EBR-II. A preliminary study is being conducted of some aspects of the performance of "typical" FFTF test subassemblies in EBR-II and of their effect on EBR-II performance. Two "typical" FFTF test subassemblies were considered during the study: one designated as the ANL-GE type, and the other as the PNL type. The ANL-GE type was studied first, and the results were modified for the study of the PNL type.

(a) ANL-GE Type. A description of the ANL-GE test subassembly is given in Table I.E.9. The reactivity worth of replacing an EBR-II driver with a test subassembly was obtained with X-Y SNARG calculations along with the change in power density. The reactivity worths for various uranium enrichment and subassembly positions, as well as the ratio of the power density in the test subassembly to the driver that was replaced, are given in Table I.E.10. The reactivity worth of the replacement is presented as a function of change in the loading of ^{235}U (equivalent) in Fig. I.E.9, where ^{239}Pu is assumed to have twice the reactivity of ^{235}U .

TABLE I.E.9. Description of ANL, GE, and PNL Types of Oxide Test Subassembly

	ANL	GE	PNL
Composition	UO_2 -20 w/o PuO_2	UO_2 -25 w/o PuO_2	UO_2 -25 w/o PuO_2
Pellet diameter (in.)	0.245	0.243	0.210
Clad OD (in.)	0.290	0.290	0.250
Clad thickness (in.)	0.020	0.020	0.015
Smear density (%)	~84	~85	83 ^a
Height (in.)	11.0	13.5	13.5
Linear power (kW/ft)	~17	~20	5-17
U enrichment (a/o)	93	93	0, 43, 93
Pu enrichment (a/o)	91	91	91

^aTheoretical density = 93%.

TABLE I.E.10. Percent Reactivity Change and Power-density Ratio for ANL-GE Subassembly versus Driver Fuel

Enrichment (a/o)	Percent Reactivity Change					Power-density Ratio (Oxide/Driver)
	Row 2	Row 3	Row 4	Row 5	Row 6	
93	+0.52	+0.42	+0.32	+0.24	+0.16	1.163
43	-0.07	-0.07	-0.05	-0.02	-0.003	0.708
0	-0.64	-0.53	-0.40	-0.30	-0.21	0.377

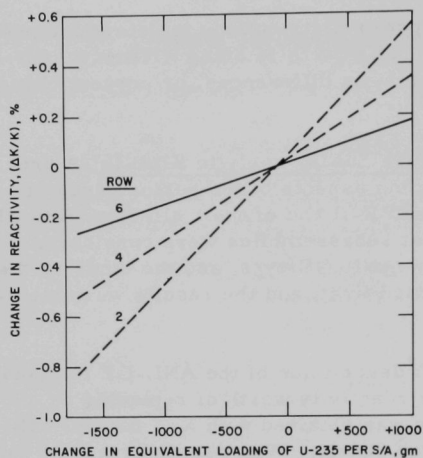


Fig. I.E.9

Reactivity Change Produced by Changing the ^{235}U
(Equivalent) Loading in a Subassembly for Various
Row Positions in EBR-II

The results for linear power generation in ANL-GE oxide, shown in Table I.E.11, were obtained by correcting for the difference in power density and the length of fuel pins between the test and driver subassemblies. The number of days to achieve 1 a/o burnup for the mixed-oxide fuel, shown in Table I.E.12, was obtained by correcting the driver-fuel value of 2735 MWd/1 a/o burnup in the center position.

TABLE I.E.11. Linear Power Generation (in kW/ft, avg) of
ANL-GE Oxide Test Subassemblies

Enrichment (a/o)	Row 2	Row 3	Row 4	Row 5	Row 6
93	22.8	21.1	18.5	14.8	11.4
43	13.8	12.8	11.3	9.0	6.9
0	7.3	6.8	6.0	4.7	3.6

TABLE I.E.12. Number of Days of 45-MW Operation to Attain
1% Burnup in ANL-GE Oxide Test Subassembly

Enrichment (a/o)	Row 2	Row 3	Row 4	Row 5	Row 6
93	48	52	60	74	96
43	80	86	99	122	160
0	150	160	186	228	300

Two-dimensional calculations determined the worth of fuel expansion according to position in EBR-II. In considering the safety aspect of the oxide-fuel loading, a conservative fuel-expansion coefficient of zero was taken. The loss of the reactivity decrement at 45 MW due to an oxide subassembly is given in Table I.E.13 as a function of core position.

TABLE I.E.13. Loss of Power Defect due to Absence of Axial Expansion in Oxide Test Subassembly

	Subassembly Position			
	Row 1	Rows 2, 3	Rows 4, 5	Row 6
Loss per Subassembly, 1h	1.3	1.0	0.63	0.47

(b) PNL Type. The performance of PNL type of subassembly (see Table I.E.9) was based on the results for the ANL-GE type. The reactivity worths and power-density ratio calculated are in Table I.E.14, the linear power generation in Table I.E.15, and burnup rates in Table I.E.16; all are based on the relative ^{235}U (equivalent) loadings of the PNL and ANL-GE types. The loss of the reactivity defect is the same in both types since both are assumed to have a zero fuel-expansion coefficient.

TABLE I.E.14. Percent Reactivity Change and Power-density Ratio for PNL-GE Subassembly versus Driver Fuel

Enrichment (a/o)	Percent Reactivity Change					Power-density Ratio (Oxide/Driver)
	Row 1	Row 3	Row 4	Row 5	Row 6	
93	+0.12	+0.095	+0.065	+0.050	+0.030	0.92
43	-0.40	-0.33	-0.25	-0.20	-0.14	0.56
0	-0.80	-0.66	-0.52	-0.38	-0.25	0.30

TABLE I.E.15. Linear Power Generation in PNL Oxide Pins

Enrichment ^{235}U (a/o)	Power Density (kW/ft, avg)				
	Row 2	Row 3	Row 4	Row 5	Row 6
93	18.0	16.7	14.6	11.7	9.0
43	10.5	9.9	8.8	6.9	5.3
0	5.8	5.4	4.7	3.8	2.9

TABLE I.E.16. Number of Days of 45-MW Operation to Attain
1 a/o Burnup in PNL Oxide Fuel

Enrichment ^{235}U (a/o)	Days for 1 a/o Burnup				
	Row 2	Row 3	Row 4	Row 5	Row 6
93	60	65	75	92	120
43	100	107	124	152	200
0	188	200	232	285	375

(c) Summary. The preliminary study has been made to determine the maximum number of oxide test subassemblies which can be loaded into EBR-II. The determination has been based in part on an allowable loss of 10 to 15 lh in the power decrement. Based on the data in Table I.E.14, the maximum number of test subassemblies ranges between 10 (for all test subassemblies in Rows 2 and 3) and 20 (for all test subassemblies in Row 6).

(iv) Study of Power Coefficient. The linear component of the power coefficient was calculated for Run 27A and for a similar core loading surrounded by a depleted-uranium blanket. For the loading with a full blanket, referred to as Run 27-BNKT, four half-loaded subassemblies in Run 27A were replaced with fully loaded subassemblies, and the steel reflector in Rings 7 and 8 with blanket subassemblies. The calculational method was the same as that used for Runs 16, 24, 25, and 26. The values of the components of the power coefficient are given in Table I.E.17.

TABLE I.E.17. Components of Power Coefficient in
Units of Δk ($\times 10^5$) or $\Delta k/\Delta T$ ($\times 10^5$)

Component	Run 27A	Run 27-BNKT
Na--Core Δk	-41.7	-39.3
$\Delta k/\Delta T$	-0.453	-0.451
Na--Upper refl Δk	-41.3	-37.5
$\Delta k/\Delta T$	-0.225	-0.214
Na--Inner refl/bnkt Δk	-3.4	-5.6
Na--Total	-86.7	-82.4
Fuel Δk	-42.0	-44.0
$\Delta k/\Delta T$	-0.199	-0.218
Steel--Axial Δk	-17.3	-10.9
Radial Δk	-115.4	-88.7
$\Delta k/\Delta k$ In/mil	-3.42	-3.59
45 MW (no radial) Δk	-148.1	-141.3
45 MW Δk	-265.9	-244.0

The temperatures used for Runs 27A and 27-BNKT were those calculated for Runs 25 and 24, respectively. The values of the components for Run 27A are slightly more negative than those for Runs 26B and 25, which were similar in loading to Run 27A. Most coefficients for Run 27-BNKT are more negative than those for Run 24, which also had a depleted-uranium blanket but a smaller core loading than Run 27-BNKT. Note that sodium temperatures were used in calculating the steel radial expansion for Run 27-BNKT whereas the steel temperatures were used in all other calculations.

The calculations for Runs 27A and 27-BNKT indicate that the linear components of the power coefficient have not changed significantly from previous loadings. Any change in the total power coefficient would be due to a change in the pattern of radial movement of the subassemblies.

(v) EBR-II Dynamics Analysis. Analog computer studies of the EBR-II power-to-reactivity feedback curves measured in Run 26 have been made using estimated time constants for the axial fuel-expansion effect (coefficient experimentally measured in separate reactor runs), the sodium density effect (theoretical estimate of coefficient), and the control-rod-bank expansion effect. It was observed that the structural effect which must be added to the computer analog of the above effects to secure rod-drop curves matching those of Run 26 could be synthesized from at least three positive feedback coefficients with typical time constants of approximately 0.3, 2, and 6 sec. However, while the rod-drop data could be fairly well represented by this means, the transfer-function data (particularly the phase data) could not. This has led to the conclusion that it is necessary to treat the dynamic structural effect as a cooperative thermomechanical interaction between Rows 6, 7, 8, and 9. The 2-sec time constant obtained in the analog computer studies may result from dynamic radial heat transfer between Rows 6 and 7 or from dynamic cooperative thermomechanical motion between rows or possibly both.

For example, the transit time of the outer blanket sodium is 2-3 sec and could take part in such a cooperative motion. The inner plenum sodium holdup time is also 2-3 sec, but effects from the plenum sodium temperature seem to be only very small ones related to expansion of the subassemblies at their upper end.

A static bowing model constitutes a possible means of solving the above extremely complex dynamic structural problem by combination with a program for determination of differential temperatures to be inputted as a function of time. It is estimated that the present Bow II computer code must be upgraded by an order of magnitude in result accuracy to be useful in such an application. The code is being examined to determine the feasibility of such an improvement.

c. Reactor System Testing, Surveillance, and Evaluation
(B. C. Cerutti)

Last Reported: ANL-7438, pp. 46-47 (March 1968).

(i) Fuel-handling Operations. Because of operational problems with the reactor-vessel cover lock No. 3, a new plant-modification proposal to improve lock operation and reduce the possibility of electrical or mechanical damage to the lock unit has been submitted. The torque-limiter switch on this unit (which stops the drive motor) has not been dependable. Disassembly revealed a binding switch actuator and some loose electrical connections. The lock was repaired and seems to be operating properly, but the modification will be installed as soon as possible.

Binding of the vertical motion of the fuel-transfer arm at the "transfer" point has recently been encountered. The symptoms are similar to those exhibited in March 1966 immediately after the transfer-arm repair and reinsertion into the primary tank. At that time sodium oxide was believed to have been carried into the annulus between the transfer-arm support column and the plug during insertion. Continued use of the transfer arm at that time reduced the binding until the problem disappeared completely. After the recent binding, the rotational interlock solenoids were retracted, and the transfer arm was exercised both vertically and in rotation at the "transfer" point. Binding had occurred only when handling a heavy subassembly and only at the transfer position, so exercising was done with increasing subassembly weights and near the transfer positions. The binding decreased as the transfer arm was exercised until operation essentially returned to normal. A possible explanation is that there is a buildup of sodium oxide around the support column and occasionally a small quantity drops into an area of close clearance and causes the binding. Fuel-handling operations continued without difficulty after the arm was exercised. The clutch for the vertical movement mechanism on the fuel-transfer arm was reworked and set to limit the force that can be applied to 100 lb. The handle attachment was also reworked to prevent shearing of the linkage bolts.

Cleaning and level adjustment of the rotating-plug-seal alloy gave results as follows:

	<u>Large Plug</u>	<u>Small Plug</u>
Dross removed, lb	171	150
Seal alloy added, lb	224	264
Seal alloy depth after filling, in.	8	$8\frac{7}{8}$
Nominal seal alloy depth, in.	$8\frac{1}{4}$	9

(ii) Primary-sodium Purification System. To help in trouble shooting the surge-tank vacuum and argon-supply systems, a vacuum gauge was installed between the two argon-gas syphon-break valves. This gauge provides a means for determining the leak rate through the motorized bellows-sealed gate valve.

d. Fuel Swelling and Driver Surveillance (F. G. Foote)

(i) Mark IA--Investigation of Anomalous Fuel Swelling

Last Reported: ANL-7438, pp. 48-49 (March 1968).

(a) Extended Burnup of MC-S-type Fuel Pins. Matched Set No. 2, which consists of Subassemblies C-2027 and C-2036, was removed from the reactor core midway through Reactor Run 27; Subassembly C-2027 is being held in the fuel-transfer storage rack and C-2036 has been transferred to FCF for fuel-swelling surveillance. Two subassemblies (C-291 and C-2027) are now being held in the storage rack for possible reinsertion into the core for additional burnup.

(b) High-burnup Irradiations of Mark-IA Fuel. Irradiation-test Subassemblies XO15 and XO17 have been removed from the core and stored in the reactor storage basket.

(c) Effect of the Change to Mark-IA Design upon Fuel Swelling. Swelling results from Subassembly C-298 are not yet available. The conclusions that there is no effect upon swelling from design change remain unchanged (see Progress Report for February 1968, ANL-7427, pp. 54-55). A third subassembly is being prepared that contains more of the same fuel materials in additional elements of the Mark-I, Mark-IA, and Mark-IB fuel-element designs.

(d) Effect of Trace-element Impurities upon Fuel Swelling. Subassembly C-2077, which contains fuel pins cast at Illinois in the injection-casting furnace, was removed from the core at a maximum burnup level of 0.8 a/o and transferred to the FCF for fuel-swelling measurements. Results are not yet available.

(e) Effect of Heat Treatment upon Swelling of U-5 w/o Fs Alloy. Density measurements have been completed on all 12 specimens of this series. The least swelling was observed in the as-cast condition and after water quenching from the high-gamma region. Higher swelling values were obtained from specimens in the as-aged condition (1 hr at 500°C). Unfortunately, all driver fuel receives an aging treatment as part of the sodium-bonding process.

(f) Hot Laboratory Examination of Irradiated Fuel

(i) Fuel Surveillance. Ten subassemblies (L-447, C-2003, B-352, B-354, B-355, B-356, B-357, B-358, B-359, and B-360) were removed from the core near the end of Reactor Run 27. Since all of these subassemblies contain some fuel elements that may have been clad in seamless tubing, the subassemblies are considered to be potential leakers. Five have already been transferred to the FCF to survey for sodium level and for cladding leaks. Regardless of whether cladding leaks are found or not, the survey will add about 850 more data points of swelling, burnup, and temperature to our accumulation.

(g) Analysis of Fuel-pin Swelling. An attempt is being made to develop a new figure of merit. The method is based upon fitting an equation of the form

$$\% \text{ Swelling} = \alpha (\text{Bu} - 0.48)^2 + 4.4 \text{Bu} \left(\frac{\bar{T}}{T} \right)^7 - 0.7 \quad (1)$$

to the swelling, burnup (Bu), and temperature data for a given casting batch, where \bar{T} is the average temperature of the fuel elements in the set, and α is used as the figure of merit. If we assume that α is linearly dependent upon the trace-element impurities, we obtain, for 19 different casting batches,

$$\alpha = 34.577 - 0.081 (\text{Si}) - 0.013 (\text{Al}) - 0.012 (\text{Fe}) - 0.001 (\text{C}). \quad (2)$$

The factor for silicon is approximately six times larger than that for either aluminum or iron; thus, the calculations confirm the effectiveness of silicon in the production of fuel with low swelling rates. This approach to the swelling problem is being developed further. New and more accurate fuel-temperature data are now being obtained and will be used in the analysis.

(ii) TREAT Experiments

Last Reported: ANL-7438, pp. 51-52 (March 1968).

(a) Fuel-motion Studies with Mark-IA Fuel Elements
(C. J. Renken)

In a future transient experiment in TREAT, an attempt will be made to measure the fuel motion in Mark-IA fuel elements during the course of the transient. The end of the fuel will move through a pulsed induction field generated and detected by transducers that consist of groups of coaxial coils. A transducer will be provided for both the top and the bottom of the fuel. The fuel motion may be measurably independent of the motion of the sodium during the transient by analysis of the train of pulses produced by the fuel motion, and by time sampling of the individual pulses.

The resistivities of the sodium, the fuel, and the cladding will change drastically as the fuel element heats. This effect appears reconcilable by careful design of the transducer, as well as by proper choice of pulse length and sampling time. However, the success of this plan depends on the existence of a difference between the resistivities of the sodium and of the fuel pin that is great enough to produce a usable signal. The extent of this difference has been the subject of some investigation.

The experiments start by electrically heating the fuel element to a temperature high enough to melt the sodium. At 150°C, the resistivity of the sodium will be about 11 $\mu\text{ohm-cm}$, and the approximate resistivity of the unirradiated uranium-5 w/o fission fuel is estimated to be about 68 $\mu\text{ohm-cm}$. (Actual measurements are available only to up 50°C.) This difference is very favorable, but unfortunately the temperature coefficient of resistivity of molten sodium is strongly positive, while the coefficient of the gamma-quenched fuel probably is weakly negative. At the projected peak surface temperature of the fuel during the transient, 800°C, the sodium will have a resistivity of about 44 $\mu\text{ohm-cm}$, while the resistivity of the fuel could have dropped considerably from the 150°C value of 69 $\mu\text{ohm-cm}$ (at 150°C). This convergence of the resistivities will degrade the signal produced as the end of the fuel pin passes through the transducer field.

The situation will improve when measurements are attempted on irradiated fuel elements. The irradiation damage in the fuel can be expected to raise the effective resistivity. Any surface damage suffered, which is likely at the projected burnup of 1.2 a/o, will be beneficial. The fuel probably will be converted to a predominantly alpha phase during irradiation and will then possess a positive coefficient of resistivity that will help maintain a useful difference between the resistivities of the fuel and the sodium.

The uncertainty in the resistivity values of the fuel and the sodium at any given time during the transient is bound to reduce the accuracy of the motion measurement. Close attention to transducer design will be necessary to reduce this ambiguity.

e. Mark-II Driver Fuel Element Development (J. H. Kittel)

(i) Element Irradiation Tests, Metallurgy, Idaho (M. A. Pugacz)

Last Reported: ANL-7438, pp. 52-53 (March 1968).

An irradiation capsule that will contain three prototype Mark-IIA elements is being assembled for insertion in the CP-5 reactor. The objectives of the irradiation are to study the change in central temperature of the fuel due to swelling, and to determine gas-pressure buildup in the plenum due to thermal expansion, fuel swelling, and fission-gas release.

The prototype elements have the same cross-section dimensions as the Mark-II elements; however, the length dimensions have been scaled down by a factor of seven. Two of the elements are instrumented with thermocouples to measure the temperatures of the cladding and of the center of the fuel. The other element is instrumented with a "null-type" pressure transducer that will provide information of the gas pressure in the plenum.

As of April 10, the experimental fuel elements of Mark-II design were exposed to 922 MWd in Subassembly XO29 in EBR-II. The maximum calculated burnup was 0.53 a/o.

Twenty-two of the 25 capsules shipped to Idaho as replacements for capsules to be removed from experimental Subassembly XO29 were rejected because of thinning of the weld closures below the tube-wall thickness. Two improved joint designs were tested: a square butt-joint with a 10-mil undercut, and a square butt-joint with no undercut. Both designs showed excellent capability of producing sound welds consistently. The butt-joint without undercut was the easiest to prepare and was the preferred joint design, but it was also the most difficult to inspect by nondestructive inspection techniques. Several weldments and cross sections of each design were sent to Idaho for examination and evaluation. Subsequently, Idaho authorized an increase of 0.010 in. in the flange width.

End pieces have been machined in accordance with the change. Replacement tubes have been received from Idaho, and the bottom ends have been welded. Inspection of the welds by X ray is in progress.

Preliminary creep-strain calculations have been made for the Mark-II fuel cladding by assuming that at a burnup level of 5 a/o the circumferential stress of the cladding increases linearly from 0 to 16,000 psi in 366 days at 550°C (50 MW reactor operation) and 292 days at 600°C (62.5-MW reactor operation). At 550°C, Types 304L and 316 stainless steel develop 0.1% strain in ~350 and ~500 days, respectively. At 600°C, Types 304L and 316 stainless steel develop 0.1% strain in ~200 and ~300 days, respectively. These preliminary calculations indicate that the creep strain of Type 304L stainless steel cladding may limit Mark-II fuel-element lifetime to burnups less than 5 a/o; if, however, Type 316 stainless steel cladding is used for the Mark-II element, cladding strain will not limit fuel-element lifetime.

- (ii) Voids in the Fuel Cladding and the Control-rod Shroud of EBR-II (S. D. Harkness)

Last Reported: ANL-7438, pp. 49-50 (March 1968).

- (a) Mark-IA Fuel Cladding. Two additional sections of cladding were examined from the fuel element that exhibited high swelling.

These sections showed the same general microstructure; voids and Frank dislocation loops were homogeneously distributed throughout the material, but no voids were observed to lie on grain boundaries. The measured values of void-volume fraction are consistent with those observed by other workers for austenitic stainless steels that have undergone a similar fluence. Corrected values of average void size ($\langle D \rangle$), number density (N_V), and volume fraction (V_F) calculated for the four sections are listed in Table I.E.18.

TABLE I.E.18. Results of Examination of Mark-IA Fuel Cladding

Sample Number	Max Cladding Temp (°C)	Approximate Fluence ($n/cm^2 \times 10^{-22}$)	$\langle D \rangle$ (Å)	N_V (No./ $cm^3 \times 10^{-15}$)	V_F (%)
1	480	1.2	93	5.4	0.2
2	465	1.4	105	4.0	0.2
3	492	1.1	140	1.5	0.2
4	462	1.4	91	2.8	0.1

(b) EBR-II Control-rod Shroud. Sections of a Type 304 stainless steel control-rod shroud that had been irradiated in EBR-II to a peak fluence of $5 \times 10^{22} n/cm^2$ are being examined. This material is of great interest for two reasons: first, the fluence is higher than for any Type 304 stainless steel previously studied, and second, the shroud was unstressed during exposure. These points should aid in delineating the roles of fluence and stress in the void-growth process.

Density measurements for three different positions are presented in Table I.E.19. The experimentally determined standard deviation for these results was $0.002 g/cm^3$. The large amount of indicated void formation implies that the presence of stress is unimportant to the phenomenon.

TABLE I.E.19. Density Results for Control-rod Shroud

Sample Position above Bottom of Core (in.)	Irradiation Temperature (°C)	Fluence ($n/cm^2 \times 10^{22}$)	V_F (% Increase in Volume)
23.5	470	1.0	0.06
17.5	470	2.0	0.28
5.5	420	4.8	1.04

At present, one section of the shroud has been examined by transmission electron microscopy (TEM). The estimated fluence

and temperature for this section are 4.5×10^{22} n/cm² and 410°C, respectively. The general microstructure was the same as observed in the cladding. A representative micrograph is presented in Fig. I.E.10. The average void diameter was 100 Å, the number density was 4.5×10^{15} /cm³, and the calculated volume fraction was 0.25%. Since void formation is strongly temperature dependent, it is expected that sections that experienced higher irradiation temperatures will show larger void-volume fractions.



96,000X

Fig. I.E.10. Typical Microstructure from Type 304 Stainless Steel
Control-rod Shroud (Sample Fluence = 4.5×10^{22} n/cm²; Irradiation Temperature = 410°C)

f. Equipment--Fuel Related (E. Hutter)

Last Reported: ANL-7438, pp. 53-54 (March 1968).

(i) Oscillator Rod Mark II. Further evaluation of the 39-fuel-element and 22-dummy-element oscillator-rod design to replace the existing Type-II oscillator rod (see Progress Report for February 1968, ANL-7427, p. 61) has revealed that a fully fueled rod with 61 elements could be used instead and would not present major engineering problems. Additional flow holes would have to be drilled near the center of the lower shield. Hole size and location have been calculated. A more precise

method to determine exact flow orifices would require a model for experimentally sizing the holes.

(ii) Engineering Consultation

(a) SWELL: A Fuel-element-lifetime Code. A fuel-element-lifetime code, SWELL,* was written about a year ago with a threefold purpose: (1) to achieve general capability for fuel-element-lifetime calculations, (2) to aid in the design of the Mark-II fuel elements, and (3) to demonstrate that fuel-element lifetime should be treated as a dependent variable in studies of 1000-MWe LMFBR power-plant optimization.

Originally, SWELL was slanted toward oxide-fuel elements because their behavior, particularly near end of life, was better known than that of metal fuel elements. As a result, only recently has SWELL been applied successfully to metal fuel.

Present work on improving the SWELL code for estimating the time of cladding failure involves eliminating the criterion that cladding failure occurs when net growth takes place on every thermal cycle. Instead, the actual amount of growth from cycling will be considered as just another source of damage to be added to that from creep, thermal-stress fatigue, and irradiation.

Initial results from SWELL indicated that the code overestimated the cladding creep caused by thermal stresses. Therefore, the code is being changed so that as creep due to thermal stresses occurs, the thermal stresses reduce correspondingly, in much the same manner as they reduce by plastic deformation.

g. Equipment--Reactor and Primary Coolant System (B. C. Cerutti)

Last Reported: ANL-7438, pp. 54-55 (March 1968).

(i) Fuel-handling System. As the result of an operational problem in which one of the three reactor cover locks failed to torque properly, a protective circuit was designed for the cover-lock motor-control circuit to automatically de-energize the motors prior to motor damage. The circuit de-energizes the cover lock motors and prevents restarting until a check has been made of the locks.

(ii) Sodium Sampling Pump and Filter. Newly completed electrical modifications have been tested successfully. The sodium sampling pump and filter assembly has been disassembled, cleaned, and inspected. The pump and filter will be shipped to the reactor, where they will be installed in a spare nozzle of the primary-tank cover.

(iii) Intermediate Heat Exchanger Seal. The test rig has been completed. The baffle has been fabricated and is being heat treated. When the baffle has been mounted, the test rig will be soaked in 700°F sodium to determine whether the baffle's spring characteristics are affected.

*Bump, T. R., Effects of Other Power Plant Parameters on Fuel-element Lifetime, Trans. Am. Nucl. Soc. 10(2), 664 (1967).

h. Secondary Sodium and Power Systems (B. C. Cerutti)

Last Reported: ANL-7438, p. 55 (March 1968).

(i) Control System for Boiler-water Level. A series of tests were performed on a static control unit to replace the existing servo-operated control system for boiler-water level. The test results indicate that the static controller is satisfactory for use as a replacement unit. The use of the static controller will reduce the number of components in the system and should improve overall system reliability.

(ii) Study--Sodium-Water Reaction, Pressure Relief, Secondary System. Although the design of the steam generators and superheaters is intended to preclude a sodium-water reaction, because of the seriousness of potential damage if a rupture occurs in the secondary system, a study has been initiated to determine the ability of the superheater to sustain certain reaction effects.

The study is based on the need to understand the mechanisms for such reactions and the structural response for cases in which a tubular superheater is not blanketed with an inert cover gas. In existing related studies of tube failure that permits steam to leak into sodium, the descriptions of the behavior of the source of the ensuing disturbance and of the response of the structure depend very heavily on the presence of an inert cover gas.

Plans for the study have been developed and work has begun under a contract with the Illinois Institute of Technology Research Institute. In the preliminary phase of the study, models are being developed for calculating steam-to-sodium leak rates and for estimating reaction-product properties and shell response. The initial efforts included examination of the properties of superheated steam and water-steam mixtures in states neighboring the superheater process curve. The selection of a gamma-law representation of isentropic behavior in the superheated vapor is being studied. Isentropic processes in a water-steam mixture can be characterized adequately by a linear relation between specific volume v and the reciprocal of pressure, p^{-1} , as shown by

$$v - v_0 = u_0^2 \left(\frac{1}{p} - \frac{1}{p_0} \right),$$

where the subscript zero denotes a saturation state and u_0 is a function of entropy having the dimensions of velocity. These processes will form the basis for estimating leak rates as functions of reservoir pressure and back pressure in the reaction-product bubble for various possible leak locations. From these results will come expressions for mass flow rate per unit of idealized break area as a function of current steam-reservoir state and current reaction-product bubble pressure.

The second phase of the study will include calculating reaction-product bubble dynamics, estimating transient loadings on the shell and piping from pressure-pulse propagation in the sodium, analyzing the dynamic response of the shell and adjacent tubing, and evaluating the pressure-relief system.

i. New Subassemblies Design and Experimental Support (E. Hutter)

Last Reported: ANL-7427, pp. 62-64 (Feb 1968).

(i) Mark-II Core Development

(a) Fuel Subassembly. Review of the report on the Mark-II driver-fuel design continues. The cost of fabricating hardware for five Mark-II in-reactor experimental irradiation subassemblies have been estimated. Fabrication will begin when the report is approved.

(ii) Radial Blanket

(a) EBR-II Reflector Subassembly. The possibility of slightly decreasing the dimensions of the hexagonal subassembly is being evaluated. A smaller subassembly would facilitate the outward movement of the tops of the subassemblies (flowering effect), thus increasing the negative power coefficients of reactivity.

The exterior dimensions of the locating buttons that protrude from the hexagonal container near the center of the core will not be changed.

(iii) Irradiation Subassemblies

(a) Mark-A. A proposed variation of the Mark-A19 irradiation subassembly would permit experimental ceramic fuels to be irradiated at temperatures above those normal for EBR-II. To allow this, as in the mixing-type Mark-C subassembly, certain fuel-element positions would be converted to bypass flow channels so that the temperature of the sodium leaving the subassembly will be no higher than usual. However, because of the longer length of the fuel elements, only a very short (4 in.) mixing space would be available in which to combine the ~1200°F sodium from the test fuel elements with the ~700°F sodium from the bypass channels to achieve the normal subassembly outlet temperature of ~940°F.

In studies of mixing effectiveness, dye has been injected into water flowing through fourteen different mixer configurations. Some of

the configurations provide good mixing in a 6-in. length. But, although further experiments are planned, it does not seem likely that efficient mixing can be achieved in a 4-in. mixing chamber without subjecting the subassembly structure to excessive thermal stresses.

(b) Mark-B. Drawings have been completed for modifications that will allow the Mark-B7 irradiation subassembly to be used in the inner or outer blanket regions of the reactor, as well as in the core.

(c) Mark-E. Fabrication has begun on a hydraulic test model of the Mark-E "nonmelt-through" irradiation subassembly. Initial tests in a water loop will check the ability of the collection devices to retain simulated fuel fragments and debris.

(d) Mark-F. Hydraulic tests of a Mark -F37 irradiation subassembly (see Progress Report for January 1968, ANL-7419, p. 65) have shown that the predicted capability of this subassembly has been exceeded slightly.

j. Process Chemistry (D. W. Cissel)*

Last Reported: ANL-7438, pp. 58-60 (March 1968).

(i) Sodium Coolant Quality and Control

(a) Primary Sodium

(1) Sampling. The primary purification system was out of service for most of the report period because of difficulties in the surge-tank vacuum system. All samples were taken with the FERD loop sampling equipment.

(2) Radionuclides. Five samples of primary sodium were analyzed by gamma spectrometry for radionuclides. The results are listed in Table I.E.20.

TABLE I.E.20. Radionuclides in Primary Sodium

Sample Date	^{137}Cs ($\mu\text{Ci/g}$)	^{131}I ($\mu\text{Ci/g}$)	^{22}Na ($\mu\text{Ci/g}$)
3/6/68 ^{a,b}	1.6×10^{-2}		
3/26/68 ^b	2.6×10^{-2}		1.9×10^{-2}
3/30/68	1.6×10^{-2}		
4/3/68	5.3×10^{-3}	2.1×10^{-4}	
4/6/68	1.6×10^{-2}	2.0×10^{-3}	

^a Taken from purification-loop sampler; all others from FERD loop sampler.

^b Taken in Pyrex beakers; all others were in quartz beakers.

*Erratum: In Table II.E.9, p. 58 of ANL-7438, the activity unit of the isotope should be $\mu\text{Ci/g}$, not Ci/g .

(3) Trace Metals. A primary sodium sample taken on February 23, 1968, was analyzed for trace metal impurities by atomic absorption. The results are listed in Table I.E.21.

TABLE I.E.21. Trace-metal Impurities in Primary Sodium

Metal	Concentration (ppm)	Metal	Concentration (ppm)
Al	3.0	Fe	2.0
Bi	1.6	Mg	0.4
Co	<0.4	Mn	<0.2
Cr	<0.3	Ni	0.9
Cu	0.4	Sn	19.6

(4) Tritium. Four primary sodium samples (current and historical) were analyzed for tritium. The results are listed in Table I.E.22.

TABLE I.E.22. Tritium Concentration in Primary Sodium

Sample Date	Tritium Concentration (pCi/cc)
3/7/63	<150
7/9/65	2540
	3340
11/14/67	1840
2/5/68	1740

Tritium concentrations in various plant systems were reported in the Progress Report for December 1967, ANL-2403, p. 69.

(b) Primary Argon. A test program was initiated to determine the source of nitrogen in the primary-tank cover gas. The nitrogen concentration was first reduced to 1200 ppm by purging

with fresh argon. Then an attempt was made to associate increases with specific plant operations. Initial results indicate the source of nitrogen to be connected with operation of the fuel-unloading machine. However, further testing is required before a definite conclusion can be reached; testing is continuing.

(c) Expanded Capabilities for Sodium Sampling

(1) Primary Sodium. The beaker sampler for the FERD loop sampling system was successfully tested and was used to sample primary sodium during an extended shutdown of the primary purification system.

k. Experimental Irradiation and Testing (D. W. Cissel)

Last Reported: ANL-7438, pp. 60-66 (March 1968).

(i) Experimental Irradiations

(a) Status of Experiments in EBR-II. The status of experimental irradiations in EBR-II as of April 30, 1968, is shown in Table I.E.23.

All subassemblies containing encapsulated experimental fuel elements were removed from the reactor grid and stored in the storage basket in the search for the source of the fission-product releases detected on several occasions during reactor operation (see Sect. I.E.1.a).

After the end of Run 27E, structural-materials Subassemblies XO34 and XO35 from ORNL were loaded into grid positions 2F1 and 7B4, respectively.

Removal of experimental Subassembly XG05 from the storage basket was requested by the sponsors (ANL-MET and GE) after an accumulation of 12,640 MWd of reactor operation. The capsule in the subassembly having the greatest exposure was estimated to have an average burnup of approximately 6.9 a/o. After disassembly, the 14 fuel capsules were inspected by neutron radiography and weighed. All capsule weights compared favorably with the known or estimated preirradiation weights. Results of the neutron radiography are given in Sect. I.E.1.k.(ii)(2).

(b) Status of Irradiation Experiment Proposals Given Administrative Approval-in-Principle (AIP). Table I.E.24 summarizes the present status of all irradiation experiments which have been given AIP but not been inserted in the reactor.

(c) New Experimental Subassembly Design. Fabrication of a prototype of the Mark-F-37 subassembly design, originally requested by GE for their fuel-element development program, was completed, and flow testing has been started by ANL-RE.

Flow testing continued of mixing devices that might be incorporated in a Mark-A subassembly design to permit capsule irradiations having surface temperatures approaching 1200°F. This investigation for elevated capsule-surface-temperature testing is in support of the GE-Group 5 irradiation.

TABLE I.E.23. Status of EBR-II Experimental Irradiations

Subassembly (Position)	Date Charged	Capsule Content and Number of Capsules ()	Experimenter	Accumulated Exposure (MWd) 4/30/68 ^a	Estimated Goal Exposure (MWd)
XG02 ^b (7A1)	7/16/65	UO ₂ -20 w/o PuO ₂ Stainless Dummies (1)	GE	14,006	16,700
XG03 ^b (7D1)	7/16/65	UO ₂ -20 w/o PuO ₂ Stainless Dummies (1)	GE	14,006	22,300
XG04 ^b (7B1)	7/16/65	UO ₂ -20 w/o PuO ₂ Stainless Dummies (1)	GE	14,006	42,050
XA08 ^b (4F2)	12/13/65	UC-20 w/o PuC Structural (1)	ANL ANL	10,703	19,800
XO10 ^b (7F3)	3/24/66	UO ₂ -20 w/o PuO ₂ Structural (1)	GE ANL PNL	10,937	19,800
XO12 ^c (4B2)	8/10/66	UO ₂ -20 w/o PuO (1)	NUMEC	7,079	20,100
XO15 ^c (4A2)	11/15/66	UO ₂ -20 w/o PuO ₂ UO ₂ -20 w/o PuO ₂ UC-20 w/o PuC U-Fs (Mk-1A) (2)	NUMEC GE ANL ANL	5,424	11,000
XO16 (4D2)	1/13/67	Structural Structural (1)	ANL GE	4,459	7,400
XO17 ^c (4C3)	11/15/66	UO ₂ -20 w/o PuO ₂ UC-20 w/o PuC U-Fs (Mk-1A) (5)	NUMEC UNC ANL	5,424	6,500
XO18 (2B1)	12/6/66	Structural Structural Structural Structural and Heavy Metal Fission Yield Sample (1)	GE PNL ANL ANL	5,089	21,300
XO19 ^d (6D2)	1/13/67	UO ₂ -20 w/o PuO ₂ (U _{0.8} Pu _{0.2})C Structural Graphite (1)	GE UNC PNL PNL	4,193	7,500
XO20 ^d (6B5)	1/13/67	UO ₂ -PuO ₂ (U _{0.8} Pu _{0.2})C Structural Structural Graphite (1)	GE UNC PNL ANL PNL	4,193	7,500
XO21 (2D1)	2/27/67	Structural (7)	PNL	4,459	21,500
XO22 (7C4)	2/27/67	Structural (7)	PNL	4,459	5,000
XO25 (4E2)	10/10/67	Structural (1)	GE	2,811	7,400
XO26 (7D5)	10/11/67	Structural (7)	NRL	2,811	3,000
XO27 ^d (4B3)	11/22/67	UO ₂ -25 w/o PuO ₂ Structural (1)	GE PNL	1,516	7,200
XO28 ^f (4D3)	11/22/67	U-15 w/o Pu-10 w/o Zr U-Fs (4)	ANL ANL	1,634	9,200
XO29 ^f (4E3)	12/22/67	U-Fs (Mk-1B) (3)	ANL	1,015	5,100
XO31 ^e (6C1)	11/22/67	UO ₂ -25 w/o PuO ₂ (1)	PNL	1,585	2,200
XO32 ^d (6F1)	11/22/67	UO ₂ -25 w/o PuO ₂ (1)	PNL	1,516	11,000
XO33 ^e (5E2)	12/22/67	(U _{0.8} Pu _{0.2})C (1)	UNC	966	10,000
XO34 (2F1)	4/12/68	Structural (7)	ORNL	355	13,500
XO35 (7B4)	4/12/68	Structural (7)	ORNL	355	40,500
X900 (7A4)	3/20/68	Structural (1)	ANL	6419	2,700

^aAccumulated exposure during April was 587 MWd for the subassemblies that stayed in the reactor.^bRemoved to basket in March.^cRemoved to basket at end of Run 27D.^dRemoved to basket at end of Run 27E.^eRemoved to basket at end of Run 27F.^fRemoved to basket at end of Run 27G.^gIncludes 54 MWd from March 1968.

TABLE I.E.24. Status of Experiments with AIP

Sponsor	Material of Test	No. Caps.	Suggested Reactor Row ^a	Date of AIP	Estimated Date for Delivery to Idaho Site
ANL	Oxide fuel, Group O-3	19	3	9/22/67	12/68
	Carbide fuel, Group C-5	19	2	9/22/67	1/69
	Oxide fuel, (unencap)				
	Safety Program	19	4	9/6/66	6/67 ^b
	Mark-II fuel (unencap)	455	Core	9/22/67	6/68
	Mark-II fuel (encap) ^c	25	4	6/3/67	5/68
	Metal fuel, M-4	19	3	2/13/68	6/68
	Structural, Group S-9	19	4	9/22/67	6/68
	Tritium yield	-	7	6/8/67	Cancelled
	Magnetic materials	7	7	6/8/67	7/68
BMI	Nitride fuels	8	7	2/13/68	6/68
GE	Oxide fuel, Group 8-B	19	7	6/7/67	2/68 ^b
	Oxide fuel (unencap), Group 3	16	4	9/6/66	6/67 ^b
	Oxide fuel, Group 7	4	4	9/2/66	2/68 ^b
	FCR Structural Group L-15	4	2	1/4/68	11/67 ^b
	Oxide fuel (unencap), Group 9A	37	4	1/20/67	6/68
	Oxide fuel (unencap), Group 5	16		1/20/67	7/68
INC	Structural materials, Fatigue No. 1	7	7	6/6/67	3/68 ^b
	Structural materials, Fatigue No. 2	7	7	9/21/67	4/68 ^b
LASL	Oxide insulators	7	8	6/6/67	6/68
	Carbide fuels	1	2	2/27/67	3/68 ^b
		6	3		6/68
NRL	Structural materials	7	7	9/6/67	10/68
ORNL	Oxide insulators	7	8	9/21/67	7/68
PNL	Oxide fuel (unencap)				
	("low" power)	37	3	9/21/67	6/68
	Oxide fuel (unencap)				
	("normal" power)	37	4	9/21/67	7/68
	Oxide fuel (unencap)				
	("high" power)	37	3	9/21/67	8/68
	Graphite materials	7	7	7/31/67	Indefinite
	Thermocouple materials	5	4	7/31/67	7/68
UNC		2	4	7/31/67	2/68 ^b
	Oxide fuel, Group X	5	3	3/4/68	3/68 ^b
	Carbide fuel (129-147)	19	7	6/6/67	7/68
	Carbide fuel (high power)	6	3	1/20/67	7/68
W	Carbide fuel (+V-alloy)	2	3	9/21/67	6/68
	Carbide fuel (+V-alloy)	9	4	9/21/67	Indefinite

^aBased upon fission rates at a reactor power of 45 MWt.^bDate received.^cReplacements for capsules of same type whose irradiation is nearing completion (e.g., Subassembly XO29).(d) Other Work

(1) Subassembly Flow Tests. The following experimental irradiation subassemblies have been flow tested: X900, Mark-B-37-type with pressurized-tube caustic-stress-corrosion capsules; XO34 and XO35, Mark-B-7-type with materials irradiation capsules from ORNL; XO36, a Mark-A-type containing encapsulated mixed-oxide fuel elements from GE; and XO37 and XO38, Mark-B-7-type with materials irradiation capsules from Idaho Nuclear Corporation (INC).

(2) Equilibration-Internal Friction Techniques for Analysis of Oxygen in Sodium. The prototype driver subassembly for the study of the equilibration-internal friction technique for analysis of oxygen in sodium was flow tested with mockup experimental capsules installed in the subassembly outlet. No significant change in subassembly flow rate was measured.

(3) XO40 Unencapsulated Mixed-oxide Irradiation Subassembly. The steady-state temperature distribution for experimental Subassembly XO40 was calculated with the HECTIC II code.

(4) Miscellaneous. Temperature distributions were calculated with the HECTIC II code for experimental Subassembly XO29 in 5E4 and 4N1 for 50-MW reactor operation.

(ii) Nondestructive Testing

(a) Capsule Examination. Five Mark-A-19 experimental mixed-oxide fuel capsules from PNL successfully passed final examination by X ray. The capsules are intended for inclusion in the reconstructed experimental Subassembly XO11, which will be renumbered XO39. LASL returned one fueled capsule (No. 42B), which passed final examination by X ray and is also to be placed in experimental Subassembly XO39.

INC delivered seven Mark-B-7 structural-type capsules for irradiation in experimental Subassembly XO38. All capsules passed final X-ray inspection.

(b) Neutron Radiography. The 14 fueled capsules removed from experimental Subassembly XG05 were transferred to TREAT for neutron radiographs. One of the nine GE mixed-oxide capsules contained a failed element (Capsule F20) which showed evidence of melting and probable penetration of the inner cladding wall.

The three ANL mixed-carbide capsules appeared in good condition. However, ANL Capsule ND-24, one of the two ternary-alloy capsules (U-15 w/o Pu-10 w/o Zr), showed fuel separation at three axial locations. The largest separation measured about 1/4 in. and was located at the center of the fuel column. The other two separations were just visible, and occurred about 2 and 4 in., respectively, above the largest separation. The fuel column in the other ternary capsule, NC-17, revealed axial fuel swelling which had forced fuel up around the bottom of the restrainer.

(c) Antimony-Beryllium Neutron Source for Neutron Radiography in FCF. Two experimental capsules containing metallic fuel, the top adapter of an EBR-II subassembly, and a cadmium penetrometer were radiographed with the use of the antimony-beryllium source. After

several trials with poor results, attempts to radiograph the top adapter were abandoned. The parallax resulting from using short distances between the source block and the adapter resulted in pictures that lacked definition. Increasing the distance required excessive time to activate the dysprosium foils.

Efforts were directed toward optimizing collimator size to obtain the best results with fueled capsules as subjects. Neutron collimators with sizes of 2 by 2, $1\frac{1}{2}$ by $1\frac{1}{2}$, 1 by 2, and 1 by 1 in. were used to evaluate two foil exposure times, one of 7 and the other of 17 hr. There seemed to be little or no advantage in the longer exposure since the dysprosium foils approached equilibrium activation during the 7-hr exposure. The definition on the film is best with the smallest collimator, but at the sacrifice of film image density.

The $1\frac{1}{2}$ - by $1\frac{1}{2}$ -in. collimator and 0.01-in.-thick dysprosium foils were chosen as the best compromise. The front side of the foil produced a better film exposure than the back; however, exposure from the back side was of usable quality.

As a final test, the capsules and dysprosium foil were moved closer to the source for a $2\frac{1}{2}$ -hr exposure. After neutron irradiation, the foil overexposed "medical no screen" film while not completely exposing type "AA" film. This shows the possibility of significantly reducing the neutron exposure time for certain applications if the larger film grain size of the "medical no screen" film can be accepted. The beryllium source block is ready to be moved to the FCF mockup area for dry-run testing of the complete radiography system.

(iii) Handling and Examination

(a) Irradiated Capsules from Experimental Subassembly XO11. The ANL-MET Capsule SOV-3, previously in experimental Subassembly XO11, was returned to Idaho for reinsertion in the reactor in experimental Subassembly XO39, which is also to contain other capsules from XO11. Neutron radiography confirmed that the sodium bond level in Capsule SOV-3 was the same as when removed from the reactor.

(b) Testing of Subassembly Sodium-removal Procedure

(1) Cyclical Testing of Stressed Capsules of Type 304 Stainless Steel. Experimental Subassembly X900, containing the pressure-stressed tubing samples, was loaded into grid position 7A4 for a goal exposure of about 2700 MWd. This is the start of the fifth (and last) residence in the primary sodium, to be followed by normal cleaning procedures. The first four cycles did not involve neutron exposure during soaking in primary sodium.

(iv) Safety Review of Experiments. The EBR-II Irradiations Review Committee (IRC) acted on the following experiments.

(1) Experimental Subassemblies XO37 and XO38, both containing fatigue specimens of structural materials from INC, were recommended for reactor safety and operational approval.

(2) After reviewing with experimenters the weld design for experimental capsules, the IRC recommended that the meltdown flange on the capsule end fixtures be increased in width to 0.030 ± 0.002 in.

1. FCF Process Analysis and Testing (M. J. Feldman)

Last Reported: ANL-7438, p. 67 (March 1968).

(i) Test and Analytical Methods. Installation of hollow cathode lamp sources, a burner, and an optical system in the Junior Caves has been completed. After calibration, this equipment will permit determination of Mo, Ru, Rh, Pd, Fe, and Ni in "hot" fuel samples by atomic absorption. Optical alignment of the system has been completed, and calibration work is under way. Atomic absorption analysis of "hot" fuel will reduce the wet chemistry manipulations presently required for analysis of irradiated fuel.

The equipment required for foil exposure and transport for neutron radiography has been received from the vendor and is undergoing mechanical acceptability tests in the mockup facility.

m. FCF Equipment Improvement (M. J. Feldman)

Last Reported: ANL-7427, p. 76 (Feb 1968).

(i) Processing Equipment. The experimental capsules which are removed from EBR-II for surveillance must be rebonded prior to reinsertion in the reactor. The bonding technique must provide steady forces so that the fuel will not be subjected to damage from impact or vibration. Preliminary theoretical investigations showed that electromagnetic forces could be utilized to remove sodium voids while not subjecting the fuel to any shock. Feasibility tests of prototype equipment will be made.

(ii) Auxiliary Equipment. The design of the in-cask subassembly grapple is essentially complete.

(iii) Repair and Decontamination. Detail designing for the equipment-decontamination facility is being undertaken. Bids for the manipulator-decontamination facility are being evaluated.

- n. FCF Experimental Support--Hot Fuel Examination Facility (HFEF)--Feasibility and Cost Study (N. J. Swanson)

Last Reported: ANL-7438, p. 67 (March 1968).

A meeting was held with Pacific Northwest Laboratory personnel to compare the features of HFEF with those of the FFTF inert-gas-cell examination facility, as requested by DRDT. A plan was developed to enable the two projects to take advantage of each other's efforts in common areas. The basic differences in the two projects and the reasons for these differences were defined for DRDT.

Work continued toward the establishment of the HFEF/FCF interfaces. A transmittal to DRDT defined the projected overall long-range examination capabilities at the EBR-II Site, including the provisions at HFEF, FCF, and the Plutonium Chemistry Cells. This transmittal included also a summary of the functional priorities presented to the project by prospective users.

The primary factors involved with site selection have been discussed and are to be reviewed.

New approaches to the facility layout were taken. A concept in which the alpha-clean cell is provided in the basement rather than the first floor area appears quite attractive. Other major efforts include investigations of concepts for transfer penetrations and remote materials handling.

- o. Reactor Improvements, Nuclear Instrument Test Facility Study (B. C. Cerutti)

Last Reported: ANL-7438, p. 68 (March 1968).

Gamma-flux mapping of the thimble for the instrument test facility was performed at a reactor power level of 45 MWt. A plot of the gamma flux is shown in Fig. I.E.11.

Following the gamma-flux mapping, the gamma detector was removed and replaced by a fission detector. A test run was made to determine the detector position where saturation of the counting equipment occurred. Saturation (10^5 cps) occurred at 9 ft above the core centerline with the reactor operating at 45 MWt. The flux level at this position in the thimble was approximately 2.5×10^5 n/cm²-sec.

Circuit design has been completed for removal of the thimble-temperature signal from the reactor protective circuit.

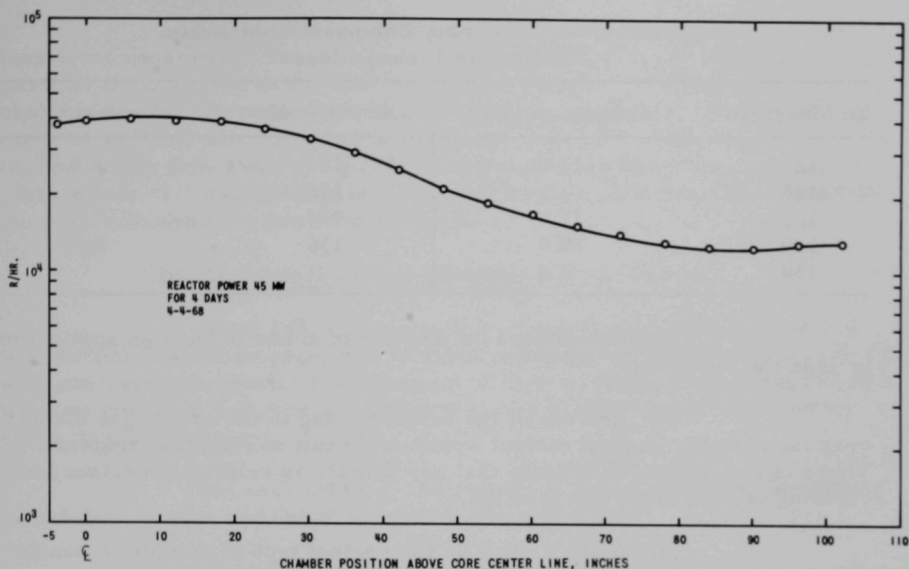


Fig. I.E.11. Gamma-flux Plot

p. Feasibility Study of Fuel Failure Detection--Chemical and Mechanical Methods

Last Reported: ANL-7438, pp. 68-70 (March 1968).

(i) Trace Elements Analytical Techniques (C. E. Crouthamel)

The technique devised for placing tagged elements in the fuel (see Progress Report for October 1967, ANL-7391, p. 106) is planned principally for metal fuels having a sodium bond between the fuel and the cladding. A shift in emphasis to other fuels (e.g., oxide or carbide) would probably require a change in the method of placement of the tag in the fuel. A complementary technique that is being evaluated, but which is somewhat outside the scope of the task as originally defined, would use fuel-element tags consisting of various mixtures of the five light xenon isotopes, namely, ^{124}Xe , ^{126}Xe , ^{128}Xe , ^{129}Xe , and ^{130}Xe , in unique ratios of isotopic composition (none of these isotopes are produced in fission in significant yields). Xenon that is highly enriched in the light isotopes is commercially available from Mound Laboratory; the isotopic composition of the mixture is given in Table I.E.25. It is anticipated that by the use of this isotopic mixture, in combination with varying amounts of isotopically pure ^{128}Xe (prepared by irradiation of iodine), many unique tags could be devised (perhaps as many as 100). Depending on the quantity of pure ^{128}Xe added, the measurement of either the $^{124}\text{Xe}/^{128}\text{Xe}$ or the $^{129}\text{Xe}/^{128}\text{Xe}$ ratio would serve to identify a specific tag.

TABLE I.E.25. Isotopic Composition of Xenon
Enriched in Light Isotopes

Xe Mass No.	Abundance (a/o)	Xe Mass No.	Abundance (a/o)
124	12.0	131	2.8
126	4.5	132	1.4
128	17.4	134	0.3
129	59.0	136	0.2
130	2.3		

Other advantages of the use of xenon in such an application include the following:

(a) Release of the xenon gas tag to the argon-gas blanket over the primary sodium coolant would not result in chemical reaction. There is experience to indicate that gas release is relatively certain for a cladding failure at any pin location.

(b) A gas sample is the easiest type of sample to handle by automated equipment. In addition, extremely small volumes of xenon can be separated from large volumes of argon by adsorption on Molecular Sieves in remotely operated equipment.

(c) The entire argon blanket can be continuously purged of xenon (by adsorption on Molecular Sieves) so that the isotopic tags can be used repeatedly.

The xenon isotopic ratios would be determined with a mass spectrometer. The analyses could be obtained with a programmed data-accumulation system, such as one presently in use in the Chemistry Division. For a concentration of xenon of $1 \text{ cm}^3/1000 \text{ ft}^3$ of argon (1 part in 2.8×10^7), it may be possible to analyze the argon directly without batch sampling and separation of the xenon.

The times required for analyses would of course, vary with the respective concentration levels of the isotopes. Analysis time (from the time of sampling to the time of data display) could be less than one hour in a fully automated system, but might be several hours in a manual operation. These estimates do not include the time that might be required for separation of xenon from argon.

(ii) Tag Confirmation Study (F. A. Cafasso)

Design of the experimental loop for evaluating the chemical stability of tags in circulating sodium continues. The stainless steel piping to be used in the construction is being tested for wall imperfections by non-destructive methods. Fabrication of a drain tank for the loop has started.

Samples of the flowing sodium are to be taken from a stainless steel reservoir. To anticipate possible problems with sampling and gas entrainment, due to the flow and mixing behavior in this reservoir, the circulation of a dye in water (whose density and viscosity approximates those of sodium) was observed in a similar reservoir made of glass. Good mixing at low flow rates (~2 gal/min) and negligible vortexing at high flow rates (up to ~8.5 gal/min) were observed, which indicate that the design of the loop-sampling reservoir is adequate.

(iii) Mechanical Failed-Fuel Locator (E. Hutter)

About 20% of the detail drawings for the prototype failed-fuel locator have been prepared. Layout drawings for the prototype test rig also are being prepared. Procurement of an electromagnetic pump for sodium flow has been deferred pending a decision to use a centrifugal sodium pump that is available.

The feasibility of using the test rig to test both the model failed-fuel locator and the prototype is being studied.

q. EBR-II Materials-Coolant Compatibility (J. E. Draley)

Last Reported: ANL-7438, pp. 70-71 (March 1968).

Assembly and inspection of many drawings and some contacts with manufacturers have made possible the compilation of a complete list of materials exposed to the primary sodium in EBR-II.

Of the materials directly exposed to liquid sodium in the primary system (see Table I.E.26), Ampco 18-13 and 18-23 (aluminum bronze), nickel, and the nickel-base alloys Colmonoy 4, Colmonoy 5, Inconel, Inconel X, and Monel may be considered of potential concern with respect to failures that are related to material dissolution. The behavior of aluminum bronze and Inconel X exposed in SURV-I (see Progress Report for November 1967, ANL-7399, pp. 88-89) at ~700°F indicates that these materials (and probably the other nickel alloys, except Monel) do not present a problem. However, some components of aluminum bronze and Inconel X are in service at ~900°F.

Monel and unalloyed nickel are exposed to sodium at ~700°F as pump bus bars. These bars are not easy to inspect as they are in locations comparable to the copper bus bars that were a problem in the past.* Monel may be suspect because of the relatively high copper content (~30%), but there has been no evidence of failure or malfunction. Data obtained at 1200°F (see Progress Report for September 1967, ANL-7382, pp. 83-86) suggests that the nickel bus bar should perform satisfactorily. There has been no indication of failure or malfunction.

*Copper from bus bars of this type dissolved into the primary coolant of EBR-II.

TABLE I.E.26. Materials Directly Exposed to EBR-II Primary Sodium

Material	Approximate Service Temperature (°F)
Ampco 18-13 Aluminum Bronze	700, 800-850, 900
Ampco 18-23 Aluminum Bronze	700
Borated (3%) Stainless Steel (probably Type 304)	700
Carbon Steel ASTM 325-55T	700
Chromium-plated 304, 410 and 420 SS	700 and 900
Colmonoy 4 and 5	900
Inconel	700
Inconel X	700
Mild Steel	700
Monel	700
Nickel	700
Stainless Steels; 303, 304, 316, 321, 347	300 to ~1000
Stainless Steels; 410 and 420	700 and 900
Steel (unspecified)	700
Steel, Type 1020 (hot-rolled)	700
Steel, SAE 4340	700
Stellites; Nos. 3 and 6	700 and 900
Tool Steels, Types 18-4-1 or 2, Rex AA, and AISI T1	700 and 900

Of perhaps most potential concern are the various "mechanical" components fabricated with ferrous alloys of relatively high carbon content, i.e., tool steel. These materials were chosen because of necessary mechanical properties such as hardness and/or strength. The relatively high carbon concentrations are necessary to achieve the required properties. It is possible that carbon has been transferring to other materials, particularly Type 304 stainless steel; this transfer may result in impairment of function of the high-carbon materials.

This possibility has led to plans to examine some of the high-carbon steel parts to check for loss of strength and hardness. Detailed plans have not yet been completed.

Many primary system materials, some of which may not be resistant to sodium, are contained within Type 304 stainless steel cladding. They are listed in Table I.E.27. Failure of at least some of the components that contain these materials may be detectable by analysis of the sodium.

TABLE I.E.27. Materials Exposed as Clad
to EBR-II Primary Sodium^a

Material	Component
Aluminum alloys 1100, 3003, 6061, 6063	Instrument thimbles
Alumina	Instrument thimbles, heat exchanger thermocouples
Boral	Instrument thimbles
Borated graphite	Neutron shielding
Carbon steel	Reactor vessel cover lift mechanism and a flowmeter
Chromel-Alumel	Heat exchanger thermocouple
Copper	Pump bus bar
Formica	Pump bus bar
Glass braid	Level control
Graphite	Neutron shielding
Lavite	Pump
Lead	Instrument thimbles
Magnesia	Flowmeter
Mica	Pump
Mild steel	Shield plug
Nylon	Instrument thimbles
Oxalloy 28 ^b	Level indicator
NaK	Pressure transducers and shutdown cooling plug
1020 steel	Magnet
Uranium	FUM-Mark-III gripper
Zirconium hydride	Instrument thimble

^aAll materials except copper and formica at ~700°F; copper and thermocouples at ~850°F; formica at 400 to 500°F.

^bCopper conductor sheathed in Type 430 stainless steel.

2. Operations--Reactor Plant

Last Reported: ANL-7438, pp. 72-76 (March 1968).

The reactor was operated for 587 MWdt in Runs 27D through 27H during April. Throughout the month the primary aim was to identify the source of fission-gas leakage from the core (see Sect. I.E.1.a). Suspected experimental subassemblies were removed from the core in four lots as leakage recurred. The last lot removed included the last of the fueled experimental subassemblies in the core, and further operation for 148 MWdt in Run 27H produced no further leakage by the end of the month. The cumulated total of EBR-II operation is 16,704 MWdt.

After startup for Run 27D on March 30, the power-reactivity decrement (PRD) was measured to be 44 lh at 45 MWt with the control rods banked at 11.00 in. [see Sect. I.E.1.a.(i)(h)]. Reactor operation was normal until April 6, when a fission-gas release occurred and the reactor was shut down. The release was indicated on the fission gas monitor (FGM) when recorded gas activity increased by a factor of 20. Radiometric analysis of the primary-tank gas blanket showed ^{133}Xe and ^{135}Xe activities to have increased by factors greater than 10. When the primary pumps were shut down another release occurred, probably because of the decreased pressure in the core. No airborne contamination developed in the reactor building during or after the release.

Experimental Subassemblies XO12, XO15, and XO17, and the special driver subassembly (C-2138) containing nineteen 70% enriched pins were removed from the reactor, and reactivity adjustments were made as required.

After startup for Run 27E, while reactor power was being leveled at 30 MWt, a scram occurred which was initiated by a low clutch-reference voltage for primary pump No. 2. The voltage regulator for the pump-control circuit was changed, since it was the most suspected component in the control circuit. Following reactor restart, however, a similar scram occurred, and further checkout of the control system revealed an intermittent short in the clutch-reference voltage circuit. A defective wire was replaced, and pump operation since that time has been normal. This pump problem was not related to the one reported last month (see ANL-7438, p. 73), since the present circuit involved was part of the modified brake-control circuit which had just been installed.

Following restart of the reactor on April 9, the PRD was measured to be 46.7 lh at 45 MWt with the control rods banked at 11.25 in. A spurious scram on April 12 provided the opportunity to reduce flow in the primary system in an attempt to induce a fission-gas release. Flow was reduced to about 23% for 10 min and then raised to 100%. Gas samples taken before and after the flow reduction indicated a small, gas-type fission-product release.

This release was not readily evident by observation of the FGM. Four experimental subassemblies: XO19, XO20, XO27, and XO32, were removed from the reactor as suspected leakers, and structural experiments XO34 and XO35 were installed for irradiation.

Following the start of Run 27F on April 15, the PRD was measured to be 37.7 lh at 45 MWt with the control rods banked at 12.25 in. Another fission-gas release was induced on April 16 by reducing flow, following a scram caused by the inadvertent grounding of the output signal from a primary flowmeter. The six remaining ceramic-fueled experimental subassemblies were then removed from the core.

Criticality for Run 27G was achieved on April 17, and the PRD was measured to be 42 lh at 45 MWt with the control rods banked at 11.00 in. Reactor operation continued until April 19, when a very slight increase in signal was seen on the FGM recorder. A primary-tank cover-gas sample was taken immediately, and just as radiometric analysis was completed, the FGM began indicating a definite increase in radioactivity in the cover gas. The analysis confirmed a fission-gas release and the reactor was immediately shut down. Surveillance of gas samples and of the FGM continued for almost an hour after shutdown, and the FGM indication, after increasing from 11 to 15 cps, stabilized at the higher level. Primary pumps were then shut down for about 20 min, leaving only the 6% primary flow from the auxiliary EM pump, and no further release was observed. Shortly after the main pumps were restarted, the FGM signal began to increase and ultimately reached 350 cps. ^{133}Xe and ^{135}Xe activities reflected similar large increases, and the reactor-building air activity temporarily increased. The two remaining experimental subassemblies, XO28 and XO29, were removed, and appropriate reactivity adjustments were made. A small gas release was noted when XO28 was raised from the core.

Reactor startup for Run 27H on April 25 was followed by about 24 hr of operation at 500 kWt and 10 hr of operation at 5 MWt, then by a shutdown of reactor and primary pumps to check for a fission-gas release. None was detected, and the reactor power was raised normally to 45 MWt early on April 28. Operation continued without incident through the end of the month. Table I.E.28 summarizes the loading changes in EBR-II during April.

3. Operations--Fuel Cycle Facility (M. J. Feldman)

Last Reported: ANL-7438, pp. 76-82 (March 1968).

a. Hot Line Operation. Additional runs were made to produce 70% enriched fission elements for use in experimental programs. Chopped pins of 70% enriched fission were blended by melting with a uranium-2 w/o silicon alloy to increase the silicon content of the fission to the 300-500 ppm range. The resultant alloy was then processed into acceptable elements. Table I.E.29 summarizes the production activities for the report period.

TABLE I.E.28. Loading Changes in EBR-II during April 1968

Date	Grid Position	Removed	Installed ^a	Comment
4/6	6A1	B-372	A-739	Removed because of suspected leakage
	6B1	B-373	A-773	
	4B2	XO12	C-2070	
	4A2	XO15	C-2060	
	4C3	XO17	C-2066	
	4B1	C-2138	C-2065	
				70% enriched irradiation completed
4/7	6F4	B-371	A-798	
4/12	2F1	C-2009	XO34	
4/13	6D2	XO19	B-371	Removed because of suspected leakage
	6B5	XO20	B-373	
	4B3	XO27	C-2009	
	6F1	XO32	A-789	
	7B4	A-813	XO35	
4/17	7F3	XO10	A-813	Removed because of suspected leakage
	7A1	XG02	A-748	
	7D1	XG03	A-735	
	7B1	XG04	A-799	
	5B2	XO33	C-2067	
	6C1	XO31	B-385	
4/20	6C5	B-363	A-723	Removed because of suspected leakage
	6D1	B-374	A-785	
	6C1	B-385	A-787	
	4D3	XO28	C-2068	
	4E3	XO29	C-2071	

^aA--Depleted-uranium inner-blanket subassembly;

B--Row-6-type driver-fuel subassembly;

C--Driver-fuel subassembly;

X--Experimental subassembly.

TABLE I.E.29. Production Summary for Hot Line

	4/1/68 through 4/30/68	Total This Year
1. Subassemblies received: Core, Control, Safety Other	10 1	41 6
2. Subassemblies Dismantled (for processing)	13	44
3. Subassemblies Dismantled (for examination, etc.)	2	5
4. Subassemblies Fabricated	3	13
5. Subassemblies Transferred to Reactor: Subassemblies Stored in L&O Vault and Interbuilding Corridor	5 0	17 0
6. Elements Decanned: From Irradiated Subassemblies Rejects Other Total Decanned	655 83 83 821	2,651 205 161 3,017
<u>Melt Refining</u>		
	<u>Irradiated Fuel</u>	<u>Recycle Material</u>
7. Number of Runs	2	1
8. Average Pour Yield, % 1968 to Date (Total)	90.7 16	87.7 8
<u>Processing</u>		
	<u>3/1/68 through 3/31/68</u>	<u>Total This Year</u>
9. Injection-casting Runs (Total Number)	4	26
10. Elements Processed: Accepted Rejected	325 55	1,520 232
11. Elements Welded: Rewelded	170 0	1,089 0
12. Elements Leak-tested: Accepted Rejected	51 0	1,138 18
13. Elements Bonded (including recycle)	256	1,733
14. Elements Bond-tested: Accepted Rejected	142 15	1,306 92
15. Elements to Surveillance Number of Subassemblies	157 4	838 26
<u>Waste Shipments</u>		
16. Cans to Burial Ground	10	26
17. Oxide and Glass Scrap to ICPP	0	18

Construction of a truck lock and of the second-story addition to the FCF office building has started. The truck lock will provide a ventilation barrier for loading and unloading casks from trucks, and an area for decontaminating truck beds and casks.

b. Cold Line Operation. Normal productive operations were conducted throughout the month. A summary of the month's production data is given in Table I.E.30.

TABLE I.E.30. Production Summary for Cold Line

	4/1/68 through 4/30/68	Total This Year
1. Alloy Preparation Run:		
New Fuel	0	6
Remelts	7	19
Total	7	25
2. Injection-casting Runs	13	45
3. Pins Processed:		
Accepted	1,020	3,675
Rejected	45	205
4. Elements Welded	580	2,533
Elements Rewelded	1	14
5. Elements Leak-tested:		
Accepted	580	2,644
Rejected	0	40
6. Elements Bond-tested:		
Accepted	670	2,722 ^a
Rejected	40	170
7. Subassemblies Fabricated	8	25
8. Subassemblies Sent to Reactor	2	5

^aTotal corrected. In Table II.E.17, p. 77, ANL-7348, should have been 2,052 rather than 4,116.

c. Maintenance and Repair. One of the two remotely operated cranes in the argon cell became inoperative as a result of the failure of the drive motors for the trolley and hoist. Tests were conducted remotely in an attempt to remedy the situation or aid in defining the cause of the failure. These tests were not successful, and the trolley has been removed from the shielded cells for further tests and repair. The crane hook was all the way down (floor level) at the time of failure; consequently, it was necessary to remove the block and hook before removing the trolley from the bridge. Design work is underway on an unshielded crane trolley which can be used as required as a temporary replacement.

The spare carriage for the operating manipulators was received from the vendor and is undergoing preoperational tests in the mock-up facility. This use of the carriage will allow routine removal of all the carriages for maintenance without reducing the capabilities of in-cell operations.

d. Analyses

(i) Chemical Analyses. The numbers of fuel product analyses on hot-line, cold-line, and vendor fuel samples, together with the average values and ranges, are tabulated below:

Analyzed for	Number	Average Value	Range
U (total and isotopic)	23		
U (total)		94.66 w/o	94.29-95.36
²³⁵ U (% of total U)	21	52.12 w/o	51.92-52.27
Pu (total and isotopic)	5		
Pu (total)		1270 µg/g	1200-1480
Mo	27	2.48 w/o	2.37-2.59
Ru	15	1.97 w/o	1.79-2.10
Rh	15	0.273 w/o	0.257-0.307
Pd	20	0.189 w/o	0.180-0.197
Zr	20	0.080 w/o	0.049-0.120
Nb	14	0.014 w/o	0.010-0.020
Fe	27	450 ppm	68-2060
Al	8	140 ppm	60-300
Si	53	435 ppm	270-1010
Ni	11	142 ppm	82-192
Cr	12	<23 ppm	
C	11	290 ppm	165-355

Total Analyses: 282

Analyses for surveillance of irradiated pins from the reactor are tabulated below:

Analyzed for	Number	Average Value	Range
Total U	1	94.31 w/o	
Total Pu	1	1584 µg/g	
²³⁵ U	1	51.54 w/o	
Fe	3	320 ppm	275-355
Al	1	90 ppm	
Si	16	264 ppm	100-1100
Tc	9	256 µg/g	117-455
Ni	2	78 ppm	72-84

Total Analyses: 34

(ii) Postirradiation Analyses of EBR-II Fuel. All the fuel elements from Subassemblies C-2111 and C-2113, which had been suspected of containing a leak, have undergone low-power-irradiation leak checks in TREAT. These tests failed to indicate any leaks.

It is postulated that a very small leak could be plugged with a reaction product of sodium and that the internal pressures generated within the jacket are not sufficient to dislodge this plug. Previous measurements of the level of bonding sodium in these elements showed that no sodium had been lost. Therefore, if any leak exists, it must be above the normal sodium level

in the elements. Equipment is being built to test the sections of the jackets of these elements above the top of the sodium level. The jackets will be cut approximately 5 in. from the top of the element, washed to remove any sodium deposits, and subjected to internal pressures of 1-2000 psi of helium.

As a part of the surveillance program to evaluate the irradiation performance of driver fuel produced in the FCF cold line, three subassemblies were installed in the EBR-II core during Run 27. These subassemblies: C-2124, C-2121, and B-388, are three of six which will be irradiated to burnup increments in the range of 0.6 to 1.2 a/o. The remaining subassemblies of this program: C-2120, C-2129, and C-2130, are scheduled to begin irradiation at the beginning of Run 28.

As a part of the EBR-II Driver Fuel Anomalous Swelling Program, a total of 182 elements from Subassemblies C-295 and C-2036 have been subjected to normal surveillance examinations following irradiation to calculated fuel burnup of 1.09 a/o and 1.20 a/o, respectively. Subassembly C-295 is intended to provide data concerning the effects of differences of fuel enrichment (nominal 52% ^{235}U versus 48% ^{235}U) on irradiation swelling of the fuel. As expected, preliminary results obtained from examination of these elements indicate little effect of fuel enrichment on the irradiation swelling of the fuel pins.

Subassembly C-2036 is one of a pair of subassemblies (the other being C-2027 which is being held in the reactor storage basket following irradiation to 1.2 a/o burnup) which contain only fuel from the same casting batches. These batches were expected to exhibit minimal irradiation swelling, and it was believed that one subassembly of the pair (C-2027) could become a candidate for irradiation to a fuel burnup greater than 1.2 a/o if postirradiation examination of its companion (C-2036) indicates this to be feasible. Only preliminary results of the examination are currently available for C-2036, but these data indicate low swelling for the fuel. It is expected that a request for irradiation of C-2027 to a burnup greater than 1.2 a/o will be made as soon as final results are evaluated.

A total of 48 elements from five irradiated subassemblies were given postirradiation examinations to determine fuel swelling as a part of the continuing FCF Product Analysis Program. In this program, each production batch of fuel is evaluated for its irradiation performance, and this information is correlated to production parameters, chemical analyses, metallographic analyses, etc.

Indications of possible cracking of the seamless-tube cladding of an irradiated driver-fuel element (Element 16 from spent Subassembly C-249) during metallographic analysis conducted by ANL-MET prompted a review of FCF subassembly-fabrication records in order to indicate those

which possibly contained elements utilizing seamless tubing. The review showed that 10 subassemblies in the reactor possibly fitted this category. The decision was made to remove these subassemblies (B-352, B-354, B-355, B-356, B-357, B-358, B-359, B-360, C-2003, and L-447) from the core. These subassemblies are currently being subjected to normal post-irradiation examinations in the FCF. This effort should provide information concerning the adequacy of seamless tubing in driver-fuel elements.

Subassembly C-2138, containing 19 elements enriched to 70%, has been removed from the reactor after having been irradiated to 0.3 a/o burnup. Postirradiation surveillance of these elements will be conducted before subjecting companion subassemblies containing 70% enriched elements to higher burnups. The use of the 70% enriched alloy is a part of the Higher Power Operations test program.

Postirradiation examination of five 6th-row, B-type subassemblies (B-354, B-355, B-357, B-358, and B-359) revealed that fuel pins fabricated from four specific U-5 w/o Fs casting batches displayed unexpectedly high irradiation swelling. Following irradiation to a maximum subassembly burnup of approximately 0.99 a/o (0.83 a/o average), preliminary maximum values of volume swelling for some fuel pins were as follows: Batch 4126--16%; 4130--13%; 4131--13%; and 4132--11%. These values compare with a maximum swelling of 10% that would be predicted for fuel categorized as "high swelling type" at this burnup level.

Upon obtaining these results, it was ascertained that no fuel fabricated from these casting batches is present in EBR-II. The swelling values cannot be correlated with fuel silicon content because this analysis was not made at the time of injection casting of the fuel. Pin sampling for chemical and burnup analyses and metallographic investigation have been initiated in an effort to provide further information regarding the unexpected swelling.

PUBLICATIONS

LIQUID-METAL FAST BREEDER REACTORS--CIVILIAN

Selected Fission Cross Sections for ^{232}Th , ^{233}U , ^{234}U , ^{235}U , ^{236}U , ^{237}Np , ^{238}U , ^{239}Pu , ^{240}Pu , ^{241}Pu , and ^{242}Pu

W. G. Davey

Nucl. Sci. Eng. 32, 35-45 (April 1968)

Argon Cell Used to Reprocess Reactor Fuel

W. F. Holcomb

Cryogenic Eng. News 3, 21-25 (April 1968)

An Exploratory Study of the Behavior of Niobium- and Vanadium-base Alloys in Oxygen-contaminated Sodium

Harry A. Levin and Sherman Greenberg

ANL-6982 (Jan 1968)

Tube-Burst Tests on Irradiated EBR-II Type 304L Stainless Steel Fuel Cladding

W. F. Murphy and H. E. Strohm

Nucl. Appl. 4, 222-229 (April 1968)

Technology of Sodium Cooled Fast Reactor Fuels in the U.S.

J. M. Simmons, E. R. Astley, E. A. Evans, J. H. Kittel, D. A. Moss, and A. Strasser

Fast Breeder Reactors, Proc. Conf., London, May 17-19, 1966.

Pergamon Press, Oxford, 1967, p. 615

II. GENERAL REACTOR TECHNOLOGY

A. Applied and Reactor Physics Development-- Research and Development

1. Reactor Code Center (M. Butler)

Last Reported: ANL-7438, p. 84 (March 1968).

During the first quarter of 1968 the Center distributed a total of 171 program packages. This is somewhat lower than anticipated due to the changeover to the larger-core 1401 computer and associated downtime. This change will allow standard utilization of 800-bits per inch (bpi) recording rather than the 556 bpi used previously.

New programs assimilated into the Center library include an IBM-360 version of AISITE2 from Atomics International, GAKIN and GAMBLE5 from Gulf General Atomic, NAP from Illinois Institute of Technology Research Institute, and DESTHEC-DP, KANT, PROCOPE, and CDC-1604 versions of AIREK-MOD and MAC-RAD from the ENEA Computer Programme Library. These programs are now available for distribution upon request.

Corrected versions of the Center programs: 251, SAFE-AXISYM for the IBM-7044, and 252, SAFE-PLANE for the Univac 1108, have replaced the original IBM-7044 programs.

2. Theoretical Reactor Physics

a. Cross Section Data Evaluation (C. N. Kelber)

Last Reported: ANL-7438, p. 84 (March 1968).

(i) ENDF/B Processing. Many of the ENDF/B materials, which were processed through ETØE and MERMC2 on the CDC-3600, have now been processed through the system 360 versions of these codes. Difficulties arose in running ETØE for some materials because of differences in the two systems. Most of these problems were solved by making minor changes in ETØE. Some DAMMET problems had to be rerun to provide new input tapes to ETØE because the Fortran BACKSPACE statement on the 360 system will work properly only with unblocked data.

(ii) ^{235}U Evaluation. The Fortran program which calculates infinite-dilution capture and fission cross sections from unresolved resonance parameters by integrating over the appropriate statistical distributions has been extended. The scattering cross sections are now calculated, and the program varies fission widths and reduced neutron widths internally

for $\ell = 0$ neutrons in order to give agreement with input average fission and capture cross sections. A set of unresolved resonance parameters has been derived for ^{235}U and is being combined with the ENDF/B data which do not now have unresolved parameters.

(iii) ^{239}Pu Evaluation. The OS-360 versions of CODILLI and CURVEPLOT were used in an attempted multilevel analysis of the Sacloy data for ^{239}Pu fission in the energy range from 46 to 70 eV. The process has revealed a discrepancy between the two codes; this is not due to numerical errors, as conversion to double precision has shown. In cooperation with F. T. and D. B. Adler the results were compared to results obtained with their version of the codes using the same data and parameters. The tentative conclusion appears to be that there is a logical error in CODILLI which will have to be found and corrected before the data analysis proceeds further.

b. Reactor Computations and Code Development (B. J. Toppel)

Last Reported: ANL-7419, pp. 90-95 (Jan 1968).

(i) ARC System Development. The ARC system utilities are being improved to permit users to simply modify, or add to input data when rerunning a previous calculation. The new capability requires the user to supply only new data and eliminates the need to duplicate input data previously saved and retrievable in the ARC system data pool.

(ii) Phase-1 Fuel-cycle Package. Test runs are continuing on the one-dimensional system. Output edits have been debugged. The major portions of the work remaining are a cleanup of the output formats, implementation of the general input processor, and inclusion of special search routines for the initial steps of the solution.

The special search procedures will give a rapid approximate solution in order to save running time in the more accurate, but time-consuming, regular searches. Consider an equilibrium problem with scatter-reloading, for which the required fresh fuel enrichment e and the burnup time Δt_B are unknown. Given guesses of these values, $e^{(0)}$ and $\Delta t_B^{(0)}$, the problem is to find approximately correct values and approximate atom-density vectors for the partially burned portions of the reactor charge at the start of the burn step (t_0).

The solution procedure is as follows. First, assume that the fresh feed-density vector $n_1^{(0)}(t_0)$ for each material applies to all partially burned fuel for that material. Solve for the flux $\phi^{(0)}(t_0)$. Now determine the burn matrices $B^{(0)}[\Delta t_B^{(0)}]$ and find the partially burned fuel-density vectors $n_1^{(0)}[t_0]$ and $n_1^{(0)}[t_0 + \Delta t_B^{(0)}]$ for all fractions of each material. Test the burnup

of the batch fractions to be discharged at $[t_0 + \Delta t_B^{(0)}]$ and adjust Δt_B until the burnup criterion is satisfied. For this new burn time $\Delta t_B^{(1)}$ find $n_i^{(1)}[t_0]$ and $n_i^{(1)}[t_0 + \Delta t_B^{(1)}]$ for all materials and batch fractions as above.

Now define

$$k_\infty = \frac{\text{Production}}{\text{Absorption}} = \frac{\int_{\vec{r}} \int_E \nu \Sigma_f(\vec{r}, E) \phi^{(0)}(t_0, \vec{r}, E) dE d\vec{r}}{\int_{\vec{r}} \int_E \Sigma_a(\vec{r}, E) \phi^{(0)}(t_0, \vec{r}, E) dE d\vec{r}}.$$

Compute $\Delta k_\infty = k_\infty[t_0 + \Delta t_B^{(1)}] - k_\infty[t_0]$ and assume that $\Delta k_{\text{eff}} \equiv \Delta k_\infty$. Given the required k_{eff} at the time $[t_0 + \Delta t_B^{(1)}]$, the end of the burn step, find

$$k_{\text{eff}}[t_0] = k_{\text{eff}}[t_0 + \Delta t_B^{(1)}] - \Delta k_{\text{eff}}.$$

Now perform an enrichment search to $k_{\text{eff}}(t_0)$ at t_0 with no control poison in the system. Each change in $e^{(k)}$ requires recalculation of all density factors $n_i(t_0)$, using the burn matrices $B^{(0)}[\Delta t_B^{(1)}]$.

When the enrichment search is completed, one has improved estimates of required burnup time, fresh-fuel enrichments, and atom-density vectors of the partially burned fuel in the reactor at the start of the burn. Normal search procedures are now initiated.

Two-dimensional problems are being tested. Since the burnup modules and routines are independent of the dimensionality of the neutronics model, this system is already in an advanced state of development consistent with the advanced status of the two-dimensional diffusion-theory modules in the ARC system. Problems to date have been related to the greatly increased storage requirements of two dimensional cases.

(iii) Flux Synthesis. A finite-difference formulation of the differential equations arising in connection with the variational flux synthesis technique reported in ANL-7419 has been completed. Flow charting of the algorithms to execute its solution with the IBM-360 computer in the ARC system is near completion.

In preparation for numerical experimentation with the flux-synthesis algorithms, an ARC system standard path has been written to generate a set of one-dimensional neutron-diffusion-theory solutions for use as trial functions. Owing to the ease with which modules and standard paths may be linked in the ARC system, generation of this new path involved only a trivial Fortran exercise.

B. Reactor Fuels and Materials Development

1. Fuels and Claddings--Behavior of Reactor Materials

a. Irradiation Behavior of Advanced Ceramic Materials (L. C. Michels)

Last Reported: ANL-7438, pp. 91-92 (March 1968).

Neutron radiography of the specimens in capsule ANL-56-8 has been completed. This capsule was removed from the MTR at the end of Cycle 272 after an anomalous temperature excursion. The capsule contained four specimens of uranium sulfide pellets and two specimens of vibratorily compacted UC-PuC powders. Corrected data for the specimens are given in Table II.B.1.

TABLE II.B.1. Specimens in Capsule ANL-56-8

Specimen Number	Design Parameters ^a		Operating Conditions		
	Fuel Composition (w/o)	Effective Density (%)	Max Cladding Temp (°C)	Estimated Burnup to Date	
				U + Pu (a/o)	fiss/cc x 10 ^{-20b}
MV-3	UC-20 PuC	81	715	9.9	28
MV-5	UC-20 PuC	80	705	9.6	27
S-7	US	80 ^c	535	8.0	15
S-8	US	89	725	10.2	20
S-9	US	76 ^c	750	10.2	19
S-10	US	91	690	10.2	22

^aAll cladding is Nb-1 w/o Zr alloy of 0.281-in. OD and 0.012-in. thickness.

^bBased on effective density.

^cPartially annular pellets; Specimen S-7 contained a center thermocouple.

Specimens S-7, S-8, and S-10, all of which contained uranium sulfide pellets, exhibited some indication of diametral swelling, pellet cracking, and pellet separation. However, Specimen S-9, which also contained uranium sulfide pellets, appeared intact with no detectable changes. The pellets in Specimen S-9 were annular in contrast with the solid pellets in Specimens S-8 and S-10. Specimen S-7, which also contained annular pellets, had a sheathed thermocouple inserted in the annulus.

The fuel density of one of the two UC-PuC specimens, MV-3, appeared to vary along the length of the pin. The other specimen, MV-6, showed no evidence of this variation.

b. Structures and Properties of Advanced Fuel Materials
(J. H. Handwerk)

Last Reported: ANL-7438, pp. 92-95 (March 1968).

(i) Thermodynamic Properties of PuO₂. The heat capacity equation

$$C_p = 22.18 \times 2.080 \times 10^{-4} T - 4.935 \times 10^5 T^{-2}, \quad (3)$$

given in ANL-7438, is plotted in Fig. II.B.1 along with Sandenaw's low-temperature values.* The coincidence of the two curves in the region near room temperature effectively confirms the low-temperature data.

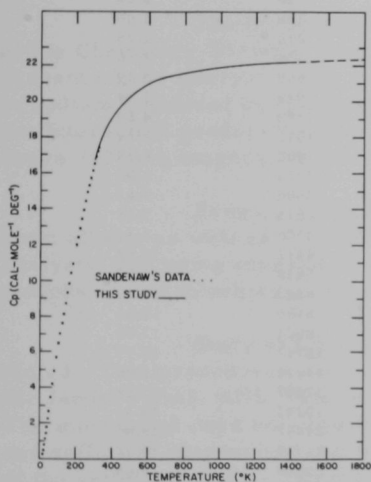


Fig. II.B.1. Heat Capacity of PuO₂ as a Function of Temperature

heat capacity of approximately $23 \pm 1 \text{ cal mole}^{-1} \text{ deg}^{-1}$ for PuO₂ at its melting point of $2663 \pm 20^\circ\text{K}$.†

c. Fundamentals of Corrosion in Liquid Metals (S. Greenberg)

Last Reported: ANL-7427, pp. 99-101 (Feb 1968).

(i) Corrosion Inhibition by Dissolved Getters in Liquid Sodium Environment. The results of analyses of vanadium-alloy samples before

*Sandenaw, T. A., J. Nucl. Mater. 10, 165 (1963).

**Forsythe, G. E., J. Soc. Indust. Appl. Math. 5, 74 (1957).

†Lyon, W. L., and Baily, W. E., General Electric Report GEAP-4878 (1966).

and after exposure to 650°C sodium that contained about 100 ppm magnesium are given in Table II.B.3. Less than 2% of the weight gains were attributable to magnesium, and less than about 10% were due to nickel. Additional samples were subjected to general survey spectro-analysis of "order-of-magnitude" accuracy; results show that V-15 w/o Cr-5 w/o Ti picked up small amounts of iron in addition to the other elements listed in Table II.B.3.

TABLE II.B.2. Molar Thermodynamic Properties of PuO_2

T (°K)	C_P° (cal mole ⁻¹ deg ⁻¹)	$S_T^\circ - S_{0^\circ\text{K}}^\circ$ (cal mole ⁻¹ deg ⁻¹)	$H_T^\circ - H_{0^\circ\text{K}}^\circ$ (cal mole ⁻¹)	$-(G_T^\circ - H_{0^\circ\text{K}}^\circ)/T$ (cal mole ⁻¹ deg ⁻¹)
25	0.80	0.43	7	0.15
50	2.62	1.50	48	0.54
75	4.58	2.94	138	1.09
100	6.35	4.50	276	1.75
125	7.89	6.09	454	2.46
150	9.28	7.65	669	3.19
175	10.61	9.18	918	3.94
200	11.92	10.69	1199	4.69
225	13.20	12.16	1513	5.44
250	14.42	13.62	1858	6.18
275	15.56	15.05	2233	6.92
298.16	16.50	16.34	2605	7.61
300	16.57	16.44	2635	7.66
350	18.15	19.12	3506	9.11
400	19.19	21.62	4441	10.52
450	19.85	23.92	5418	11.88
500	20.30	26.04	6423	13.19
600	20.93	29.80	8486	15.66
700	21.33	33.06	10601	17.91
800	21.57	35.92	12747	19.99
900	21.76	38.47	14914	21.90
1000	21.90	40.76	17097	23.68
1100	22.00	42.87	19293	25.33
1200	22.08	44.79	21497	26.87
1300	22.17	46.56	23710	28.32
1400	22.22	48.20	25929	29.68
1500 ^a	22.27	49.74	28153	30.97
1600 ^a	22.32	51.17	30383	32.19
1700 ^a	22.36	52.53	32617	33.34
1800 ^a	22.39	53.81	34855	34.44

^aExtrapolated.

TABLE II.B.3. Relative Amount of Gravimetric Weight Change after Exposure of Vanadium Alloys to Magnesium-gettered Sodium at 650°C^a

Element	Weight Change (%)			
	V-20 w/o Ti		V-15 w/o Cr-5 w/o Ti	
	Coupon	Foil	Coupon	Foil
C	86.5	90.6	78.9	92 ^b
H	-1.5	0.11	-0.7	0.22
O	5.4	-0.55	15.9	-0.55
N	11.5	2.56	3.1	1.87
Total	101.9	92.7	97.2	93.5

^aCoupons were exposed for 180 hr, and foils subsequently for 168 hr.

^bResult based on analyses of a second section of this foil after first result indicated only 57% carbon.

Carbon contributed most to the weight gains. From thermodynamic considerations, magnesium would not be expected to protect these alloys from carbon interaction. Examination of samples exposed for longer times may reveal whether the carbon interaction warrants attempts to provide inhibition.

The magnesium concentration in the loop sodium has been increased to a value closer to that originally intended. (Previously, interaction of magnesium with the nickel loop resulted in a low concentration of magnesium in sodium.) The new value, 740 ppm, is based on analysis of a dip sample taken at 650°C. A nickel concentration of 160 ppm was also reported.

The method of chemical analysis developed by K. Jensen of the Chemistry Division recovers magnesium from the interaction product present on the interior of the nickel sampler, as well as magnesium present in sodium contained by the sampler. (The nickel analysis did not include the interaction product retained on the sampler wall.) Seventy ppm of the above 740 ppm magnesium were recovered from the interaction product.

Freshly prepared coupon and foil samples of the two vanadium alloys, as well as a vanadium-wire sample for later internal friction analysis, are being exposed to the gettered sodium at 650°C. Exposure periods of one month are planned.

Study of the magnesium-nickel interaction has been completed. Test procedures were described previously (see Progress Report for January 1968, ANL-7419, p. 106). Table II.B.4 summarizes the results. The interaction does not constitute a hazard in present loop experiments, and sufficient magnesium can be maintained in solution for the purposes of the gettering study. The nickel results of Table II.B.4 are not well understood; insert weight gains were higher than may be accounted for by magnesium pickup alone.

TABLE II.B.4. Interaction Product on Nickel Surfaces That Contact Na-Mg Solution at 650°C

Capsule	Time at 650°C (hr)	Insert Weight Gain (mg/cm ²)	Average Thickness of Two- layer Surface Product (μ)		Analysis of Sodium ^a after Test (mg)	
			Inner Layer	Outer Layer	Mg	Ni
DG 13	17	0.551	1.7	2.7	23.2	1.8
DG 14	108	0.597	2.0	3.6	8.6	0.9
DG 16	159	0.652	2.6	3.4	5.2	0.9
DG 15	175	0.840	4.2	2.8	5.5	2.1
DG 17	319	1.67	3.9	5.1	2.0	1.1

^aQuantities of materials loaded into each capsule were 5 g sodium and 46 mg magnesium for 63 cm² of nickel surface in contact with the sodium.

Electron microprobe analysis of the interaction product on Capsule DG 15 yielded the results given in Table II.B.5. The corrected concentration for carbon would probably be higher than that shown, but accurate correction data are not available.

TABLE II.B.5. Composition of Mg-Ni Interaction Product of Capsule DG 15^a

Element	Measured Concentration (w/o)	Concentration Corrected for X-ray Absorption (w/o)
Ni	83.7	
Mg	4.6	11.2
C	1.7	

^aSpecimen prepared by wet-polishing techniques that would not preserve surface sodium.

Metallographic preparation techniques are being tested that are designed to preserve any sodium present in the interaction product, as well as in the surface product of exposed vanadium alloy samples.

2. Fuels and Claddings--Chemistry of Irradiated Materials

- a. Development of Analytical Facilities, Microstructure Sampling Techniques, and Analytical Procedures for Analysis of Irradiated Fuels (C. E. Crouthamel)

Last Reported: ANL-7438, pp. 95-96 (March 1968).

Construction of a shielded fuel-evaluation facility continues. Minor difficulties with the operation of the transfer locks have been corrected. The pressure-control system for the inert-atmosphere enclosure is operational. Two instruments, a cathodic etcher and a vapor deposition unit, have been installed in the cell for testing the high-vacuum system that services these instruments.

A pneumatic-tube system will be used to transport samples between the shielded fuel-evaluation facility and the analytical-instrument complex. A mockup of the pneumatic system has been set up, and the operation of various components is being tested.

Outside contracting work on the analytical-instrument facility has been completed. The control instruments for the spark-source mass spectrometer have been assembled in a single relay rack to provide greater

flexibility of operation. The internally shielded electron microprobe has been moved to the analytical complex; realignment of the electron and X-ray optical systems is in progress.

b. Postirradiation Studies of Reactor Fuels (M. D. Adams)

Last Reported: ANL-7427, pp. 102-105 (Feb 1968).

(i) Mass-spectrometric Analysis of Laser-vaporized Samples.

Laser-beam vaporization is being used to obtain very small samples of irradiated fuels for analysis. In recent work, two laser-vaporized samples from a UO_2 fuel pin (13% enriched, 6.8 a/o burnup) have been examined with a thermal-ionization mass spectrometer. The two samples, which weighed $\sim 10^{-9}$ g each, were from a series of samples prepared previously (see ANL-7427, p. 105) for alpha- and gamma-spectrometric analysis. One specimen, 1C, was taken from a porous inclusion near the periphery of the fuel. Electron microprobe analysis had previously indicated that these porous inclusions were high-burnup regions associated with fully enriched UO_2 particles in the original fuel material (see Progress Report for May 1967, ANL-7342, p. 90). The second specimen, 7A, was taken from the UO_2 matrix adjacent to the porous inclusion.

In preparation for mass-spectrometric analysis, the samples were dissolved from their glass mounts with HNO_3 containing a trace of HF , and were mounted on the filament of the mass spectrometer by evaporation to dryness. Results of uranium isotopic analysis of both specimens were as follows:

Mass No.	Relative Concentrations	
	1C	7A
234	0.25	0.26
235	13.17	6.83
236	2.07	1.21
238	84.52	91.71

The relatively higher concentrations of ^{235}U and ^{236}U in sample 1C are a further indication that the porous inclusions are associated with particles of highly enriched UO_2 .

In the mass regions of the fission product elements, peaks were observed corresponding to the following elements: for sample 1C, barium, cesium, niobium, strontium, gadolinium, praseodymium, lanthanum, cadmium, and tellurium; for sample 7A, barium, cesium, strontium, gadolinium, and praseodymium. The concentrations of rare earths observed in the porous inclusion (1C) were relatively higher than those in the UO_2 matrix (7A); these data also indicate that sample 1C was from a high-burnup region.

Other elements that were detected, namely, calcium, potassium, chromium, and vanadium, were probably impurities introduced either in preparation of the fuel material (e.g., chromium) or in preparation of the samples for analysis.

3. Fuels and Claddings--Thermodynamics of Fuel Materials

- a. Total Vapor Pressures and Carbon Potentials in the Ternary System U-C-Pu (P. E. Blackburn and M. Tetenbaum)

Last Reported: ANL-7419, p. 109 (Jan 1968).

A study of the vaporization behavior of the uranium-carbon system continues. Measurements of the total pressure of uranium-bearing species and carbon activity are being made as functions of temperature and UC_x composition, using the transpiration method with hydrogen-methane mixtures as carrier gases.

Our preliminary results at 2290°K indicate trends that are consistent with expectations for single-phase uranium monocarbide, namely, a sharp increase in total uranium pressure and a sharp decrease in carbon activity as the composition of the condensed phase approaches the metal-rich phase boundary. Our data appear to be in rough agreement with the uranium pressures and carbon activities obtained by Storms from mass-spectrometric measurements.*

Storms' activity measurements were made only at 2100 to 2300°K; activity measurements were not made near the metal-rich phase boundary U(1)-UC. We are initially planning to measure activities with the transpiration technique over a wider range of temperatures and compositions than those reported by Storms. Measurements of the total pressure of uranium-bearing species in the single-phase region above the miscibility gap will also be made.

4. Techniques of Fabrication and Testing--Basic Fabricability--Research and Development

- a. Development of Nondestructive Testing Techniques (H. Berger)

Last Reported: ANL-7438, pp. 96-97 (March 1968).

(i) Neutron Techniques. Work has continued in four areas of investigation:

(1) Studies of small-source techniques with the ²⁴¹Am-²⁴²Cm-Be source of 10⁹ neutrons/sec yield are being extended to evaluate a range of collimation parameters in both BeO and water moderators.

*Storms, E. K., Thermodynamics of Nuclear Materials, IAEA, Vienna (1966), Vol. I, pp. 315, 330; The Refractory Carbides, Academic Press (1967), p. 211.

(2) The reduction in reciprocity-law failure by means of cooling the scintillator-film combination has been confirmed for several different films. Quantitative measurements are underway.

(3) New scintillator mixtures have been designed, and are being tested for efficiency, inherent unsharpness, contrast, and gamma discrimination.

(4) A new test-block system has been designed, and four identical models are under construction. The models will be used to compare test characteristics between the 20 or more laboratories that now perform neutron radiography.

(ii) Passive Ultrasonic Techniques. As described previously (see Progress Report for January 1968, ANL-7419, p. 112), a lithium niobate piezoelectric element has been bonded to a Type 304 stainless steel plate with gold foil. The lithium niobate element appeared to be firmly attached to the Type 304 stainless steel capsule. Subsequently, the same method was used to manufacture a prototype acoustic sensor. The sensor was accidentally dropped, and the element broke loose. Examination of the surfaces revealed that nonuniform bonding caused the failure.

Methods for improving the bond are being evaluated. Sample sheets of Type 304 stainless steel have been plated with nickel or nickel and platinum by a vendor. Several types of metal pastes are being considered for the joining operation.

(iii) Development of an Electrodynamic Transducer. The electrodynamic method of sound generation utilizes the force produced by the interaction of mutually perpendicular electric and magnetic fields to induce mechanical (acoustic) vibrations in materials. Houck et al.* have reported the generation, but not the detection, of acoustic waves in this manner; their model assumes that the external electromagnetic fields of the coil couple directly with the electromagnetic fields of the acoustic wave.

Initially, the test piece (a 6.0-cm-long aluminum bar) was glued to a copper strap and current passed through the strap to supply the necessary electric field. This system has been simplified by eliminating the physical connection to the test piece; the copper strap has been replaced with a coil that does not touch the test piece. This arrangement has been successful both to detect and to generate acoustic waves at 5 and 20 MHz, but the system was not adequate to generate and to detect simultaneously.

Large increases in the sensitivity of the electrodynamic transducer have been achieved with a coil in a "pancake" design. This increase in sensitivity was sufficient to demonstrate, at 5 MHz, the use of the electrodynamic

*Houck, J. R., et al., Direct Electromagnetic Generation of Acoustic Waves, Phys. Rev. Letters 19, 224 (1967).

transducer for a pulse-echo technique. Additional changes in the coil design have further increased response, and other improvements in the coil system are being considered to bring the sensitivity up to that of a piezoelectric transducer.

5. Engineering Properties of Reactor Materials--Research and Development

a. High Temperature Mechanical Properties of Fuel Oxides (R. J. Beals)

Last Reported: ANL-7427, pp. 108-110 (Feb 1968).

(i) Elastic and Anelastic Properties in a Polycrystalline System $\text{UO}_2\text{-PuO}_2$. New facilities for sintering $(\text{U,Pu})\text{O}_2$ bars have now been installed and tested. Grinding techniques that will produce a specimen with a parallel-face tolerance of ± 0.001 cm have been perfected, and a different mode of sample suspension is being tried with the hope of detecting sample torsional resonance.

A solution of 75 v/o HF and 25 v/o HNO_3 has proven somewhat effective in etching $\text{U}_{0.8}\text{Pu}_{0.2}\text{O}_2$. However, a room-temperature etching time of approximately 15 hr is required to produce an acceptable etched surface.

Ceramographic studies conducted with 8.16-g/cm^3 $\text{U}_{0.8}\text{Pu}_{0.2}\text{O}_{1.98}$ (Sample No. 1) gave no indication of the presence of second-phase material. Results of efforts conducted to isolate the "skin effect" are inconclusive, and work is continuing in this area. Results of a microprobe analysis indicated that Sample No. 1 was composed of homogeneous solid solution, as indicated by about ± 4 a/o cationic variation from the mean value of Pu = 20 a/o and U = 80 a/o. The grain size of Sample No. 1 was determined by the linear intercept method and found to have an effective spherical grain diameter of 6μ .

C. Engineering Development--Research and Development

1. Development of Master-Slave Manipulator Systems (R. C. Goertz)

Last Reported: ANL-7438, p. 98 (March 1968).

a. Development of Manipulator Systems

(i) Electric Master-Slave Manipulator, Mark E4A. The irradiation test of a servo drive unit is still in progress. In order to speed up the test, the unit was moved closer to the source to obtain an exposure rate of 2.25×10^6 R/hr (more than double the previous rate). The higher exposure rate increases the temperature of the unit to 50°C .

The irradiation test was interrupted after exposures of 1.2×10^8 R and 5.9×10^8 R to make performance tests of the servo drive unit. During these tests, the motors were heat cycled 10 times between 25 and 180°C. The fields of each motor were switched on and off (150 V per field) 10 times to test for possible electrical breakdown during these transients. The measurements show that no changes have occurred in any of the motor, tachometer, or brake-solenoid parameters. There was also no change in the friction of the overall drive unit. The friction of the brake slip clutch decreased to about 75% of the original value.

As expected, the Teflon insulation on the lead wires of the synchro had failed by an exposure of 1.2×10^8 R. New synchros are being ordered with better radiation-resistant substitutes for the lead wire, bearing lubrication, and impregnating varnish.

b. Study of Remote Handling for LMFBR Facilities. A meeting was held with General Electric (GE) personnel, to discuss remote-handling problems, approaches, and current technology. Remote Control Division (ANL) participants described the manipulator-system development program at ANL. GE participants described the fuel-handling system in SEFOR, the current fuel-handling concepts for the FFTF backup, the 300-MWe plant and the 1000-MWe plant. In each of these designs, GE is providing a shielded cell over the reactor, but are planning on men entering the cells to carry out many operations and repair tasks, assuming that manned entry is possible whenever these tasks must be done. If the cell becomes contaminated, or if fuel-handling mechanisms fail, other approaches must be used. ANL pointed out that advanced electric master-slave systems--capable of working throughout the cell--could alleviate many such problems if these systems are incorporated early in the facility design. (After-thought additions are more expensive and generally less useful.) If electric master-slave systems are incorporated, they should be relied upon to do all of the in-cell tasks. GE participants will study this concept further.

Sections 1, 2, 3, and 8 of the LMFBR Program Plan were briefly surveyed to assess the remote repair, maintenance, and handling problems expected. The need for efficient ways of making remote repairs and replacements is well recognized in many areas of the Plan. In the main, the problems are noted only in general terms and the current documents contain almost no information on possible solutions. However, to maintain a high overall plant availability, advanced manipulator systems will definitely be needed. A few meetings have been held with members of the Program Office to discuss remote-handling problems and manipulator-system technology.

Remote Control Division people met with management personnel of the two principal manipulator manufacturers: Central Research Labs, and Programmed and Remote Systems. Present and future manipulator systems as well as other remote-handling problems were discussed.

Both companies stated that they consider the present condition of the Mark E4A to be state-of-the-art, and more highly developed and reliable than many other pieces of equipment going into hot facilities. Central Research went so far as to say they are planning to prepare a sheet stating the availability of the Mark E4A as one of their supplied manipulators.

2. Heat Transfer, Fluid Flow, and Mechanics of Materials

a. High Temperature Boiling Sodium Experiments (J. V. Tokar)

Last Reported: ANL-7438, p. 99 (March 1968).

(i) Niobium-1% Zirconium Loop. Since the 41 boiling runs were completed in February, the facility has been down for repairs and modifications to the radiation boiler and preheater sections, the condenser shutter-drive mechanism, and the liquid-metal helical induction pump.

As noted in ANL-7438, the liquid-metal pump has not performed properly. The vendor of the pump checked the electrical circuitry and found it in order. More operational tests are planned.

Further analysis of the experimental data from the loop has shown that installation of a flow orifice before the boiler section may help to achieve boiling stability; the size of such an orifice is being estimated. A valve will be used rather than a fixed orifice so as to provide some margin and variable control.

b. Heat Transfer in Liquid Metal Cooled Reactor Channels (R. P. Stein)

Last Reported: ANL-7438, pp. 102-105 (March 1968).

Investigations of the engineering-type relationships to account for forced-convection heat transfer during flux transients continue. In Figs. II.C.1, II.C.2, and II.C.3 are graphs which compare errors in computed transient surface temperatures when predicted by the customarily used heat-transfer-coefficient relation and by the "first" and "second" approximation forms of the new engineering-type relationships (see Eqs. 2, 3, and 4, ANL-7438, p. 104). Temperatures are predicted for the flux transient represented by

$$q = q_m e^{\alpha \tau} \sin \pi(\ell/L), \quad (1)$$

where q is the heat-flux density to the fluid in Btu/hr-ft², q_m is the initial maximum value of q , α is the exponential inverse period in sec⁻¹, τ is the time in seconds, ℓ is the axial position along the channel measured from the inlet in feet, and L is channel length in feet.

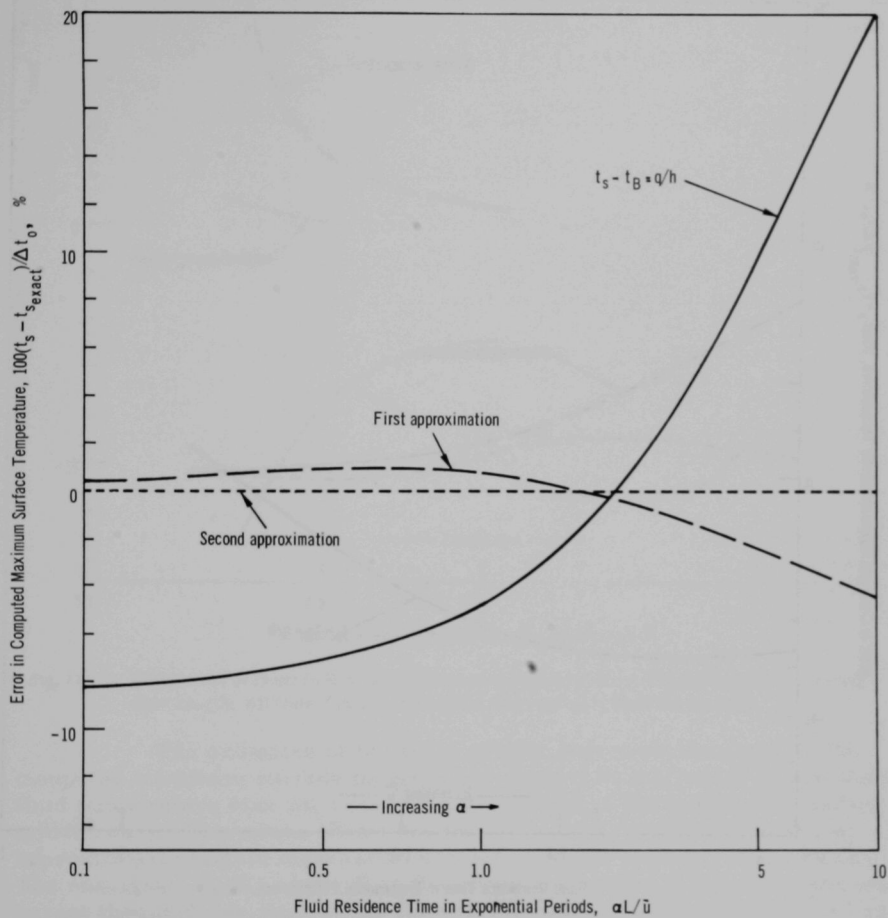


Fig. II.C.1. Comparison of Errors in Computed Transient Maximum Surface Temperatures for Decreasing Exponential Period; All Other Conditions Constant

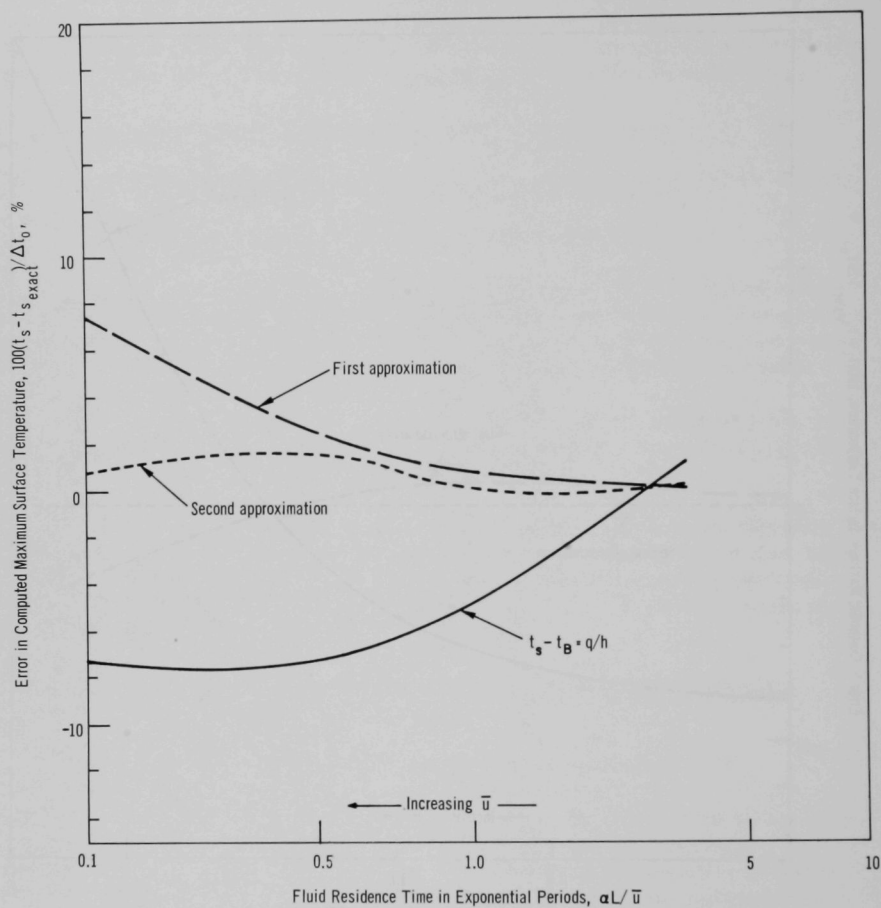


Fig. ILC.2. Comparison in Errors in Computed Transient Maximum Surface Temperatures for Increasing Fluid Velocity; All Other Conditions Constant Except Reynolds Number

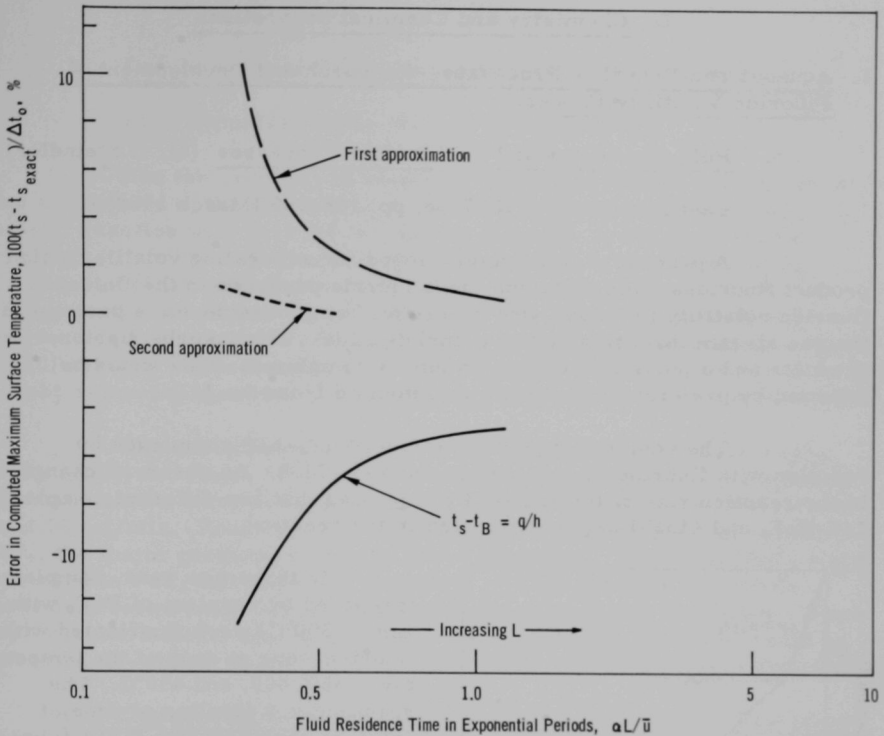


Fig. II.C.3. Comparison of Errors in Computed Transient Maximum Surface Temperatures for Increasing Duct Length; All Other Conditions Constant Except Length-to-Diameter Ratio

The ordinates of the three graphs represent the error in the computed maximum surface temperature divided by the initial steady-state fluid temperature rise Δt_0 over the entire length of the heated duct (outlet minus inlet). The values shown are for $\alpha\tau = 2.25$, which represents an approximately tenfold increase in flux from an initial steady-state value. The abscissas $\alpha L/\bar{u}$, where \bar{u} is the cross-sectional average velocity, represent the residence time of the fluid in the duct in exponential periods. For all three figures, the Prandtl number is 0.003, $\alpha\tau$ is 2.25, and, at $\alpha L/\bar{u} = 1$, the length-to-diameter ratio is 200 and the Reynolds number is 100,000.

Figure II.C.1 shows the significantly improved accuracy obtained by using the relatively simple first-approximation relationship over a hundredfold range of α . Figures II.C.2 and II.C.3 illustrate that the accuracy of the first-approximation relationship tends to become no better than the usual heat-transfer-coefficient equation when the actual fluid residence time (L/\bar{u}) decreases. For the cases explored, however, the second-approximation relationship always appears to improve accuracy significantly.

D. Chemistry and Chemical Separations

1. Aqueous and Volatility Processes--Research and Development-- Fluoride Volatility Process

a. PuF_6 Chemistry and Purification Processes (M. J. Steindler)

Last Reported: ANL-7438, pp. 108-109 (March 1968).

A procedure is being developed for separating volatile fission product fluorides from plutonium hexafluoride produced in the fluid-bed fluoride volatility process. One procedure being considered is passage of the gas stream through a bed of granulated LiF, which sorbs fission products and a portion of the plutonium as complexes. This would be followed by preferential removal of plutonium from the LiF.

The removal of plutonium from PuF_4 -LiF complexes by reaction with fluorine was described in ANL-7438. An observed change in the reaction rate of the LiF- PuF_4 suggested that two different complexes, $\text{LiF} \cdot \text{PuF}_4$ and $4\text{LiF} \cdot \text{PuF}_4$, participated in the reaction.

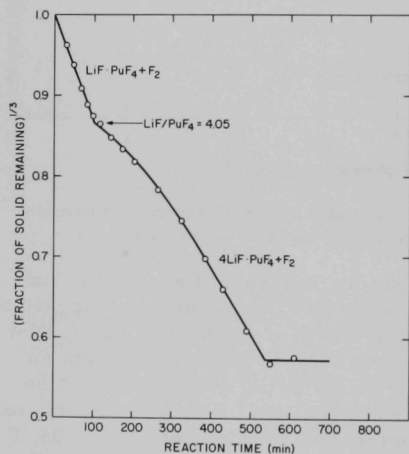


Fig. II.D.1. Reaction of LiF- PuF_4 Complexes with Fluorine at 450°C

In three new runs, samples (prepared by reaction of PuF_6 with LiF at 300°C) were fluorinated with fluorine--one at each of the temperatures 350, 400, and 450°C. The reaction as a function of time at 450°C is shown in Fig. II.D.1 (similar curves were obtained at 350 and 400°C). The discontinuities observed are consistent with a hypothetical phase diagram based on earlier work. The phase diagram predicts that at a total mole ratio of LiF to PuF_4 of 4.0, a discontinuity in reaction rate should occur signifying depletion of the $\text{LiF} \cdot \text{PuF}_4$ complex and fluorination of the $4\text{LiF} \cdot \text{PuF}_4$ complex during the remainder of the reaction. The discontinuities at mole ratios 4.2, 3.9, and 4.05 are consistent with this prediction.

Furthermore, samples of the solid phase taken after the change in reaction rate were tentatively identified as $4\text{LiF} \cdot \text{PuF}_4$ on the basis of their X-ray patterns.

b. Development of Decladding Procedures (R. L. Jarry)

Last Reported: ANL-7419, p. 122 (Jan 1968).

For the recovery of stainless steel-clad mixed-oxide fuels, a step subsequent to the HF-oxygen decladding step has been proposed, namely, reaction with pure HF to convert the oxide products of the decladding to fluorides. Such a step would potentially have the following advantages: (1) eliminate a major portion of the oxygen in the fluid-bed charge for the subsequent fluorination with fluorine, thereby reducing the fluorine requirements and simplifying recycle of the fluorinating gas phase, and (2) possibly convert some of the decladding products to volatile fluorides, thereby removing them from the fluid bed prior to the reaction with fluorine.

The reactions of pure HF with each of the compounds Fe_2O_3 , Cr_2O_3 , MoO_3 , and Nb_2O_5 have been examined, using a boat reactor system. The experiments were performed at 550°C for 2 hr with a HF flow rate of about 50 ml/min. Reaction with MoO_3 formed a small amount of volatile MoF_5 , the major products being the lower fluorides. Fe_2O_3 and Nb_2O_5 were converted to FeF_2 and NbF_3 , respectively, neither of which is volatile. Chromium sesquioxide did not react with HF under these conditions. Since these results indicate that it is unlikely that decladding products would be converted to volatile fluorides, no further work on this method is anticipated.

c. Engineering Development of Fluid-bed Fluorination Procedures
(D. Ramaswami)

Last Reported: ANL-7427, p. 121 (Feb 1968).

Engineering-scale studies are being planned to determine the feasibility of decladding and fluorinating typical fast breeder reactor (FBR) fuel bundles and to establish the process reliability. Modification for these studies of a 3-in.-dia nickel column and its auxiliaries has been initiated.

In these studies, we shall evaluate the desirability of pulsed flow of gas through a bed of inert particles instead of the steady gas flow used conventionally for fluid beds. In pulsed flow, the gas flow rate during a pulse is much greater than during conventional operation. The entire bed expands during a pulse, then contracts during the interval when the gas flow is shut off. Possible advantages of pulsed-bed operation for fluid-bed fluoride volatility processes are as follows:

1. capability for using wider ranges of particle sizes;
2. better solid-gas contacting and improved reactant utilization efficiency;

3. improved heat- and mass-transfer rates;
4. greater gas throughputs and consequently shorter fluorination times;
5. decreased elutriation of particles out of the bed.

Exploratory tests with pulsed beds were made to gain operating experience, to examine the characteristics of pulsed beds, and to compare the behavior of pulsed and steady-flow beds. The apparatus for these tests consisted of a 3-in.-dia Pyrex glass column, 72 in. long, and the auxiliaries needed to pulse the feed stream. Five sizes of granular alumina with mean particle sizes from 2380 to $2\ \mu$ were charged to the column in layers; the largest-sized alumina was charged first, then the next smaller size, and so on. The particle sizes, mass of the bed, operating time, and total gas throughput were similar to those expected during decladding and fluorinating of FBR fuels. Six runs were made, three each with pulsed and steady-flow beds.

Bed expansion was consistently greater for pulsed beds than for steady-flow beds at similar average gas flow rates. The entire bed expanded with the pulsed gas flow, whereas only top layers expanded with steady gas flow.

In the pulsed-bed runs, the layers, initially completely segregated, mixed thoroughly within about 10 to 15 min of the start of the run and remained well mixed for the remainder of the 6-hr operation. Mixing was confirmed with sieve analysis of successive portions of the bed. However, in the steady-flow runs the two lower layers remained intact for the entire period. These results suggest that the pulsed-bed mode of operation may effect mixing throughout the bed of the coarse products resulting from chemical decladding of stainless steel-clad fuels. This would avoid any problems such as caking tendencies encountered when coarse material settles to the bottom of the bed.

A Lucite mockup of a FBR fuel bundle is being constructed. This will be placed in the Pyrex column that will be operated in the pulsed-bed and steady-flow modes, permitting observation of the movement of bed material in the voids of the bundle and selection of the proper operating conditions for the 3-in.-dia nickel column to be used in future work.

d. Engineering-scale Development for $\text{UO}_2\text{-PuO}_2$ Fuel (N. M. Levitz)

Last Reported: ANL-7438, pp. 111-112 (March 1968).

Conceptual-design studies of fluoride-volatility-processing plants for LMFBR fuel are in progress. Priority of work has been placed on a large

central-plant case (uranium and plutonium load equivalent to 15,000 MWe generation rate, $\sim 10^6$ - 10^7 DF*). Various process-flowsheet alternatives are being examined. Mechanical versus chemical head-end schemes and batch versus continuous processing are being considered in these preliminary flowsheets. Specific problems examined during the report period are as follows:

(i) Method of removing sodium from fuel pins logged due to cladding failure. Early removal of sodium, before fuel-element disassembly, appeared desirable. In one scheme the fuel element, still with its shroud, would be placed in a specially designed canister. Inert gas would be forced around the fuel pins while maintaining the element at a temperature above the boiling point of sodium. The sodium would be expected to boil out of the logged tubes through the openings in the cladding. Alternatively, the sodium might be boiled off from cut fuel sections after a chopping operation.

(ii) Character of stainless steel after long irradiation. Data are needed to evaluate mechanical separation of the fuel from the cladding.

(iii) Behavior of stainless steel components in a flowsheet that includes decladding with HF-O₂ and fluorination with fluorine.

(iv) Role of interhalogens in the flowsheet as a possible alternative to a fluorine-only process, although greater current interest is in the latter process.

A reference design for the fuel assembly, selected to satisfy the present stage of our study, is from Atomics International. The design is a nonvented fuel element having a pin diameter of 0.25 in. and a cladding thickness of 0.015 in. Other ground rules, presented to this Division by the AEC for use in flowsheet development, include

Core specific power:	200 MWt/metric ton
Average core burnup:	100,000 MWd/metric ton
Composition:	Core--20% PuO ₂ -UO ₂
	Blanket--2% PuO ₂ -UO ₂
	Cladding--stainless steel
	Bonding--gas, but it is assumed that 1% of the fuel is sodium-logged.

2. Closed Cycle Processes--Research and Development--Compact Pyrochemical Processes

a. Process Chemistry of Molten Salt Systems (I. Johnson)

Last Reported: ANL-7419, pp. 123-124 (Jan 1968).

A CaCl₂-20 m/o CaF₂ salt mixture is being considered for use in the reduction step of the reference flowsheet for pyrochemical processing

*DF--decontamination factor = $\frac{\text{Quantity of Contaminant in the Product}}{\text{Quantity of Contaminant in the Feed}}$

of fast breeder reactor oxide fuels. Because CaO is a product of the reduction reaction, the $\text{CaCl}_2\text{-CaF}_2\text{-CaO}$ phase diagram is being studied.

Both the $\text{CaCl}_2\text{-CaF}_2$ and the $\text{CaCl}_2\text{-CaO}$ binary systems are being studied as part of the overall investigation. Recent experiments have shown that the $\text{CaCl}_2\text{-CaF}_2$ binary has a eutectic at about 19 m/o CaF_2 and 645°C . The $\text{CaCl}_2\text{-CaO}$ binary has a eutectic at about 7 m/o CaO and 750°C . There also appears to be a peritectic point at about 19 m/o CaO and 835°C , although the compound that forms below 835°C has not yet been identified.

b. Unit Operations Development (R. D. Pierce)

Last Reported: ANL-7427, p. 124 (Feb 1968).

Two experiments have been performed to study the removal of stainless steel cladding from oxide fuels by dissolution of the cladding in molten zinc. In these experiments, Runs ZD-3 and ZD-4, simulated subassemblies loaded with pellets and fines of UO_2 were immersed in molten zinc at 800°C . The subassemblies were constructed of Type 304 stainless steel and contained 13 tubes, of $3/8$ -in. ID and $12\frac{1}{2}$ in. long, with a wall thickness of 35 mils. The tubes were welded to three round plates each 4 in. in diameter by $1/4$ in. thick. The subassemblies contained 6.68 kg of stainless steel and were loaded with 2.49 kg of UO_2 .

Each subassembly was dissolved in 84.5 kg of molten zinc contained in a $9\frac{3}{8}$ -in.-ID tungsten crucible. About 6 kg of $\text{CaCl}_2\text{-15 w/o CaF}_2$ salt were added to the melt to retard vaporization of the zinc, and to wet and collect the UO_2 fines which are ultimately reduced in the reduction step. After ~ 30 -min immersion at 800°C , the stainless steel tubing was completely dissolved, but the round plates were relatively unaffected. The subassembly was immersed for an additional 7 hr to insure complete dissolution of the stainless steel. Filtered samples were taken during the

course of the experiments to follow the progress of the dissolution. The results of the analysis of the samples from Run ZD-3 (see Fig. II.D.2) show that ~ 4 hr were required to dissolve all of the stainless steel in the subassembly.

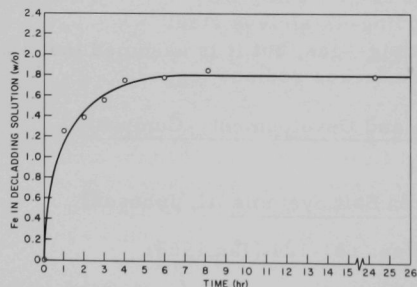


Fig. II.D.2. Progress of Decladding Experiment

After dissolution, a heated transfer line was introduced and the molten zinc-stainless steel solution was removed from the vessel. The furnace was subsequently cooled to room temperature and opened.

No undissolved stainless steel was observed. The UO_2 pellets were distributed in a fairly uniform layer on the vessel bottom and were partially covered with a zinc heel.

The furnace was then reassembled and heated to 800°C . A vacuum line was introduced through the top of the furnace, and the furnace was evacuated through a condenser in the vacuum line. Under these conditions, the zinc remaining in the crucible vaporized through the salt phase and collected in the condenser. No major operational problems were experienced during the decladding and zinc vaporization procedures in either experiment. The relatively zinc-free pellets remaining in the crucible after the decladding and zinc-removal procedures appear to be suitable for the subsequent oxide-reduction step of the reference pyrochemical flowsheet (see Progress Report for November 1967, ANL-7399, p. 137).

A facility for retorting the uranium and plutonium product solutions from pyrochemical processes has been modified to minimize atmospheric contamination of the materials processed. In recent tests, the furnace was operated at 0.01 Torr. No detectable pressure increase occurred when the unit was isolated from the vacuum pumping system for 4 hr. The equipment has been tested at temperatures up to about 700°C . Final test will be performed at temperatures up to 1200°C before the unit is used to retort solvent metals away from uranium and plutonium product solutions.

Studies are being made of various designs for continuous and semicontinuous metal-salt contacting equipment, such as mixer-settlers, that could be used in pyrochemical-processing equipment.

A solid-rotor pump has been designed (see Fig. II.D.3) that is capable of lifting molten metal or salt from one vessel and moving it to another vessel. A small working model of the pump was fabricated from Lucite and tested with water. The pump consists of a rotor containing two passages through which the molten salt or metal flows. Subsequent to the water tests, another pump of the same design was constructed of mild steel and tested with a molten Cu-33 w/o Mg alloy. The pump was placed inside a crucible containing the alloy. This crucible was placed inside a second taller crucible that acted as a receiver for the material pumped from the inner crucible. The alloy was heated to 650°C , and the pump was positioned so that the bottom of the solid rotor was immersed

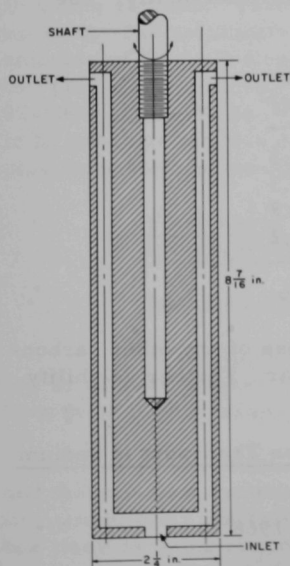


Fig. II.D.3

Solid-rotor Pump for Liquid Metals and Molten Salts

in the alloy, while the top of the rotor was above the top rim of the inner crucible and below the top rim of the outer crucible. The rotor was then spun at 2200 rpm for about 20 sec. One and one-half kilograms of metal were pumped up $6\frac{5}{8}$ in. from the inner crucible and discharged into the outer crucible. The design of a mixer-settler employing a pump of this type is currently being developed.

3. General Chemistry and Chemical Engineering--Research and Development

a. Characterization of Carbon-bearing Species in Sodium (F. A. Cafasso)

Last Reported: ANL-7403, p. 124 (Dec 1967).

(i) Solubility of NaCN in Liquid Sodium. Information on the corrosion of structural materials by cyanide in liquid sodium systems is lacking. As a first step toward obtaining such information, the solubility of NaCN in liquid sodium is being determined.

Solubility measurements were made between 400 and 550°C by taking a sample of the equilibrated melt through a 5μ -porosity stainless steel filter press-fitted into a tantalum tube, dissolving the entire sample in water, and analyzing the solution for cyanide colorimetrically. The results* obtained were:

Temperature (°C)	Solubility (ppm CN)
402	0.8 ± 0.3
425	3.0 ± 1.3
450	2.7 ± 0.8
476	5.3 ± 2.2
500	41 ± 8
549	181 ± 26

These solubilities are considerably higher than those of any other carbon-containing compounds that have been studied thus far. Further solubility measurements are in progress.

b. Identification of Mechanism(s) of Carbon Transport in Sodium Systems (F. A. Cafasso)

Last Reported: ANL-7419, p. 126 (Jan 1968).

The current objective of this study is to characterize the carbon-bearing species that migrate between structural materials in contact with liquid sodium.

*The values given supersede previously reported solubilities.

Previously it was shown that as much as 1.7 ppm of labeled carbon compound(s) existed in sodium during transport of ^{14}C -bearing species at 650°C from a Fe- ^{14}C steel to Type 304 stainless steel. Attempts are being made to deduce the nature of the migrating species. The sodium samples taken during the transport experiment have been reacted with water, and the ^{14}C -labeled reaction products in the off-gases, solutions, and residues are being assayed and identified.

Considerable effort has been devoted to developing a capability for the requisite analyses.

(i) Off-gas Analysis. The off-gas from the dissolution of sodium in water will be analyzed by a technique in which chromatographic separation/identification of the compounds is followed by their radioassay in a proportional gas content. The equipment has been assembled and tested and is undergoing calibration.

(ii) Solution Analysis. After removal of the off-gas, the aqueous solution is acidified,* filtered, and assayed for its ^{14}C content. To carry out this assay, an existing analytical train was modified to incorporate a wet combustion method. This method** involves refluxing the aqueous sample in the presence of a strong oxidant, passing the resultant gases over hot CuO (800°C) to ensure that carbon is oxidized to CO_2 , and absorbing the CO_2 in Hyamine solution. Then, a liquid scintillator is added, and the solution is counted. The reliability of the method was tested by converting known amounts of ^{14}C , dissolved in sodium sulfate solution as benzoic acid-1- ^{14}C , to $^{14}\text{CO}_2$. Oxidation was essentially complete as indicated by recovery of 90-100% of the ^{14}C as $^{14}\text{CO}_2$. The wet combustion method, therefore, appears to be adequate for this study. Analysis of aqueous solutions of sodium samples from the aforementioned transport experiment is now underway.

c. Total Vapor Pressure and Oxygen Potentials in the Ternary System U-Pu-O (P. E. Blackburn and J. W. Reishus)

Last Reported: ANL-7419, pp. 127-128 (Jan 1968).

The components of the high-temperature transpiration apparatus are in various stages of assembly and testing. The Cahn microbalance has been tested; several leaks were found and repaired.

The vacuum bell jar system, containing the Cahn microbalance, and the gas-flow system (containing moisture monitor, flowmeters, recirculating pump, etc.) are being assembled in the glovebox. In addition, the glovebox itself is being connected to the helium-purification system, and utilities are being installed in the box.

*Acidification precludes the presence of cyanide in these solutions.

**Ingram, G., "Organic Analysis: Carbon and Hydrogen," in *Treatise on Analytical Chemistry*, Part II, Vol. 11, p. 384, Kolthoff, I. M., and Elving, P. J., (eds.), Interscience Publishers, New York-London (1965).

The remaining work will involve completing the assembly and final checking of the equipment.

d. Vapor Species Partial Pressures in the Ternary U-Pu-O System
(P. E. Blackburn and J. E. Battles)

Last Reported: ANL-7419, pp. 128-130 (Jan 1968).

Mass-spectrometric studies of the volatilization behavior of the U-Pu-O system continue to determine (1) the apparent composition of the vapor phase in equilibrium with the condensed phase(s), (2) the partial pressures of the vapor species as a function of temperature, and (3) the thermodynamic properties of the vapor species.

The binary Pu-O system is being investigated first since no mass-spectrometric work has been done to establish the relationships between the gaseous Pu, PuO, and PuO₂ species and the condensed plutonia phase. The initial work relating to hypostoichiometric plutonia (PuO_{2-x}) has been completed.

As previously reported (ANL-7419, p. 128), vapor species characteristic of the vaporization of tungsten or rhenium oxides are observed mass spectrometrically when stoichiometric PuO₂(s) is heated at about 1200°C or higher in tungsten or rhenium effusion cells. After the initial heating, the intensity of these vapor species was greatly reduced; however, some WO₂⁺ and WO₃⁺ or ReO₂⁺ and ReO₃⁺ were detectable in the vapor phase throughout the duration of the experiments. Because of the reaction of tungsten and rhenium with plutonia, additional experiments were

conducted using effusion cells of iridium, which, according to the available data, should be nonreactive. When samples of initially stoichiometric PuO₂(s) were heated above 1500°C in iridium effusion cells, a strong vaporization of oxygen was observed; however, the absence of iridium oxide species in the vapor phase confirmed that plutonia does not react with iridium.

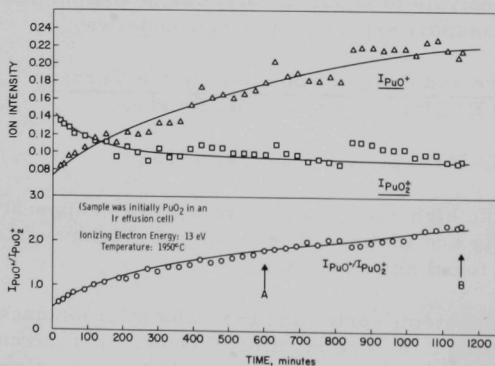


Fig. II.D.4. Intensities of PuO₂⁺ and PuO⁺, and the Ratio $I_{PuO^+}/I_{PuO_2^+}$ as a Function of Time at Constant Temperature for Run PI-1

Figure II.D.4 shows the variation of the ion intensities of PuO₂⁺ and PuO⁺, as well as the ratio $I_{PuO^+}/I_{PuO_2^+}$, as a

function of time when a sample of $\text{PuO}_2(\text{s})$ was heated at 1950°C in an iridium effusion cell. Since the sample lost considerable oxygen during the heat-up, the actual composition was unknown for the starting time at 1950°C . The measured ion intensity of PuO_2^+ exhibited a gradual decrease with time, while that of PuO^+ and the ratio of $I_{\text{PuO}^+}/I_{\text{PuO}_2^+}$ increased.

After about 10 hr at 1950°C , at Point A in Fig. II.D.4, a sample was removed for oxygen analysis. The atom ratio of oxygen to plutonium was 1.88. The sample was then heated an additional 9 hr to Point B in Fig. II.D.4, before starting temperature-dependence and rate-of-effusion measurements. At this point, the atom ratio was 1.83. No further reduction was observed during the temperature-dependence measurements (see Runs PI-1B, PI-1D, and PI-2A in Table II.D.1). Similar behavior was observed when rhenium effusion cells were used.

TABLE II.D.1. Mass-spectrometrically Determined Partial Heats of Sublimation for the Vapor Species of Plutonia

Run No.	Cell Material	Ionizing Electron Energy (eV)	Partial Heat of Sublimation (kcal/mole)			Ratio $I_{\text{PuO}^+}/I_{\text{PuO}_2^+}$ at 2175°K	Atom Ratio of Oxygen to Plutonium in Solid
			PuO_2	PuO	Pu		
P-5A	Re	13.0	140.2 ± 1.8	125.1 ± 1.0	136	2.6	1.83
P-5B	Re	13.0	137.8 ± 1.6	123.5 ± 0.9		2.8	1.81
P-5B	Re	17.0	138.2 ± 1.9	128.5 ± 1.3		2.2	1.81
PI-1B	Ir	13.0	137.8 ± 1.2	130.4 ± 0.9		2.6	1.83 ₄
PI-1D	Ir	13.0	139.6 ± 1.3	128.9 ± 1.1		3.0	1.83 ₉
PI-2A	Ir	13.0	138.8 ± 1.4	125.9 ± 1.4		3.0	1.83 ₄

The temperature dependence of the plutonium-bearing vapor species in equilibrium with condensed plutonia has been determined in several series of measurements using both rhenium and iridium effusion cells. The variation of the ion intensity of PuO^+ and PuO_2^+ plotted as a function of reciprocal temperature ($\log I T$ versus $1/T$) is shown in Fig. II.D.5

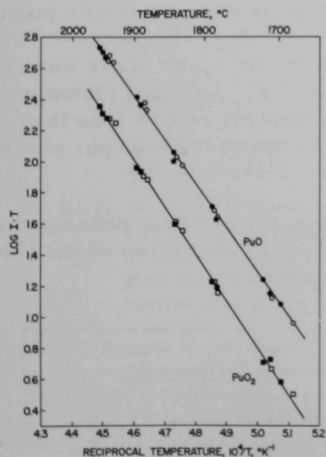


Fig. II.D.5

Variation of Ion Intensities of PuO_2^+ and PuO^+ Observed over Plutonia as a Function of Reciprocal Temperature for an Ionizing Electron Energy of 13 eV

for a typical series of measurements. About half of the data points were taken as the temperature was systematically decreased (open points) and the other points as the temperature was systematically increased (solid points). The concurrence of the data regardless of the direction of temperature variation gives assurance that equilibrium among the phases was achieved.

The partial heats of sublimation, determined from a least-squares analysis of the data, are summarized in Table II.D.1. The errors listed are standard deviations. The ionizing electron energy was 13 eV except for Run P-5B, in which it was 17 eV. The data were normalized at the mid-temperature and re-evaluated by the method of least squares to obtain single values for the partial heats of sublimation: 127.2 ± 2.7 and 138.8 ± 1.1 kcal/mole for PuO(g) and $\text{PuO}_2\text{(g)}$, respectively. The intensity ratio of PuO^+ to PuO_2^+ at 2175°K ranged from 2.6 to 3.0 (excluding Run P-5B at 17 eV), with an average value of 2.8. The last column in Table II.D.1 shows the composition of the condensed phase.

To determine the composition of the vapor phase, the measured ion intensities must be corrected for the ionization cross sections, multiplier efficiencies, and energy differences. The Otvos-Stevenson* method was used to correct for ionization cross section, and the multiplier efficiency was assumed to be proportional to the inverse square root of the mass. These two corrections offset each other, and, since the combined correction is less than the experimental errors, they have been neglected. The correction for the energy difference is given by the relationship

$$\frac{I'_{\text{PuO}}}{I'_{\text{PuO}_2}} = \frac{I_{\text{PuO}}(E - AP_{\text{PuO}_2})}{I_{\text{PuO}_2}(E - AP_{\text{PuO}})}, \quad (1)$$

where E is the ionizing electron energy and AP is the appearance potential.

After applying the above correction, the vapor phase was computed to be 57 w/o PuO and 43 w/o PuO_2 at 2219°K. Although plutonium atoms also exist in the vapor phase, their concentration was less than 1 w/o of the total vapor. The small quantity of free oxygen in the vapor phase has also been neglected.

From knowledge of the composition of the vapor phase and the rate of effusion at a given temperature, the partial pressures of the vapor species were calculated from the effusion equation

$$P_i(\text{atm}) = 2.256 \times 10^{-2} \frac{wF_i}{\text{AtK}} \sqrt{\frac{T}{M_i}}, \quad (2)$$

*Otvos, J. W., and Stevenson, D. P., J. Am. Chem. Soc. 78, 546 (1956).

where w/At is the rate of effusion in $g/(cm^2)(sec)$, F_i is the fraction of total vapor, K is the Clausing correction factor for molecular flow through short channels, T is the absolute temperature, and M_i is the molecular weight. The rate of effusion at 2219°K was determined by the weight-loss method using iridium effusion cells. The orifice area was corrected for thermal expansion, and the rate of effusion was corrected for the small weight loss of iridium that occurred during the run.

The partial pressures as a function of temperature are shown in Fig. II.D.6. These data were obtained by combining the measured partial pressures at 2219°K with the heats of sublimation from the temperature-dependence measurements. The indicated datum point represents the average of four measurements of the rate of effusion at 2219°K.

The vapor pressure of plutonia has been measured by a number of investigators,* and the results from these studies agree very well, except for the data of Phipps *et al.*, who used tantalum effusion cells. The previous results, except those of Phipps *et al.*, are shown in Fig. II.D.7 along with the results from this study. In all the previous studies, the vapor phase was assumed to be entirely $PuO_2(g)$.

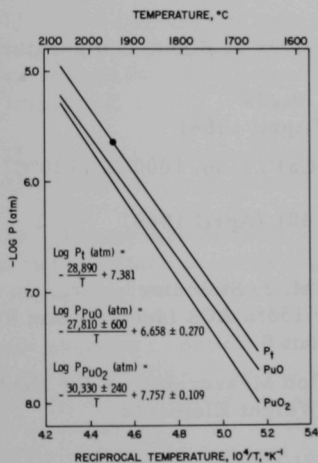


Fig. II.D.6. Temperature Dependence of the Partial Pressures of $PuO_2(g)$ and $PuO(g)$. (The temperature dependence of total pressure is represented by the P_t curve.)

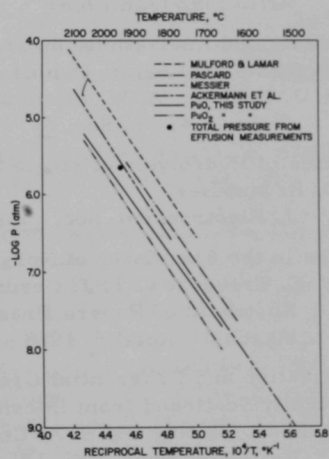


Fig. II.D.7. Temperature Dependence of the Vapor Pressure of Plutonia from Previous Studies

*Phipps, T. E., Sears, G. W., and Simpson, O. C., *J. Chem. Phys.* **18**, 724 (1950); Mulford, R. N. R., and Lamar, L. E., in *Plutonium 1960*, Grison, E., Lord, W. B. H., and Fowler, R. D., Ed. Cleaver-Hume Press. Ltd., London (1961); Ackermann, R. J., Faircloth, R. L., and Rand, M. H., *J. Phys. Chem.* **70**, 3698 (1966); Pascard, R., CEA, Paper submitted to the panel on Thermodynamic Properties of Plutonium Oxides held in Vienna, Oct 1966, reported in Ohse R. W., and Ciani, V., presented at Third International Symposium on High Temperature Technology, Aslomar, California (Sept. 17-20, 1967); Messier, D. R., submitted for publication in *J. Am. Ceram. Soc.*

PUBLICATIONS

GENERAL REACTOR TECHNOLOGY

Determination of Isotope Distribution in the Microstructure of Irradiated Ceramic Fuels

M. D. Adams, S. C. Tong, and L. E. Ross

Abstracts of Papers Presented at 155th ACS Meeting, San Francisco,
March 31-April 5, 1968 Abstract 0-19

Physical Properties of Nuclear Ceramics

J. E. Battles, J. W. Reishus, and W. A. Shinn

Bull. Am. Ceram. Soc. 47(4), 414 (April 1968) Abstract

Behavior of Urania-Rare Earth Oxides at Elevated Temperatures

R. J. Beals and J. H. Handwerk

Bull. Am. Ceram. Soc. 47(4), 414 (April 1968) Abstract

Blowback of Sintered-metal Filters: A Review of Tests and Operating Experience

Erwin L. Carls and Norman M. Levitz

ANL-7392 (Jan 1968)

Elasticity and Anelasticity of Uranium Oxides at Room Temperature:

II. Hyperstoichiometric Oxides

R. J. Forlano, A. W. Allen, and R. J. Beals

J. Am. Ceram. Soc. 51, 192-195 (April 1968)Kinetics of Hydrolysis of Single Crystal CaF_2 from 1000 to 1120°C

D. R. Messier

J. Electrochem. Soc. 115(4), 397-401 (April 1968)Studies in the Chemistry of NpF_6

L. E. Trevorow, T. J. Gerding, and M. J. Steindler

Abstracts of Papers Presented at 155th ACS Meeting, San Francisco,
March 31-April 5, 1968 Abstract 0-25Polarization and Differential Cross-Section Measurements for Neutrons
Elastically Scattered from Intermediate Weight Elements

E. E. D. Whiting and S. A. Cox

Bull. Am. Phys. Soc. 13, 681 (April 1968) Abstract

III. NUCLEAR SAFETY

A. Other Reactor Kinetics--Research and Development

1. Accident Analysis and Safety Evaluation (G. J. Fischer)

Last Reported: ANL-7427, pp. 134-137 (Feb 1968).

A safety-analysis computer code, SASIA, has been developed. Results achieved with a preliminary version have been reported by MacFarlane *et al.** This code has given particularly useful results for those accidents which are related to loss of sodium. In some calculations of loss-of-sodium accidents, the momentum of the ejecting sodium creates an irreversible rate of reactivity addition which can overwhelm the Doppler effect and lead to a severe disassembly accident.

In order to calculate the energy release of this disassembly accident a modified version of MARS,** MARS/SAS, has been produced. The following are some of the significant improvements made for MARS/SAS.

- 1) Two subroutines in the MARS program, namely, point kinetics and finding the solution of a system of first-order differential equations, have been rewritten. With these replacements, the numerical stability has greatly improved.
- 2) An option is provided to print out temperature and pressure distributions within the core at any time interval the user desires.
- 3) An alternative treatment of discontinuous power-density distribution at the interface between two adjacent regions with continuous derivative of material reactivity worths has been planned. The method makes a smooth power density distribution at the interface, i.e., it makes an arithmetic average of power density at interface of these two regions. In the original MARS, this problem was treated by introducing two thin surface regions, one on each side, at the interface; it further assumed that the pressure at interface is zero. It is to be noted that the proposed method is more realistic than the original, since power density is directly related to pressure through the equation of state, and the pressure at the interface should be somewhere between the pressures inside these two regions. Results using these two approaches were compared; it was found that there is no appreciable difference between them.

* MacFarlane, D. R., *et al.*, Theoretical Studies of the Response of Fast Reactors during Sodium Boiling Accidents, Paper presented at the International Conference on the Safety of Fast Reactors, Aix-en-Provence (France), Sept. 19-22, 1967.

** Hirakawa, N., MARS, A Two-dimensional Excursion Code, APDA-198. We are grateful to A. Klickman of APDA for his generous cooperation in this adaptation.

4) A treatment of discontinuous derivative of material reactivity worth at the interface between two adjacent regions is being incorporated into MARS/SAS. Recent results from MACH-1* and CANDID** calculations indicate that the derivative of material reactivity worth at the interface between two core regions with different enrichments (and also at the interface between core and blanket) is discontinuous. This problem has not been treated in MARS, and it was assumed explicitly that the derivative of material worth at interface is continuous. Jankus[†] has proposed a method to treat the interface between core and blanket regions with discontinuous derivative of material worth, and his method has been extended to two core regions with different compositions (or enrichments). This is done by replacing p in Jankus' original derivative (ANL-6512, p. 9, Eq. 5) with $p_1 - p_2$, where p_1 and p_2 are pressures inside core regions 1 and 2, respectively. Accordingly, the total reactivity reduction can be generalized to a core with n core regions and blanket as follows:

$$\begin{aligned} \frac{d^2k}{dt^2} = & \int_{V_i} p_i (\nabla^2 W_i) dV_i - \int_{S_i} (p_i - p_{i+1}) \frac{\delta_{i+1} C_{i+1}}{\delta_i C_i + \delta_{i+1} C_{i+1}} (\nabla W_i - \nabla W_{i+1}) \cdot ds \\ & - \int_{S \text{ at interface between core and blanket}} \frac{\delta_b C_b}{p_n \delta_n C_n + \delta_b C_b} (\nabla W_n - \nabla W_b) \cdot ds; \\ i = & 1, 2, \dots, n-1, \end{aligned}$$

where W_i and W_b designate the material reactivity worth of core region i and blanket, respectively; $\delta_i C_i$ and $\delta_b C_b$ are wave impedances of core region i and blanket, respectively.

2. Fuel Meltdown Studies with TREAT

a. Meltdown Studies

(i) Ceramic Fuel Studies (C. E. Dickerman)

Last Reported: ANL-7438, p. 125 (March 1968).

(a) UO₂ "Checkout" Experiment with Mark II TREAT Sodium Loop. A high-specific-energy loop experiment is planned as a "checkout" test for the Mark-II TREAT Integral Sodium Loop now under

*Meneley, D. A., Kvitek, L. C., and O'Shea, D. M., MACH-1, A One-dimensional Diffusion Theory Package, ANL-7223 (1966).

**Leaf, G. K., Kennedy, A. S., and Jensen, G., A Two-dimensional, Diffusion Theory Code Based on CANDID2D, ANL-CANDID, ANL-7305 (Sept 1967).

[†]Jankus, V. Z., A Theoretical Study of Destructive Nuclear Bursts in Fast Power Reactors, ANL-6512 (1962).

development [see below, Sect. (ii)]. The checkout test, to be performed with a UO_2 sample, is to provide (1) a demonstration of the capabilities of loop containment and also (2) data on the thermal interaction of high-temperature oxide and sodium coolant inside a typical coolant channel geometry. The goals include coolant-expulsion and pressure-surge data from the flowmeters and pressure transducers located at both inlet and outlet for use in development of models describing the energy transfer to sodium after a high-temperature oxide-pin failure and the subsequent transient coolant-vapor generation. Two TREAT runs are planned: one, a preliminary transient clipped early to limit the sample fuel temperature $\sim 1500^\circ\text{C}$; the second, a high-energy transient for which a total sample energy of $\sim 2 \times 10^5 \text{ J}$ is desired. The sample is to consist of a single, 13% enriched pin of 0.247-in.-dia UO_2 pellets, clad by a 0.020-in.-thick Type 304L stainless steel tube of 0.290-in. OD. The pin is to be surrounded by a ring of 6 hollow dummy pins, all seven pins located on a triangular pitch with nominal 0.056-in.-dia spiral spacer wires. This pin design is based on that of the "standard" 0.290-in.-OD mixed-oxide pin of the ANL Fuel Development programs and is similar (except for use of UO_2 instead of mixed oxide) to the 19 mixed oxide pins to be irradiated in EBR-II (see ANL-7438, p. 125).

(ii) Experimental Development (C. E. Dickerman)

Last Reported: ANL-7427, pp. 137-138 (Feb 1968).

(a) Mark-II Integral Sodium Loop Development. A second generation of integral sodium loops is under development that will have a capability for much higher pressures and more extensive instrumentation than the Mark-I integral sodium loops now in use.

The prototype loop has been instrumented with an electromagnetic flowmeter and a pressure-transducer subassembly at both inlet and outlet of the test section. Heaters and control cables are being adapted to the loop. Originally the prototype loop had been provisionally rated at 200 atm (a 180-atm rupture disk specified). Review of the loop welds and component walls as built has led to the decision that the loop actually should be rated at the same level as the other IIB loops, or 267 atm. Accordingly, a proof-test sequence has been established for running the loop at 538°C at pressures up to 333 atm. Facilities for performing such proof tests on each loop in maximum safety to equipment and personnel are being arranged.

The length of each annular linear induction pump is to be tailored to fit a specific assembled loop. Pump assembly is underway for the prototype and the three IIB (267-atm rating at 538°C) loops. Because the thermal expansion between room temperature and operating temperature is not the same for the T316 stainless steel loop body and the Inconel X-750 pump tube, the room-temperature length of the pump is

specified to be 0.020 in. longer than the pump gap. This preloading of the loop by the pump is designed to minimize the differential thermal stresses over the operating range.

(iii) Analysis (C. E. Dickerman)

Last Reported: ANL-7403, pp. 142-143 (Dec 1967).

(a) Development of Advanced Transient Heat-transfer Calculations. An "experimental" version of the ARGUS transient heat-transfer code has been assembled using the new solid-region equations which permit a more accurate representation of regions with temperature-dependent thermal conductivity. Difficulties have been encountered in modifying the equations for "thin regions" like fuel-pin cladding, and improvement of the thin-region equations has been deferred. The current version is being used, and an internal memo describing it is in preparation. The extent of subsequent changes will be determined by experience with the new version.

3. Materials Behavior, Equation of State, and Energy Transfer

a. Equation of State (C. E. Dickerman)

Last Reported: ANL-7403, pp. 143-145 (Dec 1967).

In addition to the need for the equation of state of iron and its alloys, including steel, for application to reactor safety problems, there is a strong interest in the subject for ordnance, geophysical, and astrophysical studies, and much information is contained in the literature of these subjects in addition to the usual physics and engineering publications. Because of their importance as prime materials of construction, these substances have been studied extensively, and a wealth of complexity has been revealed.

Most of the information obtained for the pressure-volume relation for solid iron at high applied stresses has been obtained by dynamic studies,* although static** and dynamic results have been brought into good

*McQueen, R. G., "Laboratory Techniques for Very High Pressures and the Behavior of Metals Under Dynamic Loading," Metallurgy at High Pressures and High Temperatures, ed. by K. A. Gschneider, Jr., M. T. Hepworth, and N. A. D. Parlee, Gordon & Breach Publishers, New York (1964), p. 44-132; van Thiel, M., Kusubov, A. S., Mitchell, A. C., and Davis, V. W., Compendium of Shock Wave Data, UCRL-50108 (June 1966); Altschuler, L. V., Krupnikov, K. K., Lebedev, B. N., Zhuchikhin, V. I., and Brazhnik, M. I., Dynamic Compressibility and Equation of State of Iron Under High Pressure, Soviet Physics-JETP, 7, 606-614 (1958); Skidmore, I. C., and Morris, E., "Experimental Equation of State Data for Uranium and Its Interpretation in the Critical Region," Thermodynamics of Nuclear Materials, International Atomic Energy Agency, p. 173, Vienna, 1962 (STI/PUB/58); see also E. Morris, The Equation of State and Uranium in the Critical Region, AWRE-0-61/62 (1962).

**Clendenin, R. L., and Drickamer, H. G., The Effect of Pressure on the Lattice Parameters of Ruthenium and Iron, J. Phys. Chem. Solids 25, 865-868 (1964); Takahashi, T., and Bassett, W. A., High-pressure Polymorph of Iron, Science 145, 483 (1964); Bundy, F. P., Pressure-Temperature Phase Diagram of Iron to 200 kbar, 900°C, J. App. Phys. 36, 616-620 (1965); Mao, H. K., Bassett, W. A., and Takahashi, T., Effect of Pressure on Crystal Structure and Lattice Parameters of Iron up to 300 kbar, J. App. Phys. 38, 272-276 (1967); Erratum 38, 2142 (1967).

agreement in recent years by improved experimental technique, calibration, and understanding of the phenomena.

The dynamic stress-strain curve represents the path followed by a material as a wave front moves through it. This path is a function of

1. the strain rate and the wave shape;
2. temperature;
3. composition: alloying agents and impurities;
4. previous history: residual strain and dislocations.

As the wave front moves through the solid, the strain rate reaches a maximum value and then decreases after the peak stress is reached. This peak stress σ_H has been found to be very close to the quasi-static value, and it is the most useful point to serve as a basis for conversion to isentropic and isothermal conditions for comparison with ultrasonic and hydrostatic experiments. This maximum stress-strain data is called the Hugoniot for the material.

The Hugoniot curve differs from the isentropic hydrostat P_S by two important ways. First, the entropy increase due to the shock front causes the material to be at a higher temperature on the Hugoniot for a given strain, or specific volume, than on the isentrope; second, the Hugoniot represents the state of stress composed of the spherical component of the hydrostat plus a deviatoric component due to the material yield strength Y .

A simple relation between the quasi-static uniaxial stress flow condition and the uniaxial strain flow condition is used, although this flow condition may be strain-rate, temperature, composition, and strain-history dependent. During compression the spherical component or pressure on the shock hydrostat P_H is related to the Hugoniot stress σ_H and yield stress Y by

$$P_H = \sigma_H - \frac{2}{3} Y. \quad (1)$$

The strains along the Hugoniot, ϵ_X , are related to the uniaxial strain ϵ by

$$\epsilon_X = \frac{3}{2} \epsilon - (Y/6K) = 1 - (V/V_0), \quad (2)$$

where K is the bulk modulus, defined by

$$K = -V \frac{\partial P}{\partial V}, \quad (3)$$

V is the volume, and V_0 is the volume at the initial pressure (usually taken as one atmosphere and equivalent to zero pressure on the scale of the phenomena considered here).

Since the bulk modulus has been found to be linear* over a wide range of pressure,

$$K(V, T) = K_0(T) + K'(T)P(V), \quad (4)$$

Eqs. 3 and 4 can be combined to give the Murnahagn equation of state in the purely elastic region:

$$P = \frac{K_0}{K'} \left[\left(\frac{V_0}{V} \right)^{K'} - 1 \right]; \quad 0 \leq \sigma_H \leq Y. \quad (5)$$

This form of the pressure-volume relation fits experimental data for both isentropic and isothermal compression in the elastic region and can be made to fit the elastic-plastic** and purely plastic regions to be introduced below in spite of phase changes which take place at higher pressures. The internal energy can be found from $E = -\int PdV$.

The wave structure in shock-compressed iron depends on the magnitude of the stress. Below the Hugoniot elastic yield point stress, a single elastic wave is found. In pure annealed iron, a slower plastic wave of greater stress amplitude is found above the Hugoniot elastic limit (HEL). Above 129 ± 1 kbar and a strain ϵ_{trans} of 0.0640 ± 0.0005 , a second plastic wave appears corresponding to a polymorphic phase transition† between the bcc structure of α -iron and the denser hcp phase of ϵ -iron. This transformation is complete at 330 kbar, and the elastic and only the second plastic wave are found between this pressure and about 660 kbar when the plastic(II) wave outruns the elastic wave and a single wave structure is observed at higher pressures.

These transitions are composition- and temperature-dependent, but only the behavior of pure iron will be described here.

Although the experimental relation between shock velocity U_S and particle velocity U_P in the linear form

$$U_P = C_0 + S U_S \quad (6)$$

*Anderson, O. L., The Use of Ultrasonic Measurements Under Modest Pressures to Estimate Compression at High Pressure, J. Phys. Chem. Solids **27**, 547-565 (1966); Drickamer, H. G., Lynch, R. W., Glendenin, R. L., and Perez-Albuern, E. A., X-ray Diffraction Studies of the Lattice Parameters of Solids Under Very High Pressure, Solid State Physics **19**, 135-228 (1966); Rotter, C. A., and Smith, C. S., Ultrasonic Equation of State of Iron. I. Low Pressure, Room Temperature, J. Phys. Chem. Solids **27**, 267-276 (1966).

*†Huang, Y. K., and Davids, N., Shock Dynamics of Hypervelocity Impact of Metals, J. Franklin Inst. **276**, 39 (1963).

†Takahashi, T., and Bassett, W. A., High-pressure Polymorph of Iron, Science **145**, 483 (1964).

is often convenient for describing the Hugoniot equation of state, the transitions make this useful only in the purely plastic region. Constants for the Murnahagn Eq. (5) have been fitted to both the static* and dynamic** results in the regions of multiple waves.

Constants to be used are the ultrasonic isothermal values of Rotter and Smith† at 300°K for fcc iron up to 3.6 kbar:

$$K_0^T = 1640 \text{ kbar}; \quad \rho_0 = 7.85 \text{ g/cc} = 1/V_0; \quad K^{T'} = \frac{dK^T}{dP} = 5.938.$$

Isentropic values are similar:

$$K_0^S = 1669 \text{ kbar}; \quad K^{S'} = 5.97.$$

These values agree well with the static measurements*

$$K_0^T \text{ fcc} = 1628; \quad K^{T'} = 5.92; \quad \rho_0 = 7.87 \text{ g/cc for } P < 130 \text{ kbar at } 23^\circ\text{C},$$

and

$$K_0^T \text{ hcp} = 1658; \quad K^{T'} = 5.10; \quad \rho_0 = 8.32; \quad \text{and } 300 > P > 130 \text{ kbar}.$$

The yield stress of iron and steel has been studied extensively as a function of composition, temperature, strain rate, and strain history. A yield stress of 12 kbar is recommended for annealed pure iron, and the strain rate dependence is

$$Y_{\text{dynamic}} = Y_{\text{static}} \left[\left\{ \frac{d\epsilon}{dT} / 40.4 \right\}^{1/5} + 1 \right] \quad (7)$$

as fitted to the data of Manjoine†† for mild steel. The temperature dependence suggested by Bell§ for annealed fcc metals in plastic deformation is

$$Y_{\text{static}} = 5.47 \text{ kbar} \left(1 - \frac{T^\circ\text{K}}{T_m^\circ\text{K}} \right) \epsilon^{1/2}, \quad (8)$$

*Mao, H. K., Bassett, W. A., and Takahashi, T., Effect of Pressure on Crystal Structure and Lattice Parameters of Iron up to 300 kbar, J. App. Phys. 38, 272-276 (1967); Erratum 38, 2142 (1967).

**Huang, Y. K., and Davids, N., Shock Dynamics of Hypervelocity Impact of Metals, J. Franklin Inst. 276, 39 (1963).

†Rotter, C. A., and Smith, C. S., Ultrasonic Equation of State of Iron. I. Low Pressure, Room Temperature, J. Phys. Chem. Solids 27, 267-276 (1966).

††Manjoine, M. J., Influence of Rate of Strain and Temperature on Yield Stresses of Mild Steel, J. App. Mech. 11, A211-A219 (1944).

§Bell, J. F., Single, Temperature-dependent Stress-Strain Law for Dynamic Plastic Deformation of Annealed Face-centered Cubic Metals, J. App. Phys. 34, 134 (1963).

where T_m is the absolute melting temperature. The effect of pressure on melting is given by the relation*

$$T_m (^{\circ}\text{K}) = 1807 + 3.8 \times P (\text{kbar}).$$

It should be noted that the yield-stress phenomena completely disappear in samples prepressurized to 10 kbar due to the reduction of dislocations.**

Above the elastic-plastic region, the constants for the linear shock velocity-partial velocity Eq. (6) can be chosen from Table III.A.1.

TABLE III.A.1. Shock-velocity Constants for Iron and Steel^a

Author	ρ_0 (g/cc)	C (mm/ μ sec)	S	Pressure Range (kbar)
Altschuler ^b	7.85	3.80	1.58	400-500
Skidmore and Morris ^c	7.84	3.67	1.645	1000-3000

^aOther data can be found in the compilation of van Thiel, M., et al., UCRL-50108 (June 1966).

^bAltschuler, L. V., et al., Soviet Physics-JETP 7, 606 (1958).

^cSkidmore, I. C., and Morris, E., "Experimental Equation of State Data for Uranium and Its Interpretation in the Critical Region," Thermodynamics of Nuclear Materials, International Atomic Energy Agency, p. 173, Vienna, 1962 (STI/PUB/58); see also E. Morris, The Equation of State and Uranium in the Critical Region, AWRE-0-61/62 (1962).

The shock hydrostats can be corrected to the isentropes and isotherms by using the Grüneisen equation

$$P - P_H = \frac{\gamma(V)}{V} (E - E_H). \quad (9)$$

The volume dependence of the Grüneisen coefficient γ is not well-known, although the assumption $\gamma/V = \gamma_0/V_0$ has been widely used and agrees reasonably well with experiment.[†]

*Sterrett, K. F., Klement, W., Jr., and Kennedy, G. C., Effect of Pressure on the Melting of Iron, J. Geophys. Res. 70, 1979-1985 (1965).

**Bullen, F. P., Henderson, F., Hutchison, M. M., and Wain, H. L., The Effect of Hydrostatic Pressure on Yielding in Iron, Phil. Mag. 9, 285-297 (1964).

†Taylor, J. W., Residual Temperature in Shocked Copper, J. App. Phys. 34, 2727-2731 (1963).

Alder* has suggested that $\gamma/\sqrt{V} = \gamma_0/\sqrt{V_0}$ is more nearly correct for iron. Values of γ for the hcp phase are not available, but the value 2.29 is suggested for ϵ -iron, and 1.633 for α -iron is calculated from the data in Rotter and Smith.** The volume dependence of γ is still under active study.

b. Materials Behavior and Energy Transfer

(i) Interactions of Fuel, Cladding, and Coolant (R. O. Ivins)

Last Reported: ANL-7419, pp. 146-149 (Jan 1968).

Currently, experiments are being conducted on the dynamics of fragmentation of low-melting metals dropped into water. An extension of the CHLOE procedure for measuring surface area of fragments (ANL-7419, p. 147) is being developed for the determination of size distribution of the particles resulting from a fragmentation experiment. Earlier data will be re-evaluated using the new procedure and will be reported in terms of size distribution.

The data given in ANL-7419 are presented graphically in Fig. III.A.1 to illustrate more clearly the effects of drop temperature and entrance velocity on fragmentation.

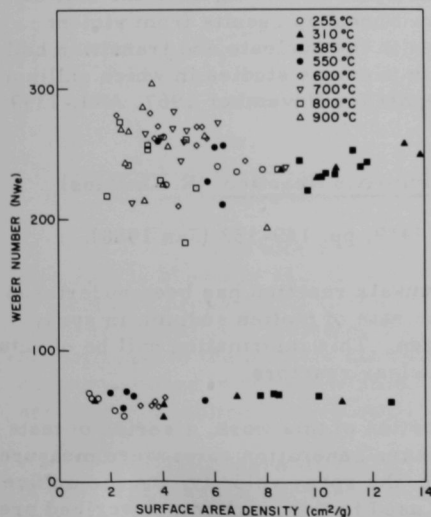


Fig. III.A.1. Fragmentation of Tin in Room-temperature Water (20°C)

In this series of experiments, single drops of molten tin at various temperatures were dropped into room temperature water at entrance velocities of magnitudes 243 and 486 cm/sec (corresponding to drop heights of 1.0 and 4.0 ft, respectively). A run was made by heating a piece of tin (weight, ~0.4 g; spherical surface area, ~0.6 cm^2) in a quartz dropper placed in an electric resistance heater. A single drop was expelled by exerting a slight overpressure in the dropper.

A dimensionless parameter, the Weber Number (N_{We}),[†] was calculated for all of the runs. The Weber Number is a measure of the ratio of dynamic to surface forces on a spherical drop.

*Alder, B. J., Is the Mantle Soluble in the Core?, J. Geophys. Res. 71, 4973-4979 (1966).

**Rotter, C. A., and Smith, C. S., Ultrasonic Equation of State of Iron. I. Low Pressure, Room Temperature, J. Phys. Chem. Solids 27, 267-276 (1966).

[†] $N_{We} = \rho D V^2 / \sigma$, where ρ is the density of water, D the diameter of the drop, V the entrance velocity of the drop, and σ the metal-quenching medium interfacial tension.

The fragments are assumed to be two-dimensional plates for the surface-area calculations (i.e., the projected cross-sectional area as determined by CHLOE has been doubled).

From Fig. III.A.1 it can be observed that runs made at temperatures either considerably below (255°C) or above (550 and 600°C) the critical temperature of water (373°C) resulted in the formation of fragments having roughly the same surface-area density* for similar Weber Numbers. However, at 310 and 385°C (temperatures which bracket the critical temperature of water), there is a significant increase in the surface-area density and an increased scatter of the data, particularly at low Weber Numbers.

Still photographs were taken with stroboscopic illumination of the fragmentation event at drop temperatures of 330 and 685°C. At 330°C, fragmentation was observed to take place at points from the air-water interface to as deep as 2 cm below the surface. The extent of fragmentation increased with increasing depth of the event. At 685°C, fragmentation was not nearly as violent as at 330°C, and occurred within 0.5 cm of the surface.

These observations indicate that a pronounced thermal contribution to the fragmentation process may be occurring near the critical temperature of water, i.e., that enhanced breakup results from violent formation and collapse of vapor bubbles in the nucleate and transition boiling regimes. This is in agreement with previous studies in which gallium fragmented in water (see Progress Report for November 1967, ANL-7399, p. 163).

(ii) Violently Sprayed Sodium-Air Reaction (R. O. Ivins)

Last Reported: ANL-7419, pp. 149-152 (Jan 1968).

The study of the sodium-air reaction has been undertaken to provide knowledge about the reaction rate of molten sodium, in spray form, with air and air depleted in oxygen. This information will be of value in safety analyses of sodium-cooled nuclear reactors.

In the experimental portion of this work, a series of tests have been completed in which the pressure generation rates were measured while the ambient oxygen concentration, the spray velocity, and the orifice diameter were varied. The apparatus used in this work was described previously (see Progress Report for January 1967, ANL-7302, p. 93).

In order to remove the restrictions of the spray-chamber geometry and the mass flow rate of sodium, a reduced-pressure rise rate,

*Surface area in cm^2 per gram of material dropped.

in $(\text{atm/sec})/(\text{g Na/cm}^3)$, has been used. The pseudoconcentration term, g Na/cm^3 , is the weight of in-flight sodium at any time after the spray reaches the top of the chamber divided by the volume of the chamber. It is also assumed that the sodium adheres and stops burning when it strikes the top of the chamber; thus, the amount of in-flight sodium remains constant.

Figure III.A.2 shows the effect of the ambient oxygen concentration on the experimental rate of pressure rise. The scatter of the data is caused by differences in the initial sodium temperature, which has a significant effect on the time required to attain ignition. (A variation in ignition time was observed in the high-speed movies taken of these runs.) At an initial ambient oxygen concentration of 4 m/o, no visible combustion was evident. This is in agreement with the theoretical analysis which predicted that vapor-phase combustion ceases when the oxygen concentration falls below 5 m/o (see ANL-7419, p. 151).

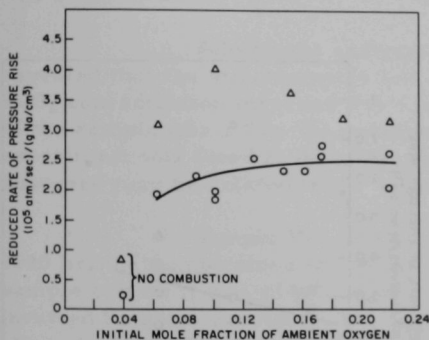


Fig. III.A.2

Effect of Concentration of Ambient Oxygen on Experimental Rate of Pressure Rise

Initial Conditions:

Ambient pressure: 1.0 atm
 Ambient temperature: 298°K
 Sodium temperature: O ≡ 623°K; Δ ≡ 698°K
 Diameter of each of seven orifices: 0.0762 cm
 Drive pressure: 1000 psig ≡ spray velocity of magnitude, 350 ft/sec

The effect of orifice diameter on the experimental pressure rise rate is shown in Fig. III.A.3. As indicated, the rate of pressure rise is inversely proportional to the orifice diameter raised to the 2.26 power. Theoretical analysis indicated that the rate of pressure rise is inversely proportional to the particle diameter to the 1.5 power. Since a one-to-one correspondence is not expected between particle size and orifice size, the agreement exhibited here is considered to be satisfactory.

Figure III.A.4 shows the effect of spray velocity on the rate of pressure rise. A portion of this variation is attributed to the decrease in particle size which probably accompanies an increase in the spray velocity.

Figure III.A.5 is a plot of the total amount of oxygen reacted in all of the experiments as a function of the concentration of ambient oxygen. As would be expected, the curve for oxygen consumption has the same characteristics as the relationship for rate of pressure rise. It should also be noted that, as the particle size decreases because of increased velocity or decreased orifice size, the oxygen consumption increases.

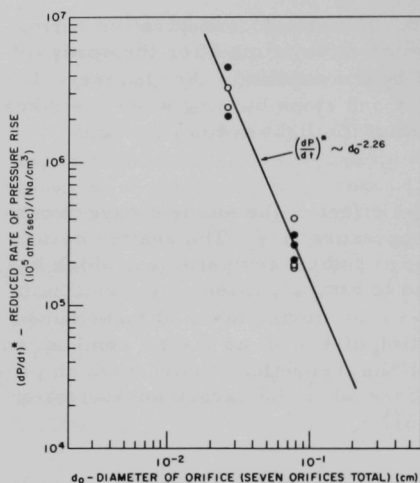


Fig. III.A.4

Effect of Spray Velocity on Experimental Rate of Pressure Rise

Initial Conditions:

Ambient pressure: 1.0 atm
 Ambient temperature: 298°K
 Sodium temperature: $\circ \cong 623^\circ\text{K}$; $\Delta \cong 698^\circ\text{K}$
 Diameter of each of seven orifices: 0.0762 cm

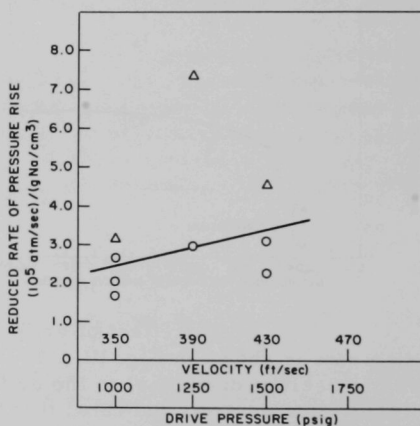
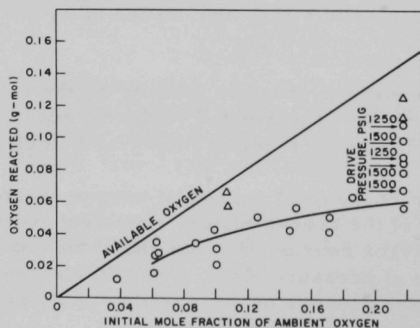


Fig. III.A.5

Oxygen Consumption in the Sprayed Sodium-Air (Depleted Air) Reaction Experiments

Initial Conditions:

Ambient pressure: 1.0 atm
 Ambient temperature: 298°K
 Sodium temperature: 623-698°K
 Orifice diameter (seven orifices total) and drive pressure: \circ - 0.0762 cm, 1000 psig (unless otherwise noted); Δ - 0.0254 cm, 1500 psig



(iii) Segregation in Ceramic Fuels (M. G. Chasanov)

Last Reported: ANL-7419, pp. 152-153 (Jan 1968).

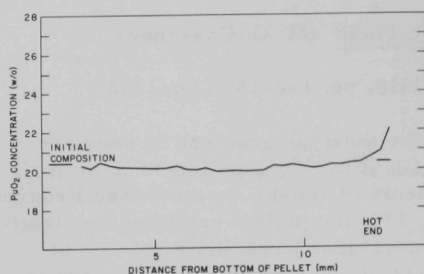
Experiments utilizing the thermal-gradient furnace are currently in progress with cylindrical ($U_{0.8}Pu_{0.2}O_{2.00}$) pellets, 1/2 in. high by 1/2 in. in diameter. In two experiments of 100-hr duration (see Progress Report for October 1967, ANL-7391, p. 178) the pellets exhibited no significant migration (pellet top surface temperatures were about 2000°C) of plutonium. In two additional experiments of 500-hr duration, reported in ANL-7419, under conditions similar to the 100-hr experiments, no significant migration was exhibited in a sample (P-3) heated inside an inverted tungsten crucible which acted as a barrier to vaporization; the other sample (P-4) heated without the crucible showed some enhancement of PuO_2 content in the hotter portion of the pellet. For P-4, a peak concentration of 22 w/o PuO_2 was found; the nominal starting composition of the pellet was 20 w/o PuO_2 .

Subsequent analysis of sections of sample P-4 for oxygen revealed that the stoichiometry had indeed changed in the region where the PuO_2 concentration increase was found. The initial oxygen-to-metal ratio of the sample was 2.009; the ratio in the upper third of the pellet after the experiment was found to be 1.946. Thus, the change in PuO_2 concentration observed may be related to the stoichiometry change found.

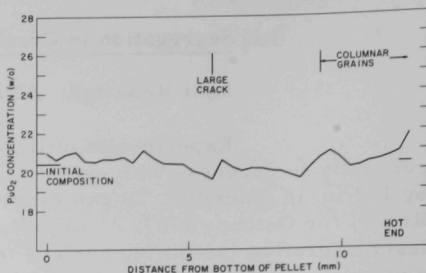
Sample P-5 was heated in the thermal-gradient furnace for 1020 hr; the temperature at the sample top was 1970°C, whereas at the sample bottom it was 1140°C. Like P-3, this specimen was heated in an inverted tungsten crucible. The results of an electron microprobe analysis along the longitudinal axis of the sample after the heating had been completed are shown in Fig. III.A.6a. There seems to be clear evidence of an increase in plutonia concentration at the hotter end of the specimen. The relative smoothness of this increase implies that it is probably not due to segregation originally present in the unheated sample.

Sample P-8 was heated in a tungsten crucible for 123 hr; the top temperature was 2340°C (which was considerably higher than heretofore achieved) and the bottom temperature was 1220°C. The probe analyses are given in Fig. III.A.6b for a scan along the longitudinal axis of the sample. Although the variations in plutonia concentration are greater than for sample P-5, the concentration increase at the hotter end is quite evident.

An experiment with temperature conditions similar to those in experiment P-8 but with a longer heating time is now in progress.



a. Pellet P-5 (in tungsten crucible); $T_{\text{top}} = 1970^{\circ}\text{C}$, $T_{\text{bottom}} = 1140^{\circ}\text{C}$; 1020 hr.



b. Pellet P-8 (in tungsten crucible); $T_{\text{top}} = 2340^{\circ}\text{C}$, $T_{\text{bottom}} = 1220^{\circ}\text{C}$; 123 hr.

Fig. III.A.6. PuO_2 Distribution in $(\text{U}_{0.8}\text{Pu}_{0.2})\text{O}_2$ Pellets Heated in a Thermal Gradient

4. Coolant Dynamics

a. Critical Flow (H. K. Fauske)

Last Reported: ANL-7438, p. 128 (March 1968).

(i) Sodium Tests. The new test section has been fabricated and is being installed in the sodium testing facility.

(ii) Sonic Velocity. The experiment facility has been modified to enable tests with steam-water mixtures. The instruments are being checked and calibrated.

(iii) Voiding Models. Extensive review of codes*,** that describe voiding rates and expulsion of liquid sodium from coolant channels during abnormal operation of a liquid-metal fast breeder reactor has shown that: (a) a realistic expulsion model must include the superheat phenomenon because it can significantly affect the voiding and, therefore, the rate of reactivity feedback; (b) in a typical fast-reactor coolant channel, whether many bubbles or a single bubble are used to describe the expulsion is of secondary importance if the heated surfaces remain wetted (in the single-bubble case, a thin liquid layer is a surface available for evaporation equivalent to many bubbles); (c) because vapor growth is controlled primarily by liquid inertia and friction, it depends strongly on the design of the reactor primary-coolant system; (d) although the assumption is made for most equilibrium analyses* that all heat input to the liquid after the saturation temperature is reached is used as latent heat of vaporization,

*Noyes, R. E., Lurie, H., and Jarrett, A. A., The Development and Growth of In-core Voids Due to Boiling during Faster Reactor Transients, Proceedings of the Conference on Safety, Fuels and Core Design in Large Fast Power Reactors, October 11-14, 1965, ANL-7120; MacFarlane, D. R., Transient Sodium Boiling Calculations-II, Nuclear Eng. & Design 6, 103-114, 1967.

**Meinhardt, W. G., Calculating Vapor Growth in a Superheated Liquid Metal Within a Heated Channel, Paper presented at the 1966 ANS Meeting, October 30-November 3, 1966, Pittsburgh, Pennsylvania.

it seems more reasonable that nearly all heat input stays in the liquid because the large liquid-to-vapor density ratios (~ 1000) mean that only a very small fraction of the liquid is needed to void a typical reactor channel.

If the superheat required to initiate nucleate boiling is known, these conclusions suggest a relatively simple model for calculating maximum, as well as fairly realistic, voiding rates in reactor coolant channels during abnormal behavior. Briefly, the calculational procedures are: (1) for a specified power or flow transient, the appropriate equations for transient heat conduction and convection give the temperatures of the fuel-cladding surface and coolant as functions of position and time; (2) the liquid-vapor interface is located by matching the coolant temperature profile with the superheat necessary to initiate boiling; (3) beyond the onset of nucleation, the heat-transfer calculations are continued as if no boiling takes place, and the maximum surface temperature of the cladding will specify the maximum available pressure (vapor pressure) to satisfy liquid inertia and friction (as long as the heated surfaces remain wetted, the cladding surface temperature remains essentially independent of the coolant density distribution because the major resistance to heat transfer lies in the fuel and cladding); (4) the motion of the liquid slugs upstream and downstream of the liquid-vapor interface is described by Newton's law.

Typical fast-reactor accidents are being calculated with this model. The results will be compared with previously published analyses.

b. Coolant Dynamics (R. M. Singer)

Last Reported: ANL-7438, pp. 128-129 (March 1968).

(i) Superheat. Data are being collected from the new superheat vessel with the artificially roughened (sand-blasted) heating surface.

(ii) Expulsion. The sodium piping is being installed, leak-checked, and insulated. All secondary piping (dump-tank lines, hot-trap loop, gas and vacuum system, etc.) has been completed, and work has started on the primary expulsion tube and test section.

c. Core Component Dynamics (M. W. Wambsganss)

Last Reported: ANL-7438, p. 129 (March 1968).

The effects on a fuel element of high-rate energy release are being determined in tests using EBR-II-type fuel-element jacket tubes as the test specimens (Type 304 stainless steel, 18 in. long, of 0.174-in. OD and 9-mil wall). The load is provided by igniting inside the tube a small amount of Bullseye pistol powder (from Hercules Powder Co.). The tests are to

(a) develop a technique for obtaining consistent loading, (b) determine the maximum amount of plastic growth before the rod ruptures, (c) measure the magnitude of the associated energy release, (d) learn how the rupture of one rod affects other rods in the bundle, and (e) study the strength provided by the helically wrapped spacer wire around each rod (by performing some tests with and others without the wrap).

A loading technique that has been found to provide consistent results involves filling the lower half of the rod (whose bottom cap is welded in place) with sand, inserting a paper wad over the sand and tamping it securely, pouring the weighed powder charge into the rod, inserting a Nichrome wire loop into the powder, using another paper wad to seal the wire above the powder charge and to compress the charge slightly, filling the rod to the top with sand, sealing the top of the rod with epoxy, and, after allowing the epoxy to cure, applying current to the resistance-heater wire to ignite the explosive.

Approximately 40 shots were fired to determine that 40 mg of powder (equivalent to an energy release of only 0.044 Btu) is the lowest charge that will rupture the rod. This might not be the absolute minimum energy for rupture because all the powder probably is not burned before venting occurs and because some other loading technique might lead to rupture with less powder.

Whether air or water was the medium outside the rod did not alter the amount of powder needed for rupture. However, the type of rupture differed with the surrounding medium. When water surrounded the rod, the wall ruptured in a single longitudinal tear. But when air surrounded the rod, the wall rupture progressed at 45° angles and several fragments broke loose. In all cases, the tear in the wall did not extend longitudinally much beyond the region where the charge had been located, and the rod diameter increased ~17% before rupture occurred.

The wire wrap had little effect except when the tube split just under the wire, in which event the wall deformed around the wire.

The effects of the rupture on other rods in the bundle and on the hexagonal can have not yet been studied extensively. However, some trends have been noted in tests of 7- and 19-rod arrays in which the center tube had 125 mg of explosive and the other tubes contained air, water, or sand. As shown in Fig. III.A.7, each array was supported at both ends and had the same dimensions as an EBR-II fuel subassembly. In all cases, the hexagonal can was visibly deformed; the can deformed the most on the side toward which the rod ruptured. As shown in Fig. III.A.8, the rods containing air were flattened and slightly bowed; those filled with sand were flattened only slightly but were bowed severely. With the 19-rod array, the outer rods in

the path of the venting gas from the explosion were deformed to almost the same degree as were those nearer the center rod or those of the 7-rod bundles. The wire wrap reduced the deformation of the rods in all bundles.

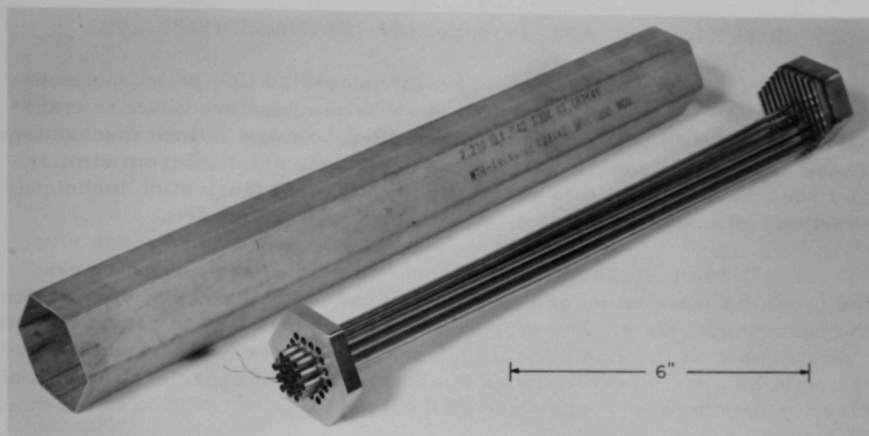


Fig. III.A.7. Test Array Consisting of 19 EBR-II-type Fuel Rods and End Supports That Will Be Installed inside Hexagonal Can before Wire Is Heated to Detonate a 125-mg Charge inside Center Tube



Fig. III.A.8. When Charge in Center Rod of Seven-rod Array (which was in water) Was Detonated, the Six Air-filled Rods Were Flattened and Slightly Bowed. Heater wire can be seen in center rod.

B. Operations

1. TREAT Operations (J. F. Boland)

Last Reported: ANL-7438, pp. 129-130 (March 1968).

a. Reactor Operations. Two Zircaloy-clad UO_2 pellet fuel rods made by ANL-MET were irradiated in room-temperature water in transparent capsules to obtain data on failure threshold and failure mechanisms. These data will be compared with data previously obtained from similar fuel rods made by BNWL to see if slightly different fabrication techniques exert an influence.

The central nine fuel elements were removed from the reactor to permit installation of a support column under the removable section of the reactor grid plate. The support column was installed to prevent possible overstressing of the grid plate if high reaction forces were transmitted to the plate by a fast pressure pulse in an experimental capsule. No signs of cladding deterioration were detected during a visual inspection of the nine elements.

Neutron radiographs were made of 14 experimental capsules from experimental subassembly XG05, an experimental capsule from MTR, and fuel rods from TREAT experiments CEN-238-T, -240-T, and -242-T.

b. Development of Automatic Power-level-control System. Computer simulation of the TREAT reactor with an automatic control system continued. Priority work for the computer at Idaho State University limited computer availability during this reporting period. Data from runs completed at the end of this reporting period are being analyzed.

A general description of control-system requirements was sent to fourteen manufacturers of hydraulic control systems to determine which ones might have an interest in fabricating a system of this general type and what experience they have had in fabricating similar systems or components.

C. Engineered Safety Features Technology--Research and Development

1. Energy Absorption Containment

a. Hydrodynamic Response of Primary Containment to High-energy Excursion (S. H. Fistedis)

Last Reported: ANL-7427, pp. 148-151 (Feb 1968).

The Rankine-Hugoniot equations for a shock wave in a solid substance are

$$U_s/(U_s - U_1) = v_0/v_1 = \sigma; \quad (1)$$

$$U_s U_1/v_0 = P_1 - P_0; \quad (2)$$

$$\frac{1}{2}U_s^2 = E_1 - E_0 = \frac{1}{2}(P_1 + P_0)(v_0 - v_1), \quad (3)$$

where v_0 , P_0 , E_0 , v_1 , P_1 , E_1 , U_1 , U_s are, respectively, the specific volume, pressure, and internal energy ahead of the shock front, the specific volume, pressure, internal energy, and velocity behind the shock front, and the shock-wave velocity.

In porous solids, particles of solid matter are separated by empty spaces so that the average specific volume is $v_{00} = mv_0$ ($m \geq 1$), where m is the degree of porosity. The Rankine-Hugoniot equations for porous material are obtained by replacing v_0 by v_{00} in Eqs. (1), (2), and (3), which gives

$$\frac{U_s(m)}{U_s(m) - U_1(m)} = m \frac{v_0}{v_1} = m\sigma; \quad (4)$$

$$U_s(m)U_1(m)/v_0 = m(P_1 - P_0); \quad (5)$$

$$\frac{1}{2}U_s^2 = E_1 - E_0 = \frac{1}{2}v_1(P_1 + P_0)(m\sigma - 1). \quad (6)$$

Because U_s and U_1 are functions of the porosity m , shock-wave experiments for specified values of m are performed on a given material. From these experiments functional relationships for U_s and U_1 can be determined so that Eqs. (4), (5), and (6) can be applied to the material for any degree of porosity.

Shock-wave compression of porous solids results in much greater heating of this material relative to solid material; thus, the usual Mie-Grüneisen equation of state is inadequate to describe the dynamic behavior of such solids because only lattice vibrations of the solid are considered. In porous material, the anharmonicity of the thermal vibrations of the atoms and ions is accounted for by the concept of an electron "gas," which, in turn, leads to a complicated equation of state in which terms representing the thermal energy and thermal pressure of the "gas" are added to the lattice components. Thus, high-temperature equations of state for porous material are written as

$$P = P_c + P_t + P_e; \quad (7)$$

$$E = E_c + E_t + E_e, \quad (8)$$

where the subscripts c , t , and e represent, respectively, the cold-compression curve, the thermal energy of electron "gas," and the thermal

pressure of electron "gas." In Eqs. (7) and (8), the Gruneisen constant γ decreases from the value of the cold-compression curve ($T = 0^\circ\text{K}$) to the value of $2/3$ corresponding to the electron gas ($T \rightarrow \infty$). Because of these complications, no general equation of state for porous solids can be given; the equation of state for each material must be determined by itself for compression and expansion.

Inherent in the above paragraphs is the assumption that the strength of the shock wave is such that shear effects can be neglected. When this is no longer true, additional complications enter the picture. To date, no experiments have been performed in which shear effects were included. Thus, this area remains open as to the best approach to follow in determining equations of state for porous material.

2. One-dimensional Code Containment Structure

a. Inelastic Response of Primary Containment to High-energy Excursion (S. H. Fistedis)

Last Reported: ANL-7403, pp. 164-166 (Dec 1967).

The dynamic axisymmetric equations of motion for the inelastic response of primary containment to a core excursion have been developed. The difference between the hydrodynamic and the inelastic responses is that the latter include the shear strength of the material, which plays the role of dissipating the energy available for damage. Thus, the hydrodynamic response represents an upper-bound case for assessment of damage to primary containment.

The three conservation laws, in cylindrical coordinates (r, z), are:

1. Conservation of Mass:

$$\rho dv = \rho_0 dv_0 \quad (\text{incremental form}); \quad (1)$$

$$\frac{d\rho}{dt} + \rho \left(\frac{\partial u^r}{\partial r} + \frac{u^r}{r} + \frac{\partial u^z}{\partial z} \right) = 0 \quad (\text{differential form}), \quad (2)$$

where ρ is the density of a deformed volume element dv , ρ_0 is the density of an undeformed element dv_0 at time $t = 0$, and u^r and u^z are the velocities of the volume element in the radial and the axial directions.

2. Conservation of Momentum:

$$\frac{d^2 r}{dt^2} = \frac{du^r}{dt} = \frac{1}{\rho} \left\{ -\frac{\partial(P - \bar{\sigma}_{rr})}{\partial r} + \frac{\partial \sigma_{rz}}{\partial z} + \frac{2\bar{\sigma}_{rr} + \bar{\sigma}_{\theta\theta}}{r} \right\} + f^r; \quad (3)$$

$$\frac{d^2 z}{dt^2} = \frac{du^z}{dt} = \frac{1}{\rho} \left\{ -\frac{\partial(P - \bar{\sigma}_{zz})}{\partial z} + \frac{\partial \sigma_{rz}}{\partial r} + \frac{\sigma_{rz}}{r} \right\} + f^z; \quad (4)$$

$$P = -\frac{1}{3}(\sigma_{rr} + \sigma_{\theta\theta} + \sigma_{zz}); \quad (5)$$

$$\bar{\sigma}_{\theta\theta} = \sigma_{\theta\theta} + P = -(\bar{\sigma}_{rr} + \bar{\sigma}_{zz}); \quad \bar{\sigma}_{zz} = \sigma_{zz} + P; \quad (6)$$

$$\bar{\sigma}_{rr} = \sigma_{rr} + P; \quad \bar{\sigma}_{ij} = \sigma_{ij} \quad (i \neq j), \quad (7)$$

where P is the hydrostatic pressure for which the equation of state is that given on p. 165 of ANL-7403, σ_{ij} represents the components of stress tensor ($i, j = r, \theta, z$), $\bar{\sigma}_{ij}$ is the stress components deviator stress tensor, and f^r and f^z are the extrinsic forces (e.g., gravity) in the radial and axial directions.

3. Conservation of Internal Energy:

$$\frac{dE}{dt} = -P \frac{dv}{dt} + \frac{1}{\rho} \left[\bar{\sigma}_{rr} \frac{\partial u^r}{\partial r} + \bar{\sigma}_{\theta\theta} \frac{u^r}{r} + \bar{\sigma}_{zz} \frac{\partial u^z}{\partial z} + \frac{\sigma_{rz}}{2} \left(\frac{\partial u^r}{\partial z} + \frac{\partial u^z}{\partial r} \right) \right], \quad (8)$$

where E is the internal energy and v is the specific volume ($v = \rho^{-1}$). The additional equation needed to complete the set is the equation of state of the materials. For purposes of computation, the equation of state will be written as a subroutine. Thus, a general form such as

$$p = p(\rho, E) \quad (9)$$

is used in deriving the finite difference equations from Eqs. (1) through (9).

Because the primary containment has various materials and, hence, interfaces between them, Lagrangian coordinates must be used in solving shock-wave problems in such media. Thus, Eqs. (1) through (9), expressed in terms of Eulerian coordinates (r, z), have been transformed into Lagrangian coordinates (k, ℓ) for computational purposes. The conservation laws in Lagrangian coordinates (k, ℓ) are:

1'. Conservation of Mass:

$$\frac{\rho_0}{\rho} = \frac{rA}{r^0 A^0}; \quad A = \frac{\partial(r, z)}{\partial(k, \ell)} \quad (\text{incremental form}), \quad (10)$$

where ρ_0 , r^0 , and A^0 are the density, radius, and area of an undeformed volume dv_0 .

2'. Conservation of Momentum:

$$\frac{d^2 r}{dt^2} = \frac{du^r}{dt} = -\frac{r}{\rho_0 r^0 A^0} \left\{ \frac{\partial(P - \bar{\sigma}_{rr}, z)}{\partial(k, \ell)} + \frac{\partial(\sigma_{rz}, r)}{\partial(k, \ell)} \right\} + \frac{2\bar{\sigma}_{rr} + \bar{\sigma}_{\theta\theta}}{\rho_0 r^0 A^0} A + f^r; \quad (11)$$

$$\frac{d^2 z}{dt^2} = \frac{du^z}{dt} = \frac{r}{\rho_0 r^0 A^0} \left\{ \frac{\partial(P - \bar{\sigma}_{zz}, r)}{\partial(k, \ell)} + \frac{\partial(\sigma_{rz}, z)}{\partial(k, \ell)} \right\} + \frac{\sigma_{rz}}{\rho_0 r^0 A^0} A + f^z; \quad (12)$$

3'. Conservation of Internal Energy:

$$\begin{aligned} \frac{dE}{dt} = & -P \frac{dv}{dt} + \frac{r}{\rho_0 r^0 A^0} \left\{ \bar{\sigma}_{rr} \frac{\partial(u^r, z)}{\partial(k, \ell)} - \sigma_{zz} \frac{\partial(u^z, r)}{\partial(k, \ell)} \right. \\ & \left. + \frac{\sigma_{rz}}{2} \left[\frac{\partial(u^z, z)}{\partial(k, \ell)} - \frac{\partial(u^r, r)}{\partial(k, \ell)} \right] \right\} + \frac{\bar{\sigma}_{\theta\theta} u^r}{\rho_0 r^0 A^0} A. \end{aligned} \quad (13)$$

The partial derivatives in Eqs. (10), (11), (12), and (13) are called Jacobians, which are defined as

$$J(F_1, F_2, \dots, F_N, X_1, X_2, \dots, X_N) = \frac{\partial(F_1, F_2, \dots, F_N)}{\partial(X_1, X_2, \dots, X_N)}$$

$$= \begin{vmatrix} \frac{\partial F_1}{\partial X_1} & \frac{\partial F_1}{\partial X_2} & \dots & \frac{\partial F_1}{\partial X_N} \\ \frac{\partial F_2}{\partial X_1} & \frac{\partial F_2}{\partial X_2} & \dots & \frac{\partial F_2}{\partial X_N} \\ \dots & \dots & \dots & \dots \\ \frac{\partial F_N}{\partial X_1} & \frac{\partial F_N}{\partial X_2} & \dots & \frac{\partial F_N}{\partial X_N} \end{vmatrix}. \quad (14)$$

Equations (10) through (14) represent the complete set of equations to be solved subject to the appropriate initial and boundary conditions. The finite-difference forms of these equations are being derived.

ARGONNE NATIONAL LAB WEST



3 4444 00011305 0